Transport Properties in Drying Process and Drying Characteristics(Dissertation_全文)

AUTHOR(S):

Okazaki, Morio

CITATION:

Okazaki, Morio. Transport Properties in Drying Process and Drying Characteristics. 京都大学, 1975, 工学博士

ISSUE DATE:

1975-05-23

URL:

https://doi.org/10.14989/doctor.r2800

TRANSPORT PROPERTIES IN DRYING PROCESS AND DRYING CHARACTERISTICS

MORIO OKAZAKI

TRANSPORT PROPERTIES
IN DRYING PROCESS
AND
DRYING CHARACTERISTICS

MORIO OKAZAKI

February 1975

CONTENTS

CHAPTER 1

INTRODUCTION

1. Historical Review and Abstracts on This Work

The phenomenological studies on drying mechanisms of T.K. Sherwood and S. Kamei have been extensively developed by R. Toei, A.H. Nissan and A.V. Luikov. For example, Toei and his coworkers have performed a lot of experiments on dryings of various materials and made clear the characteristic of drying process from a view point of simultaneous heat and mass transfer, and given the design basis for dryer of granular materials. Luikov and his coworkers have described the drying process of capillary porous solids in elegant form by using the irreversible thermodynamics.

As a result of those studies, it has become more important how to determine the transport properties, such as liquid water transfer coefficients, effective thermal conductivities of moist materials, effective gas diffusivities of pores and so on, appearing in the differential equations of heat and mass transfer on drying of solid.

The studies on these transport properties have been conducted by O.A. Hougen, O. Krischer. D.M. Newitt, R. Toei and many other workers. Particularly in this field, the enormous contributions were given by Krischer and his

coworkers.

In spite of these contributions, however, there are considerably large obstacles to predict the transport properties of porous materials appearing in industrial drying operations without any experimental data.

From the view point mentioned above, keeping accent on the transport properties of moist materials in drying process, some approaches to several unsolved problems concerning with drying mechanisms were tried in this work.

CHAPTER 2 refers to the drying process of coated film of polymer solution as an example of drying homogeneous materials. The key point of this study stayed at how to determine the diffusion coefficients in wide range of polymer concentration.

CHAPTER's 3 ∿ 6 refer to drying operation of capillary porous solids.

CHAPTER's 3 and 4 refer to the prediction method of the effective thermal conductivities of dry and wet bed of granular materials.

CHAPTER 5 refers to modeling of drying phenomena of capillary porous solids by hot air drying.

The object of CHAPTER 6 is to make clear the characteristic of super-heated vapor drying in comparing to usual hot air drying from an engineering point of view.

CHAPTER's 7 and 8 are fundamental studies on vacuum drying operation of solids.

CHAPTER 7 is a proposal of a new simple calculation

technique of narrow channel flow of rarefied gases, and CHAPTER 8 refers to a theoretical approach to gas phase mass transfer coefficient in reduced pressures and determination of accomodation coefficient of mass transfer on sublimation.

2. Publications on This Thesis

CHAPTER 2 : Journal of Chemical Engineering of Japan, 7, 99 - 105 (1974)

CHAPTER 5 : Journal of Engineering Physics (USSR), 19, 464 - 475 (1970)

CHAPTER 6 : Kagaku Kogaku (Chemical Engineering, Japan) 30, 43 - 49 (1966)
Kagaku Kogaku (Chemical Engineering, Japan) 30, 947 - 948 (1966)
Kagaku Kogaku (Chemical Engineering, Japan) 30, 949 - 950 (1966)

CHAPTER 8 : Journal of Chemical Engineering of Japan, 1, 125 - 131 (1968)

The contents of CHAPTER's 3, 4 and 7 are unpublished.

CHAPTER 2

DRYING MECHANISM OF COATED FILM OF POLYMER SOLUTION

Introduction

In the maunfacture of photographic films, synthetic fibers and many kinds of polymer products, the drying of polymer solution plays an important role. It significantly affects the qualities of the products because it is the final process in their manufacture. The histories of solvent concentration distributions and temperature are more important than the overall drying rate, however many problems are still unsolved owing to the complicated behavior of polymer solutions.

Otake et al.[9] studied the drying of cellulose-acetate-acetone solution and explained the mechanism of the process by dividing it into two periods, namely the period of forming solid skin and that of decreasing drying rate. Sano and Nishikawa[12] performed drying experiments on a drop of polyvinylalcohol aqueous solution. They solved the diffusion equation taking into account the dependency of polymer concentration on the equilibrium vapor pressure of water. However, volumetric shrinkage which takes place during the

drying and the concentration dependency of the diffusion coefficient were not considered in those studies.

The purpose of the present work is to study the drying mechanism of coated film of PVA aqueous solution and to simulate the process of drying, considering the following three points of views:

1. The concentration dependency of diffusion coefficient.
2. The concentration dependency of equilibrium vapor pressure of water.
3. The effect of volumetric shrinkage of film accompanied by evaporation of water.

1. Measurement of Mutual Diffusion Coefficients

Diffusion coefficients in polymer-solvent systems have been measured by several workers[5], but most previous data reported refer to extremely dilute solutions or nearly dried films, and there are few available data for the medium-concentration range. Therefore the diffusion coefficients for almost the whole concentration range were measured to study the drying process of PVA-water solution, using the following three methods. These were the "micro-interferometric method" for dilute concentrations, "film desorption method" for the nearly dried state and "modified micro-interferometric method" for medium concentrations.

1.1 Diffusion coefficients for low concentrations of PVA

Experimental

Although there are several methods to measure the diffusion coefficients in low polymer concentrations, the micro-interferometric method developed by Robinson[11] and by Crank and Robinson[6] was adopted in the present study because of the simplicity of the apparatus and the remarkable saving of time.

The apparatus consisted of an optical assembly, an optical wedge (diffusion cell) and a microscope. The e-line ray (5461 Å) was used for interference. The diffusion cell was an optical wedge consisting of two partially-reflecting microscope slides.

Since an interference fringe produced in the cell represents a contour line of constant optical path in the wedge, the refractive index gradient is easily determined. There is a linear relationship between the refractive index and the concentration of PVA aqueous solution, so one can easily obtain the concentration gradient. The details of this method have been treated elsewhere[7,8].

The mutual diffusion coefficient is defined by the following equation[1]:

$$j_A = -\rho D \frac{\partial \omega_A}{\partial z} \qquad (2\text{-}1)$$

The diffusion coefficient D(c) as a function of concentration

may be calculated from the concentration gradient curve, as shown in Fig. (2-1), by Boltzmann's equation (2-2);

$$D = -\frac{1}{2t}\left(\frac{dz}{d\Omega}\right)\int_0^{\Omega} z\,d\Omega \qquad (2-2)$$

in which the origin of z-axis must be chosen to establish the following equation:

$$\int_0^1 z\,d\Omega = 0 \qquad (2-3)$$

where

$$\Omega = (\omega_A - \omega_{A2})/(\omega_{A1} - \omega_{A2}) \qquad (2-4)$$

ω_{A1} and ω_{A2} are the concentrations of the two contacting solutions, respectively.

Results

The sample of PVA employed was a commercial grade having a viscosity-average molecular weight of 21,000 and a polymerization degree of 480. Linear relationships between refractive index n and concentration ω_B, as well as between specific volume and concentration, were obtained in the concentration range from pure solvent to $\omega_B \doteqdot 0.6$.

The data obtained are shown in Fig. (2-2). Measurement was carried out at 25°C and 35°C. At both temperatures the coefficient is almost independent of concentration in the range from $\omega_B = 0.15$ to 0.30, and increases with

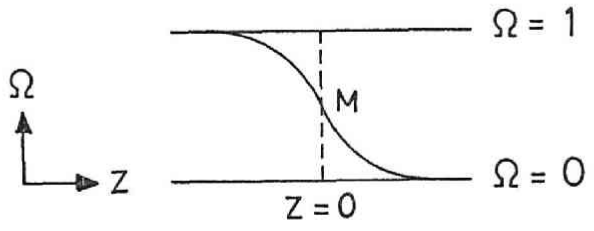

Fig. (2-1) Concentration distribution

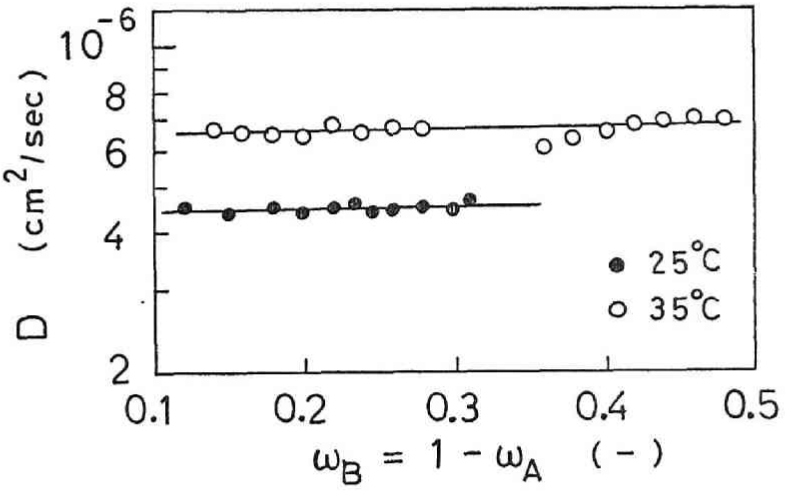

Fig. (2-2) Diffusion coefficients in low concentration range of PVA

increasing temperature. The Arrhenius activation energy is estimated to be about 5.6 kcal/mol.

1.2 Diffusion coefficients for intermediate concentrations of PVA

Experimental

Though several attempts have been made, it can be said that there has not been established a reliable method to measure the diffusion coefficient of polymer solution in the intermediate concentration range. Thus the micro-interferometric method was modified for use in such a concentration range.

The apparatus used was the same as mentioned above. A solution was put in the diffusion cell, made of two partially-reflecting microscope slides so as to be U-shaped, as shown in Fig. (2-3). Then the evaporation rate from the interior surface, A in Fig. (2-3), was suppressed, so that the solution could flow freely to the outer surface during the observing time. By means of this device the growth of a meniscus formed on the surface at B shown in Fig. (2-3), where the interference fringes were observed, was avoided. Solvent evaporation occurred at the outer surface and the concentration gradient was formed there.

Figure (2-4) shows the observed interference fringes. Polymer solution is shown at the right, air at the left and the meniscus, whose width was about 10-20μ, in the middle.

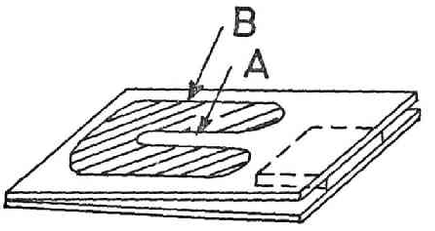

Fig. (2-3) Diffusion cell

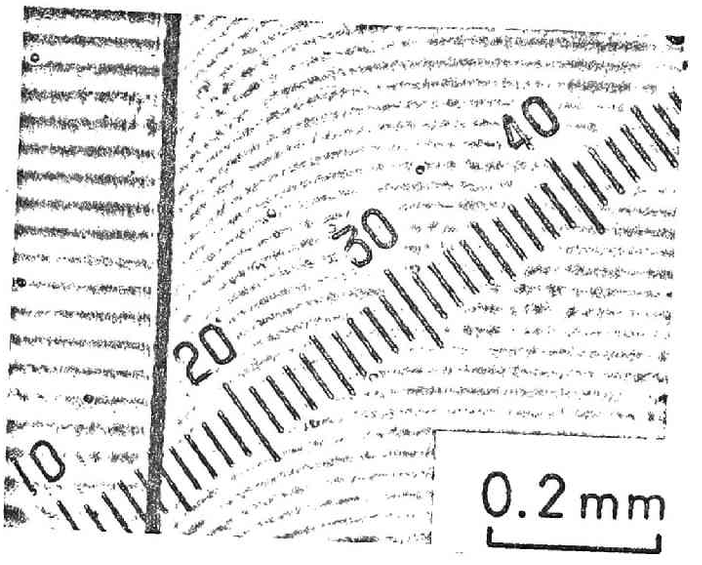

Fig. (2-4) Interference fringe

The calculation procedure of concentration gradients from the interference fringes is as follows.

In Fig. (2 -5),

$$n_1 d_1 = nd \qquad (2\text{-}5)$$

$$d_1 \fallingdotseq d + x\theta \qquad (2\text{-}6)$$

because angle θ is very small (θ = 0.008 radian). When there is a linear relationship between refractive index and concentration, Eqs. (2 -5) and (2 -6) give the relation

$$n = n_1/(1 - x\theta/d_1) \qquad (2\text{-}7)$$

whereas

$$d_1 = L\theta \qquad (2\text{-}8)$$

Therefore

$$n = n_1/(1 - x/L) \qquad (2\text{-}7')$$

As a result, the refractive index gradient is easily determined from x and L by using Eq. (2 -8).

Calculation procedure

The mass transfer equations in the system of two components are[1)]

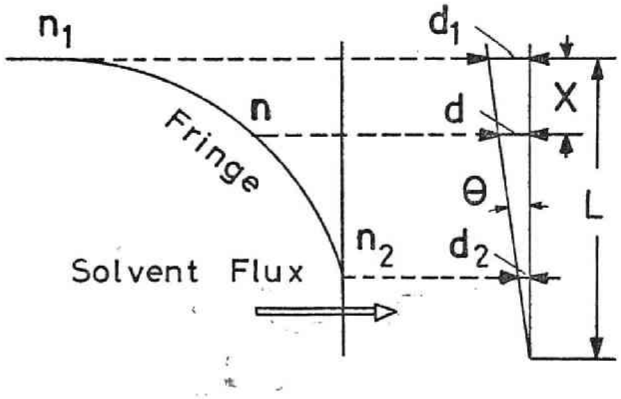

Fig. (2-5) Gradient of refractive index

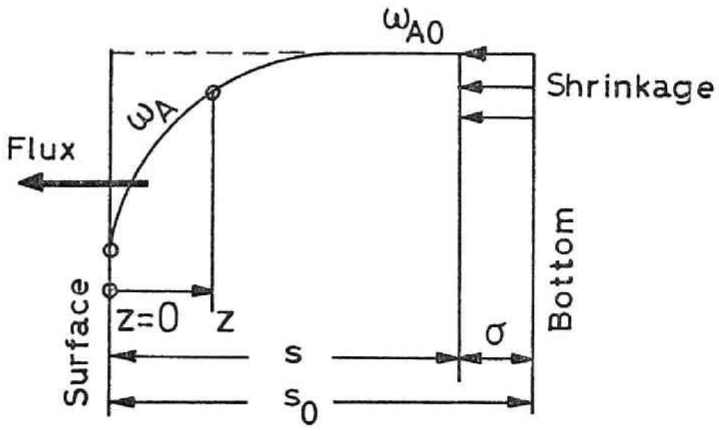

Fig. (2-6) Drying layer of polymer solution

$$\frac{\partial \rho_A}{\partial t} + \frac{\partial (\rho_A v)}{\partial z} = \frac{\partial}{\partial z}(\rho D \frac{\partial \omega_A}{\partial z}) \qquad (2-9)$$

$$\frac{\partial \rho_B}{\partial t} + \frac{\partial (\rho_B v)}{\partial z} = \frac{\partial}{\partial z}(\rho D \frac{\partial \omega_B}{\partial z}) \qquad (2-10)$$

Assuming volumetric additivity between PVA and water,

$$(\rho_A / \overset{\circ}{\rho}_A) + (\rho_B / \overset{\circ}{\rho}_B) = 1 \qquad (2-11)$$

From Eqs. (2-9)-(2-11) one can obtain the following set of transfer equations.

$$\frac{\partial v}{\partial z} = \frac{\partial}{\partial z}\left(\frac{D}{\omega_A + \hat{\omega}} \cdot \frac{\partial \omega_A}{\partial z}\right) \qquad (2-12)$$

$$\frac{\partial \omega_A}{\partial t} - (\omega_A + \hat{\omega}) \frac{\partial v}{\partial z} + v \frac{\partial \omega_A}{\partial z} = 0 \qquad (2-13)$$

where v is the velocity of the mass center and

$$\hat{\omega} = \overset{\circ}{\rho}_A / (\overset{\circ}{\rho}_B - \overset{\circ}{\rho}_A) \qquad (2-14)$$

Now let us consider a layer of polymer solution drying from one side, as shown in Fig. (2-6). The origin of z-axis is fixed at the evaporating surface. The volumetric shrinkage of the layer may occur as drying proceeds, and its amount is equal to the volume of the solvent evaporated. Let us represent the shrinkage as an advance of the bottom surface. The shrinkage σ is represented as

$$\sigma\overset{\circ}{\rho}_A + \int_0^s \rho_A dz = \int_0^{s_0} \rho_A\big|_{t=0} dz \qquad (2\text{-}15)$$

where s_0 is the initial thickness and s is that at an arbitrary time. The initial distribution of concentration is everywhere uniform. When one puts an imaginary initial bottom plane far away from the evaporation surface, the concentrations near the imaginary bottom plane are uniform and do not change appreciably. Then one obtains the following equations.

$$\sigma \doteqdot (1/\overset{\circ}{\rho}_A)\{\int_0^{s_0} (\rho_A\big|_{t=0} - \rho_A) dz + \rho_{A0}\sigma\} \qquad (2\text{-}16)$$

Then

$$\sigma \doteqdot \{1/(\overset{\circ}{\rho}_A - \rho_{A0})\}\int_0^{s_0} (\rho_A\big|_{t=0} - \rho_A) dz \qquad (2\text{-}17)$$

Therefore, one can determine s from Eq. (2-18).

$$s \doteqdot s_0 - \{1/(\overset{\circ}{\rho}_A - \rho_{A0})\}\int_0^{s_0} (\rho_A\big|_{t=0} - \rho_A) dz \qquad (2\text{-}18)$$

In applying Green's theorem to Eq. (2-9) with the boundary condition with respect to domain B on the t-z plane, as shown in Fig. (2-7),

$$\begin{aligned} &0 \leq t \leq T \\ &Z \leq z \leq s(t) \end{aligned} \qquad (2\text{-}19)$$

one can obtain

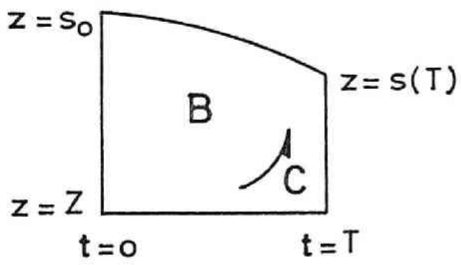

Fig. (2-7) Boundary

$$0 = \iint_B \{\frac{\partial}{\partial z}(\rho_A v - \rho D\frac{\partial \omega_A}{\partial z}) + \frac{\partial \rho_A}{\partial t}\}dzdt \qquad (2-20)$$

$$= -\int_C \{(\rho_A v - \rho D\frac{\partial \omega_A}{\partial z})dt - \rho_A dz\} \qquad (2-21)$$

There is scarcely any concentration gradient at the imaginary bottom plane, so that changing T, Z to t, z, respectively, and differentiating Eq. (2-21) by t give

$$0 = -\frac{\partial}{\partial t}\int_z^{s_0} \rho_A\Big|_{t=0} dz + \frac{\partial}{\partial t}\int_z^s \rho_A dz + (\rho_A v)\Big|_{z=s}$$

$$- \rho_A v + \rho D\frac{\partial \omega_A}{\partial z} \qquad (2-22)$$

By integrating Eq. (2-12), we obtain the equation

$$v = \frac{D}{\omega_A + \bar{\omega}}\cdot\frac{\partial \omega_A}{\partial z} + v\Big|_{z=s} \qquad (2-23)$$

Substituting Eq. (2-23) to Eq. (2-22), D is given as

$$D = -(1 + \frac{\omega_A}{\bar{\omega}})\{1/(\rho\frac{\partial \omega_A}{\partial z})\}$$

$$\times \{\frac{\partial}{\partial t}\int_z^s \rho_A dz + (\rho_A\Big|_{z=s} - \rho_A)v\Big|_{z=s}\} \qquad (2-24)$$

On the other hand, the concentration gradient at z=s(t) is always equal to zero, therefore

$$v\Big|_{z=s} = \frac{d\sigma}{dt} = -(\frac{d}{dt}\int_0^s \rho_A dz)/\mathring{\rho}_A \qquad (2-25)$$

$$D = -\left(1 + \frac{\omega_A}{\omega}\right)\left\{1/\left(\rho\frac{\partial \omega_A}{\partial z}\right)\right\}$$

$$\times \left\{\frac{\partial}{\partial t}\int_z^s \rho_A dz - \left(\rho_A\Big|_{z=s} - \rho_A\right)\left(\frac{d}{dt}\int_0^s \rho_A dz\right)/\mathring{\rho}_A\right\} \qquad (2\text{-}26)$$

One can determine the diffusion coefficients from the changes of concentration distribution curve with time by using the above equation.

Results

The distribution curves of concentration obtained are shown in Fig. (2-8). Figure (2-9) shows the diffusion coefficients calculated from Eq. (2-26). During the time of measurement, $v\big|_{z=s}$ was approximately constant and equal to about -3×10^{-6} cm/sec. The shrinkage of thickness of the imaginary layer was several percent relative to s_0. It may be attributed to the complicated calculation that there was a rather large scattering of data. However, we may rely on the results obtained by the above method, because they join those obtained in the low concentration ranges.

1.3 Diffusion coefficients for high concentrations of PVA

Experimental

The sorption method was applied to measure the diffusion coefficient in the high-concentration range. It has been reported that there is hysteresis between an adsorption process and a desorption. Thus the desorption method might

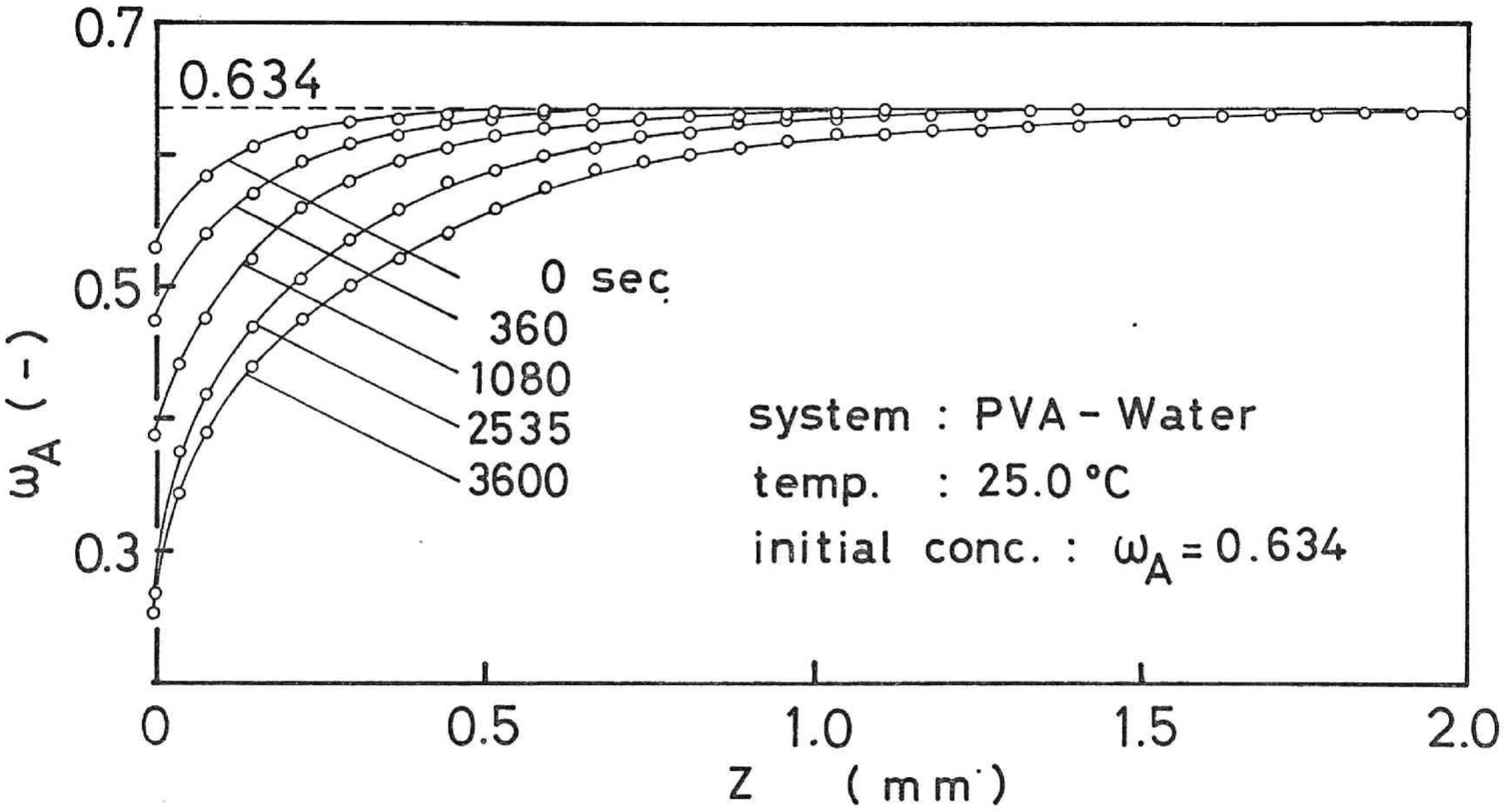

Fig. (2-8) Concentration distributions in polymer solution

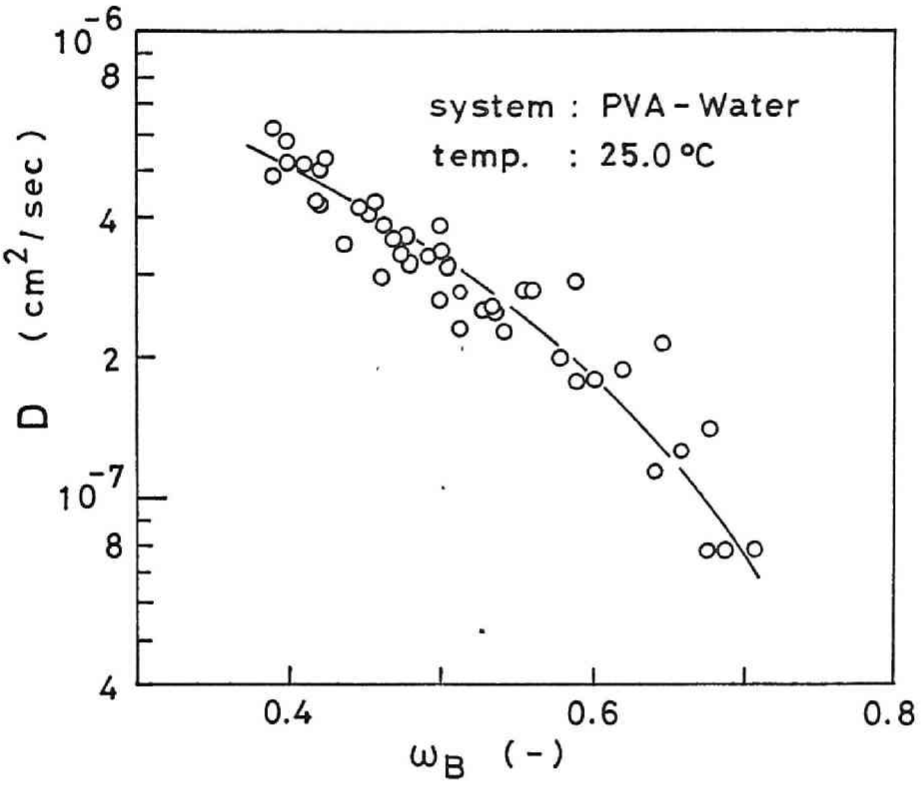

Fig. (2-9) Diffusion coefficients in middle concentration range of PVA

be favorable for application to the present purpose. The details of this method are described elsewhere[4,5,10].

If the concentration just within the surfaces of a plane sheet of thickness 2b is maintained constant, the amount of diffusant M_t taken up from the sheet in time t is given by the equation*

$$\frac{M_t}{M_\infty} = 2\sqrt{\frac{Dt}{b^2}}\left\{\frac{1}{\sqrt{\pi}} + 2\sum_{n=0}^{\infty}(-1)^n \mathrm{ierfc}\frac{nb}{\sqrt{Dt}}\right\} \qquad (2\text{-}27)$$

The downtake is considered to be a diffusion process controlled by a constant diffusion coefficient D, and M_∞ is the equilibrium sorption attained theoretically after infinite time. The value of D can be deduced from an observation of the initial gradient of a graph of M_t/M_∞ as a function of $\sqrt{t/b^2}$.

For systems in which the diffusion coefficient is concentration-dependent, the initial gradient of each desorption curve yields some mean value, $\bar{D}$, say, of the integral diffusion coefficient. Crank[3] has shown that $\bar{D}$ provides a reasonable approximation to

$$\bar{D} = (1/\omega_{A0})\int_0^{\omega_{A0}} D(\omega_A)\,d\omega_A \qquad (2\text{-}28)$$

---

*The diffusion flux of solvent and then v in Eq. (2-9) are usually very small in the sorption method. The 2nd term of left hand side of Eq. (2-9) was neglected in the derivation of Eq. (2-27).

where 0 to ω_{A0} is the concentration range existing in the sheet during the experiment. By calculating values of $\bar{D}$ for each of a series of sorption experiments, a graph showing $\bar{D}\omega_{A0}$ as a function of ω_{A0} can be drawn, and graphical differentiation with respect to ω_{A0} gives a first approximation to the relationship between D and ω_A. This first approximation was adopted in the present work.

Results

The cast films used for desorption measurements were made by the evaporation of PVA solution films on mercury. They were about 5 cm x 12 cm in scale and 10^{-2}-5 x 10^{-3} cm in thickness. From the desorption curves observed, the diffusion of the PVA-aqueous solution is of Fickian type. The deduced values of D are shown in Fig. (2-10) as well as those of $\bar{D}$.

The temperature dependency of D for the high concentration range is somewhat larger than that for the low concentration range. The activation energy was estimated to be about 7.3 kcal/mol.

2. Drying Experiments of Coated Film of PVA Aqueous Solution

Experimental

The measuring part of the apparatus used is shown in Fig. (2-11). Hot air of constant temperature and humidity

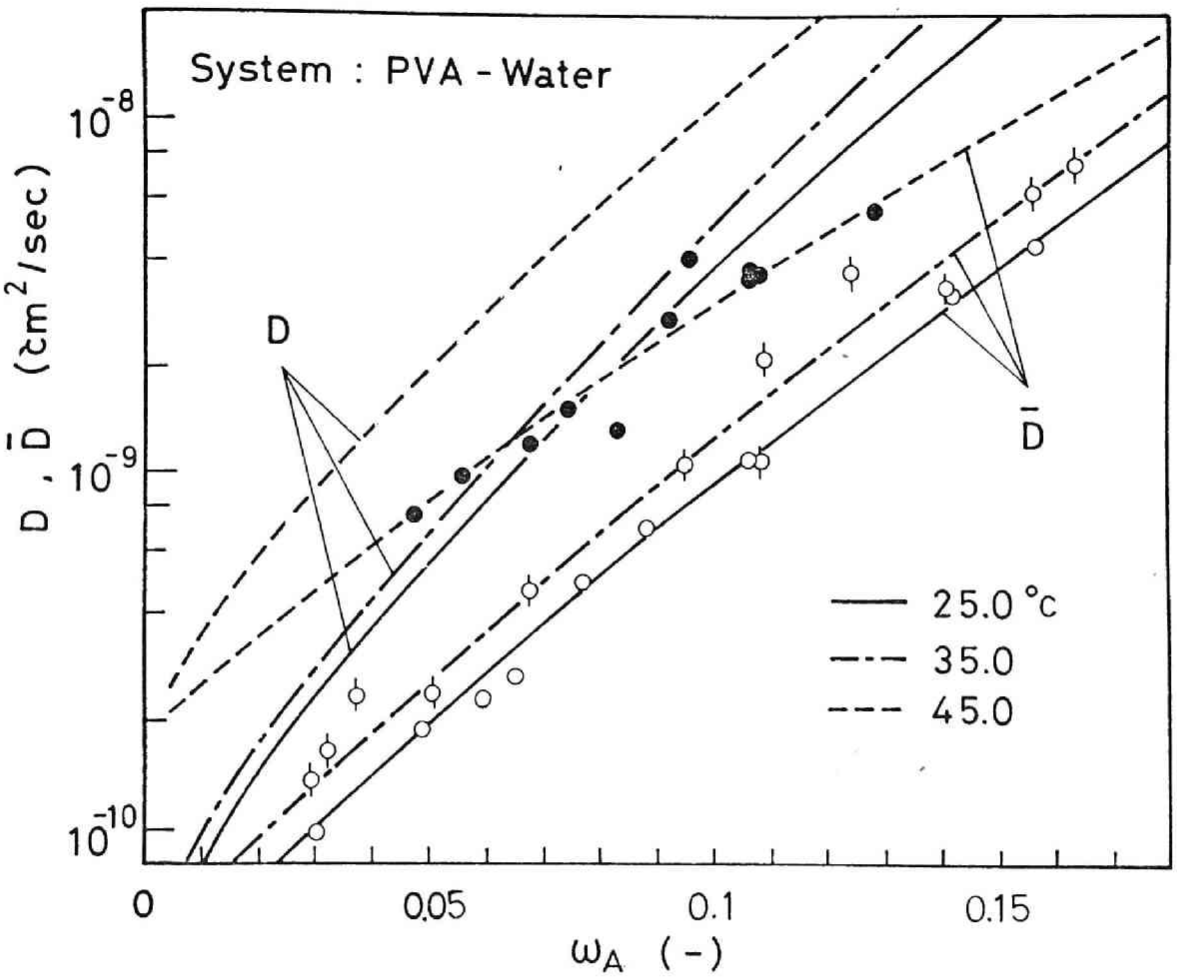

Fig. (2-10) Diffusion coefficients in high concentration range of PVA

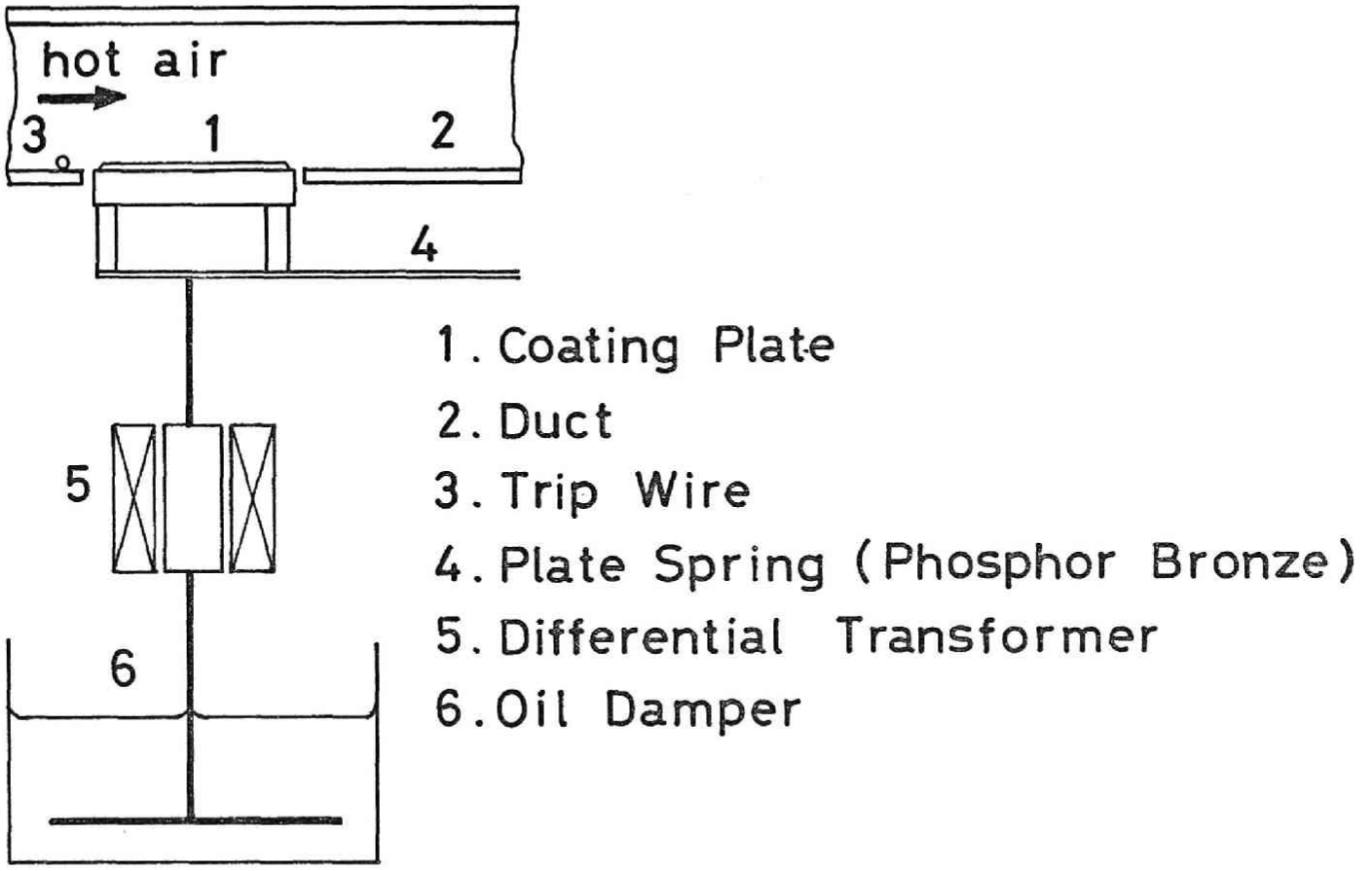

Fig. (2-11) Drying apparatus of coated film

was fed through the rectangular duct on which an assembly of coated film was put, as shown in Fig. (2 -11). The deflection of the cantilever, 4, caused by the weight change of coated film was converted to an electrical signal by a differential transformer and was recorded continuously. The oil damper was set to minimize the influence of vibration of the static pressure on the weighing. The coating plate, as shown in Fig. (2 -12), was carefully thermal-insulated by keeping the temperature of the upper aluminum plate equal to that of the coated film during the time of drying by an electronic thermo-regulator within a temperature difference of $\pm$0.1°C. The base plate for coating of PVA-solution was made of polymethylmethacrylate. The measuring error on weighing the film was within $\pm$10 mg.

Results

The experimental conditions are listed in Table (2 -1). An example of changes of weight and temperature is shown in Fig. (2 -13). Figure (2 -14) shows the drying characteristic curves observed. The drying process can be divided into two periods, that is, the constant and the decreasing drying rate period. With regard to the drying rate characteristic curve during the decreasing period, it can be recognized that the curve changes from convex for a thinner film to concave with increasing film thickness, irrespective of the same initial concentrations.

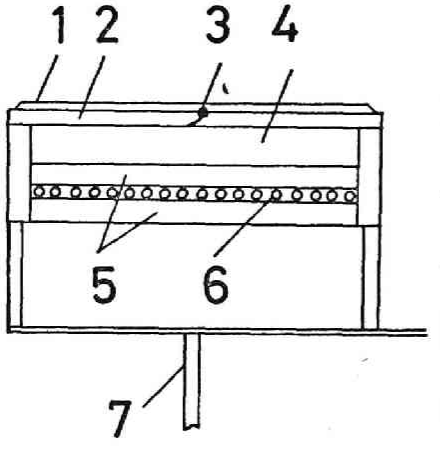

1. Coated Film
2. Coating Plate (40 x 85 mm)
3. Thermo-couple (copper-constan. 80 μΦ)
4. Thermal Insulation Material
5. Aluminum Plate
6. Electric Heater
7. Rod of INVAR Metal

Fig. (2-12) Coating plate

Table (2-1) Drying conditions of coated film

Run No.	Coated amount [g/cm^2]	Initial conc. of coated soln. ω_{A0} [g-water/g-soln.]	Initial thickness of film s_0 [cm]	Constant drying rate R_c [$g/cm^2 \cdot sec$]
110	0.0985	0.799	0.0943	2.86×10^{-5}
112	0.127	0.799	0.122	2.86×10^{-5}
117	0.0464	0.799	0.0444	2.86×10^{-5}

All the experiments were carried out at the following conditions of hot air.

Temperature: 42.0°C, Humidity: 0.0047 g-water/g-dry air, velocity: 2.7 m/sec

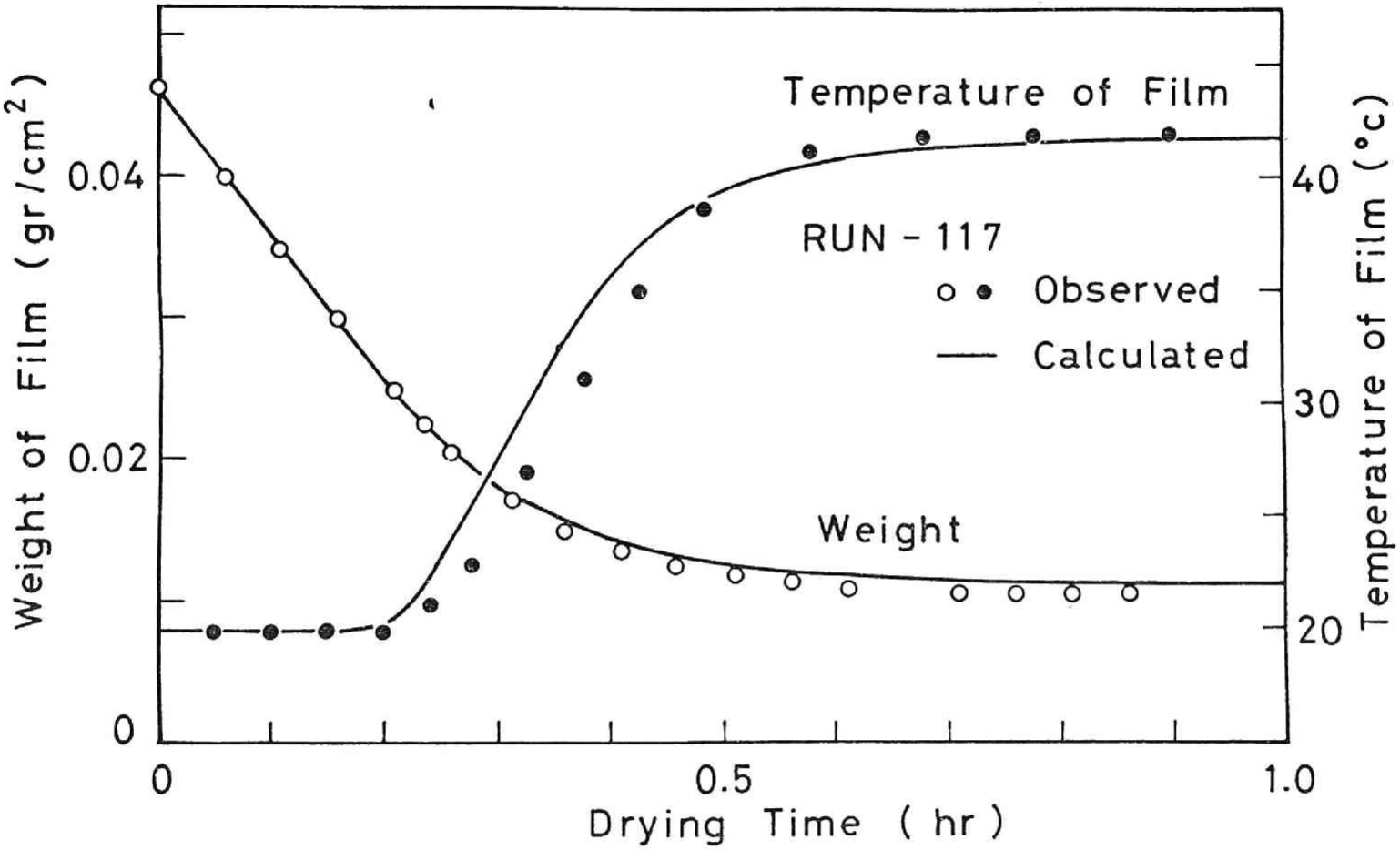

Fig. (2-13) Changes of weight and temperature of drying film

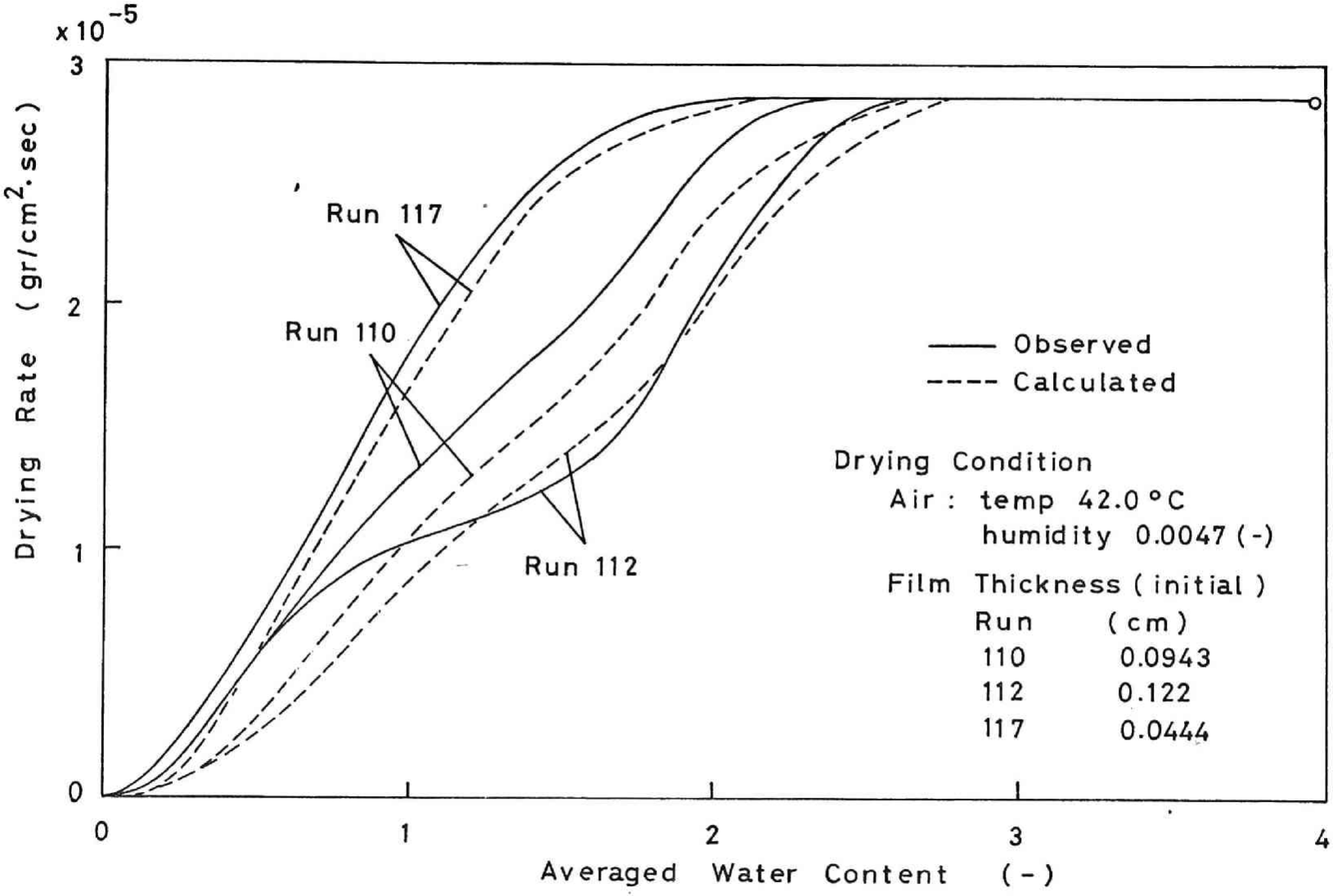

c_A=1.00 cal/g °C c_p=0.40 cal/g °C c_s=0.35 cal/g °C ω_{Ae}=0.007275
W_s=0.119 g/cm^2 ρ_A=0.994 g/cm^3 ρ_B=1.27 g/cm^3

3. Discussion of Drying Mechanism

Formulation of drying equations

Let us consider the drying process of film as shown in Fig. (2-15), where the origin is taken at the bottom of the film. Assuming that the temperature distribution is negligibly small because of the film being very thin and that there is no convective flow in the film because of the high viscosity of the solution, we can obtain the following set of equations to represent the drying process of coated film.

Elimination of v from Eqs. (2-12) and (2-13) gives the following mass transfer equation.

$$\frac{\partial \omega_A}{\partial t} + \frac{2D}{\omega_A + \hat{\omega}}\left(\frac{\partial \omega_A}{\partial z}\right)^2 = \frac{\partial}{\partial z}\left(D\frac{\partial \omega_A}{\partial z}\right) \qquad (2\text{-}29)$$

Initial conditions:

$$\text{at } t = 0, \text{ any } z : \omega_A = \omega_{A0} = \text{const.} \qquad (2\text{-}30)$$

$$\text{at } t = 0 \qquad : s = s_0 \qquad (2\text{-}31)$$

Boundary conditions:

$$\text{at } z = 0 \text{ (bottom)}, \text{ any } t : \frac{\partial \omega_A}{\partial z} = 0 \qquad (2\text{-}32)$$

at $z = s(t)$ (surface), any t :

$$-\frac{\rho D \hat{\omega}}{\omega_A + \hat{\omega}} \cdot \frac{\partial \omega_A}{\partial z} = k_g(p - p_a) \qquad (2\text{-}33)$$

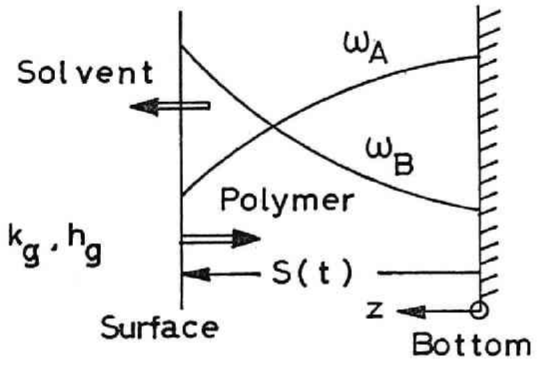

Fig. (2-15) Drying model of coated film

$$- \frac{\rho D\hat{\omega}}{\omega_A + \hat{\omega}} \cdot \frac{\partial \omega_A}{\partial z} = - \overset{\circ}{\rho}_A \frac{ds}{dt} \qquad (2-34)$$

where

$$D = D(\omega_A, \theta) \qquad (2-35)$$

$$p = p(\omega_A, \theta) \qquad (2-36)$$

Eq. (2-33) is derived by applying Green's theorem to Eq. (2-9), taking account of Eq. (2-32), and setting v=0 at t=0.

On the other hand, the heat transfer equation determining the temperature of the film is given as

$$\{W_s c_s + W(c_p + c_A w)\}\frac{d\theta}{dt} - r_A W \frac{dw}{dt} = h_g(\theta_a - \theta) \qquad (2-37)$$

the following replacements

$$\begin{aligned} &x = z/s,\ y = (\omega_A - \omega_{Ae})/(\omega_{A0} - \omega_{Ae}),\ S = s/s_0 \\ &K = D/s_0^2,\ V = v/s_0,\ \hat{y} = (\hat{\omega} + \omega_{Ae})/(\omega_{A0} - \omega_{Ae}) \end{aligned} \qquad (2-38)$$

convert Eqs. (2-29)-(2-34) and (2-37) to Eqs. (2-39)-(2-45).

$$\frac{\partial y}{\partial t} - \frac{x}{S} \cdot \frac{dS}{dt} \cdot \frac{\partial y}{\partial x} + \left(\frac{2K}{\hat{y+y}}\right)\frac{1}{S^2}\left(\frac{\partial y}{\partial x}\right)^2 = \frac{\partial}{\partial x}\left(K\frac{\partial y}{\partial x}\right) \qquad (2-39)$$

Initial conditions:

$$\text{at } t = 0, \text{ any } x : y = 1 \qquad (2-40)$$

$$\text{at } t = 0 : S = 1,\ \theta = \theta_w \qquad (2\text{-}41)$$

Boundary conditions:

$$\text{at } x = 0, \text{ any } t : \frac{\partial y}{\partial x} = 0 \qquad (2\text{-}42)$$

$$\text{at } x = 1, \text{ any } t :$$

$$-\frac{\omega\rho K}{(\dot{y}+y)S}\cdot\frac{\partial y}{\partial x} = \frac{k_g}{s_0}(p - p_a) \qquad (2\text{-}43)$$

$$\frac{k_g}{s_0}(p - p_a) = -\dot{\rho}_A\frac{dS}{dt} \qquad (2\text{-}44)$$

$$\{W_s c_s + c_p s_0(\rho_0 - \rho_{A0}) + c_A s_0(\rho_{A0} - \dot{\rho}_A) + c_A s_0\dot{\rho}_A S\}\frac{d\theta}{dt}$$

$$- r_A\dot{\rho}_A s_0\frac{dS}{dt} = h_g(\theta_a - \theta) \qquad (2\text{-}45)$$

Numerical solution

Eqs. (2-39) and (2-45) were solved simultaneously with the boundary conditions, Eqs. (2-40) - (2-44), to give the calculated results of the drying process of the coated film, as described below.

Figure (2-16) shows the diffusion coefficients observed at 25°C in the whole concentration range. The lnD was represented by a polynomial expression of 7th degree with respect to concentration, ω_A (see Appendix-1). The Arrhenius equation having ΔE = 7.3 kcal/mol was adopted to estimate the temperature dependency of the coefficients.

The equilibrium vapor pressure of water on the PVA aqueous solution was expressed by the formula

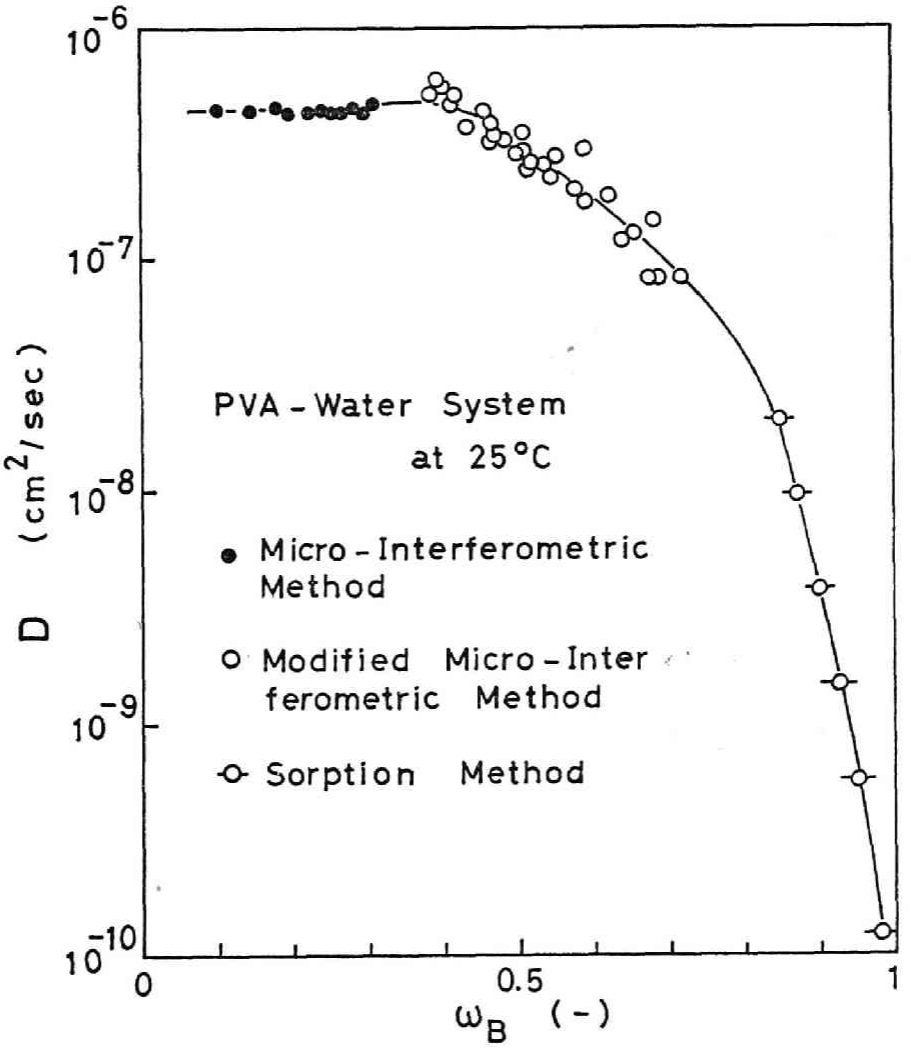

Fig. (2-16) Diffusion coefficients of PVA aqueous solution

$$p(\omega_A, T) = p_{s,T} \cdot a(\omega_A) \qquad (2\text{-}46)$$

Where $a(\omega_A)$ is the activity at the concentration of ω_A and approximately assumed to be independent of temperature over a small range of temperature, and was numerically represented by a polynomial expression of 6th degree with respect to concentration by using Sano and Nishikawa's data[12] (see Appendix-1). $p_{s,T}$ is the saturated vapor pressure of water.

The numerical calculation was done by the finite-difference method (see Appendix-2), in which Δt and Δx were 2.5 - 5.0 sec and 0.1, respectively. The numerical solutions of the set of equations are shown in Figs. (2-13), (2-14) and (2-17). An example of the calculated results representing the changes of water content distribution and film thickness with time are shown in Fig. (2-17) for Run 117. As shown in Fig. (2-13), calculated film temperature and weight were in fairly good agreement with the values observed. Values for critical water content coincided with each other too, but there were somewhat appreciable discrepancies between those of the characteristic drying rate curve, as shown in Fig. (2-14). These discrepancies, especially in the low water content range, may be due partly to the crystallization occurring in the high concentration range of polymer, which may affect both diffusion coefficient and equilibrium vapor pressure of solvent, although these effects could not be quantitatively estimated yet, and partly to the measuring methods of diffusion coefficient mentioned at 1.3,

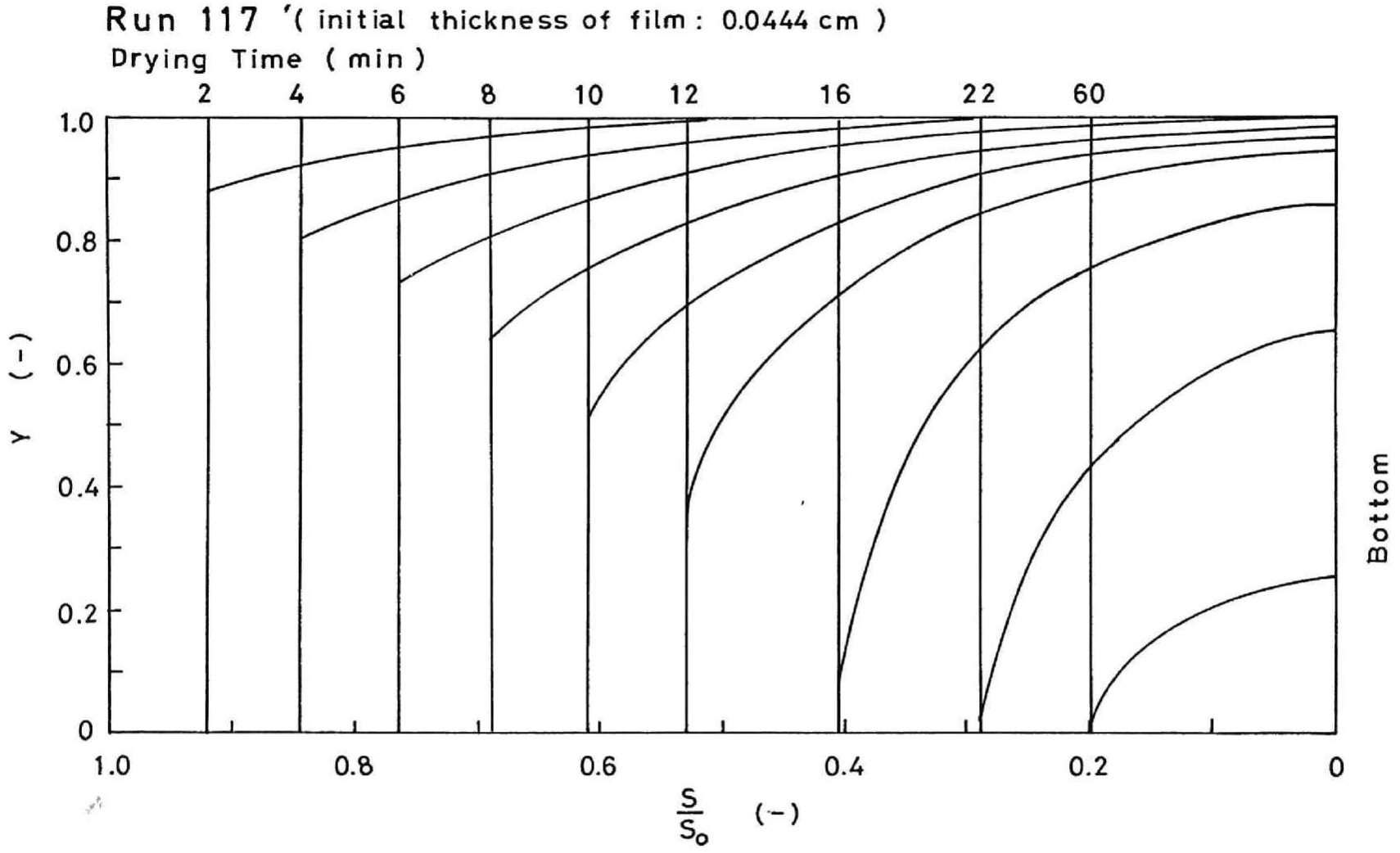

Fig. (2-17) Calculated distributions of water concentration

which neglect the influence of volumetric shrinkage assuming a small change of concentration of the system. In spite of these discrepancies, the calculated curves were similar to the observed ones as a whole.

Conclusion

Drying of coated film of polyvinylalcohol aqueous solution was studied experimentally and theoretically to determine the change of distributions of local solvent concentration and temperature of film during drying.

Measurements of diffusion coefficient of the PVA-water system were performed in the whole range of concentration. A new method for measurement in the middle range is proposed.

A set of drying equations taking account of the volumetric shrinkage accompanying the evaporation of solvent was formulated and numerically solved using the observed diffusion coefficients.

The calculated results were compared with the experimental ones obtained from drying experiments of coated film of PVA aqueous solution.

The agreement between them shows the reliability of the diffusion coefficient observed and the theoretical treatment proposed in the present work.

Appendix-1

Diffusion coefficient

$$D_{25°C}(\omega_A) = \exp\{\sum_{n=1}^{8} (1 - \omega_A)^{n-1} F_n\} \quad \text{(A-1)}$$

F_n(n=1, 2, ...,8) : -14.20662, 0.7050937, -92.66516, 718.8218, -2233.989, 3310.831, -2341.191, 627.7167

Activity of water vapor pressure

$$\text{at } \rho_B/\mathring{\rho}_B \leq 0.572 : a = 1 \quad \text{(A-2)}$$

$$\text{at } \rho_B/\mathring{\rho}_B > 0.572 : a = (\rho_B/\mathring{\rho}_B)^{n-1} F_n' \quad \text{(A-3)}$$

F_n'(n=1, 2, ...,7) : -6.000924, 33.63109, -51.77314, 31.54351, -36.5868, 64.65406, -35.46261

Appendix-2

Finite-difference equations

The integration of Eq. (2-39) by x give[13];

$$\frac{\partial}{\partial t}\int_0^x y dx = \frac{1}{S}\cdot\frac{dS}{dt}(xy - \int_0^x y dx) - \frac{2}{S^2}\int_0^x \frac{K}{y + y^*}\left(\frac{\partial y}{\partial x}\right)^2 dx + K\frac{\partial y}{\partial x} \quad \text{(A-4)}$$

Now, let k = Δt and h = Δx = 1/N.

The implicit finite-difference representation of Eq. (A-4) becomes

$$Y_{i,j+1} = Y_{i,j} + (Y_{0,j} - Y_{0,j+1}) + 2\sum_{n=1}^{i-1}(Y_{n,j} - Y_{n,j+1})$$

$$+ k\left[\frac{1}{S_{j+1}}\cdot\frac{dS}{dt}\Big|_{j+1}\{iy_{i,j} - B(y)_{i,j+1}\}\right.$$

$$+ \frac{1}{S_i}\frac{dS}{dt}\Big|_j \{iy_{i,j} - B(y)_{i,j}\}]$$

$$- 2k\{\frac{1}{S_{j+1}^2}B(K)_{i,j+1} + \frac{1}{S_j^2}B(K)_{i,j}\}$$

$$+ \frac{k}{h^2}\{K_{i,j+1}(y_{i+1,j+1} - y_{i-1,j+1})$$

$$+ K_{i,j}(y_{i+1,j} - y_{i-1,j})\} \qquad \text{(A-5)}$$

where

$$K_{i,j} = \frac{K(y_{i,j})}{y_{i,j} + \hat{y}}\left(\frac{y_{i+1,j} - y_{i-1,j}}{h}\right)^2 \qquad \text{(A-6)}$$

$$B(X)_{i,j} = \frac{1}{h}\int_0^{ih} X(x,j)\,dx$$

$$= \left(\frac{X_{i,j} + X_{0,j}}{2} + \sum_{n=1}^{i-1} X_{n,j}\right) \qquad \text{(A-7)}$$

The semi-implicit representation at the bottom (i = 0) for Eq. (2-39) is

$$y_{0,j+1} = y_{0,j} + \frac{k}{2h^2}\{K(y_{0,j}) + K(y_{1,j})\}(y_{1,j} - y_{0,j})$$

$$- \frac{2K(y_{0,j})}{y_{0,j} + \hat{y}}\cdot\frac{1}{S_j^2}(y_{1,j} - y_{0,j})^2$$

$$+ \{K(y_{0,j+1}) + K(y_{1,j+1})\}(y_{1,j+1} - y_{0,j+1})$$

$$- \frac{2K(y_{0,j+1})}{y_{0,j+1} + \hat{y}}\cdot\frac{1}{S_{j+1}^2}(y_{1,j+1} - y_{0,j+1})^2 \qquad \text{(A-8)}$$

$$\left.\frac{dS}{dt}\right|_{j+1} = (S_{j+1} - S_j)/k \qquad \text{(A-17)}$$

where $y_{N,j}$ is given from Eq. (A-15).

Eq. (2 -45) is given as follows;

$$\theta_{j+1} = \theta_j + k\{h_g(\theta_a - \theta_j) + r_A \overset{\circ}{\rho}_A s_0 \left.\frac{dS}{dt}\right|_j\}/(A_1 + A_2 S_j) \qquad \text{(A-18)}$$

where

$$A_1 = W_s c_s + c_p s_0(\rho_0 - \rho_{A0}) + c_A s_0(\rho_{A0} - \overset{\circ}{\rho}_A) \qquad \text{(A-19)}$$

$$A_2 = c_A s_0 \overset{\circ}{\rho}_A \qquad \text{(A-20)}$$

Calculation Procedures

The principle of numerical calculation is as follows.

(1) Substituting θ_j, S_j and $dS/dt|_j$ into Eq. (A-18) gives θ_{j+1}.

(2) Substituting $p^{(n)}(y_{N,j})$ which is the n-th approximate value of $p(y_{N,j})$ into Eq. (A-16) gives $S_{j+1}^{(n+1)}$, which gives $dS/dt|_{j+1}$ from Eq. (A-17)

(3) $y_{0,j+1}^{(n+1)}$ is given by substitution of $S_{j+1}^{(n+1)}$ into Eq. (A-8)

(4) By substituting $y_{0,j+1}^{(n+1)}$ into Eq. (A-5), one can obtain the values $y_{i,j+1}^{(n+1)}$ (i = 1, 2, ..., N-1) succesively.

(5) Substituting the values obtained above into Eq. (A-13) gives $Y_{N,j+1}^{(n+1,1)}$, the first approximate value of $Y_{N,j+1}^{(n+1)}$, and which gives $y_{N,j+1}^{(n+1,1)}$ from Eq. (A-15). Further substitution of $y_{N,j+1}^{(n+1,1)}$ into Eq. (A-13) and (A-15) gives $y_{N,j+1}^{(n+1,2)}$. By iteration of these calculations

$$\left.\frac{dS}{dt}\right|_{j+1} = (S_{j+1} - S_j)/k \qquad \text{(A-17)}$$

where $y_{N,j}$ is given from Eq. (A-15).

Eq.(2 -45) is given as follows;

$$\theta_{j+1} = \theta_j + k\{h_g(\theta_a - \theta_j) + r_A \overset{\circ}{\rho}_A s_0 \left.\frac{dS}{dt}\right|_j\}/(A_1 + A_2 S_j) \qquad \text{(A-18)}$$

where

$$A_1 = W_s c_s + c_p s_0(\rho_0 - \rho_{A0}) + c_A s_0(\rho_{A0} - \overset{\circ}{\rho}_A) \qquad \text{(A-19)}$$

$$A_2 = c_A s_0 \overset{\circ}{\rho}_A \qquad \text{(A-20)}$$

Calculation Procedures

The principle of numerical calculation is as follows.

(1) Substituting θ_j, S_j and $dS/dt|_j$ into Eq. (A-18) gives θ_{j+1}.

(2) Substituting $p^{(n)}(y_{N,j})$ which is the n-th approximate value of $p(y_{N,j})$ into Eq. (A-16) gives $S_{j+1}^{(n+1)}$, which gives $dS/dt|_{j+1}$ from Eq. (A-17)

(3) $y_{0,j+1}^{(n+1)}$ is given by substitution of $S_{j+1}^{(n+1)}$ into Eq. (A-8)

(4) By substituting $y_{0,j+1}^{(n+1)}$ into Eq. (A-5), one can obtain the values $y_{i,j+1}^{(n+1)}$ (i = 1, 2, ..., N-1) succesively.

(5) Substituting the values obtained above into Eq. (A-13) gives $Y_{N,j+1}^{(n+1,1)}$, the first approximate value of $Y_{N,j+1}^{(n+1)}$, and which gives $y_{N,j+1}^{(n+1,1)}$ from Eq. (A-15). Further substitution of $y_{N,j+1}^{(n+1,1)}$ into Eq. (A-13) and (A-15) gives $y_{N,j+1}^{(n+1,2)}$. By iteration of these calculations

or by Newton's Method using the derivatives which are estimated by the two-points approximation, finally one can obtain $y_{N,j+1}^{(n+1)}$ which satisfies the following criterion.

$$\left| y_{N,j+1}^{(n+1,m)} - y_{N,j+1}^{(n+1,m+1)} \right| / \left| y_{N,j} - y_{N,j+1}^{(n+1,m+1)} \right| \leq \delta_1 \tag{A-21}$$

$$\delta_1 = 10^{-6} \tag{A-22}$$

(6) $S_{j+1}^{(n+1)}$ and $dS/dt\Big|_{j+1}^{(n+1)}$ can be obtained by substitution of $y_{N,j+1}^{(n+1)}$ into Eqs. (A-18) and (A-16).

(7) Then one interates the calculation procedures from (2) to (6), and finally can obtain the value of $y_{N,j+1}$ which satisfies the following criterion;

$$\left| y_{N,j+1}^{(n)} - y_{N,j+1}^{(n+1)} \right| / \left| y_{N,j} - y_{N,j+1}^{(n+1)} \right| \leq \delta_2 \tag{A-23}$$

$$\delta_2 = 10^{-4} \tag{A-24}$$

These calculations were performed by FACOM 236-60 of the Data Processing Center of Kyoto University, in the double-precision program.

Nomenclature

b = one half of film thickness [cm]

c = heat capacity [cal/g·°C]

j_A = mass flux of A respect to mass center [g/cm^2 sec]

D = mutual diffusion coefficient in PVA-water system [cm^2/sec]

$\bar{D}$ = integral diffusion coefficient [cm^2/sec]

d = interval distance between optical wedge [cm]

h_g = heat transfer coefficient at film surface [cal/cm^2· sec·°C]

K = D/s_0^2 [1/sec]

k_g = mass transfer coefficient at film surface [g/cm^2· sec·mmHg]

L = distance from head of wedge to observed point (cf. Fig. (2-8)) [cm]

M_t = amount of diffusant at time t [g]

M_∞ = amount of diffusant in equilibrium state [g]

n = refractive index of PVA solution [-]

p = partial pressure of water vapor at film surface [mmHg]

p_a = partial pressure of water vapor in hot air [mmHg]

R = 1.987 (gas constant) [cal/g-mole·°K]

r_A = latent heat of vaporization of water [cal/g]

S = dimensionless thickness of film, s/s_0 [-]

s = thickness of film [cm]

T = absolute temperature or time [°K], [sec]

t = time [sec]

V = v/s_0 [1/sec]

v = velocity of mass center [cm/sec]

W = mass of dried-up film [g]

W_s = mass of coating plate [g]

w = averaged water content of film [g-water/g-polymer]

x = dimensionless distance, z/s [-]

y = dimensionless mass fraction of solvent

$(\omega_A - \omega_{Ae})/(\omega_{A0} - \omega_{Ae})$ [-]

$\hat{y}$ = $(\hat{\omega} + \omega_{Ae})/(\omega_{A0} - \omega_{Ae})$ [-]

z = distance [cm]

θ = temperature or wedge angle [°C], [radian]

Ω = dimensionless mass fraction

$(\omega_A - \omega_{A2})/(\omega_{A1} - \omega_{A2})$ [-]

ρ = density [g-solution/cm^3-solution]

ρ_A, ρ_B = concentration of solvent, polymer respectively [g/cm^3-solution]

$\overset{\circ}{\rho}_A$, $\overset{\circ}{\rho}_B$ = density of pure solvent, polymer respectively [g/cm^3]

σ = length of shrinkage of film [cm]

ω = mass fraction [-]

$\hat{\omega}$ = $\overset{\circ}{\rho}_A/(\overset{\circ}{\rho}_B - \overset{\circ}{\rho}_A)$ [-]

<Subscripts>

A = solvent (water)

a = hot air

B = polymer (PVA)

e = equilibrium

p = polymer (PVA)

s = coating plate

w = wet bulb temperature

0 = initial value

Literature Cited

1) Bird, R. B., W. E. Stewart and E. N. Lightfoot: "Transport Phenomena", John Wiley & Sons (1962)

2) Boltzmann, L.: Ann. Physik, 53, 959 (1894)

3) Crank, J.: "The mathematics of Diffusion", Oxford Univ. Press (1956)

4) Crank, J. and G. S. Park: Trans. Faraday Soc., 45, 240 (1949)

5) Crank, J. and G. S. Park: "Diffusion in Polymers", Academic Press, London and New York (1968)

6) Crank, J. and C. Robinson: Proc. Roy. Soc., A204, 549 (1951)

7) Nishijima, Y. and G. Oster: J. Polymer Sci., 19, 337 (1956)

8) Nishijima, Y. and G. Oster: J. Chem. Education, 38, 114 (1961)

9) Otake, T. and Y. Hachihama: Ann. Rept. Inst. Fibers (Osaka Univ.), 6, 126 (1952)

10) Prager, S. and F. A. Long: J. Am. Chem. Soc., 73, 4072 (1951)

11) Robinson, C.: Proc. Roy. Soc., A204, 339 (1950)

12) Sano, Y. and S. Nishikawa: Kagaku Kōgaku (Chem. Eng., Japan), 29, 294 (1965)

13) Wakabayashi, K.: Preprint for the symposium on drying at Toyamashi (Soc. of Chem. Eng., Japan, Nov., 1969) P. 138

CHAPTER 3

PREDICTION OF EFFECTIVE THERMAL CONDUCTIVITIES OF PACKED BEDS

Introduction

The effective thermal conductivity of packed bed or granular material filled with a stagnant fluid which conductivity is smaller than that of the particle at relatively low temperature is an important property in engineering calculation, and so has been studied experimentally and theoretically by numerous investigators. Schumann and Voss[8], Yagi and Kunii[12], Kunii and Smith[4], and Zehner and Schlünder[13] have proposed the predicting formulas by a simple theoretical consideration based on a simplified geometrical model. Deissler and Boegli[2], and Wakao and Kato[11] have obtained numerical solutions by the relaxation method to the Laplace equation for the cubic ($\varepsilon = 0.476$) and the orthorhombic ($\varepsilon = 0.395$) lattice models of spheres. Krupiczka[3] has derived and approximate solution for the cubic lattice and presented the correlating formula for the conductivity as a function of the void fraction. However these studies are those calculated only for the symmetrical axes of regular packings. Thus the purpose of the present

study is to derive a predicting formula of effective thermal conductivities of bed of random packing having an arbitrary fraction of void in the case that only the conductive heat flux is predominant and radiative or convective can be neglected.

1. Modeling for the Heat Transfer Characteristic

1.1 Coordination number and void fraction

The coordination number, that is the number of contact on one sphere made by the surrounding spheres, is of interest in the study of packed beds. Particulary when one evaluates the effective thermal conductivity, it plays a predominant role. Figure (3-1) cited from Ridgway and Tarbuck's paper[7] shows the relationship, between void fraction and coordination number for spheres of uniform size, which contains the calculated values for regular packings and also the observed by several workers[1,5,6,9,10]. The curve on the figure is the best quadratic regression line, obtained by Ridgway and Tarbuck[7], which can be fitted to the points, and has the equation

$$\varepsilon = 1.072 - 0.1193\ N + 0.00431\ N^2 \qquad (3\text{-}1)$$

$$\text{for} \quad \varepsilon \geqq 0.246$$

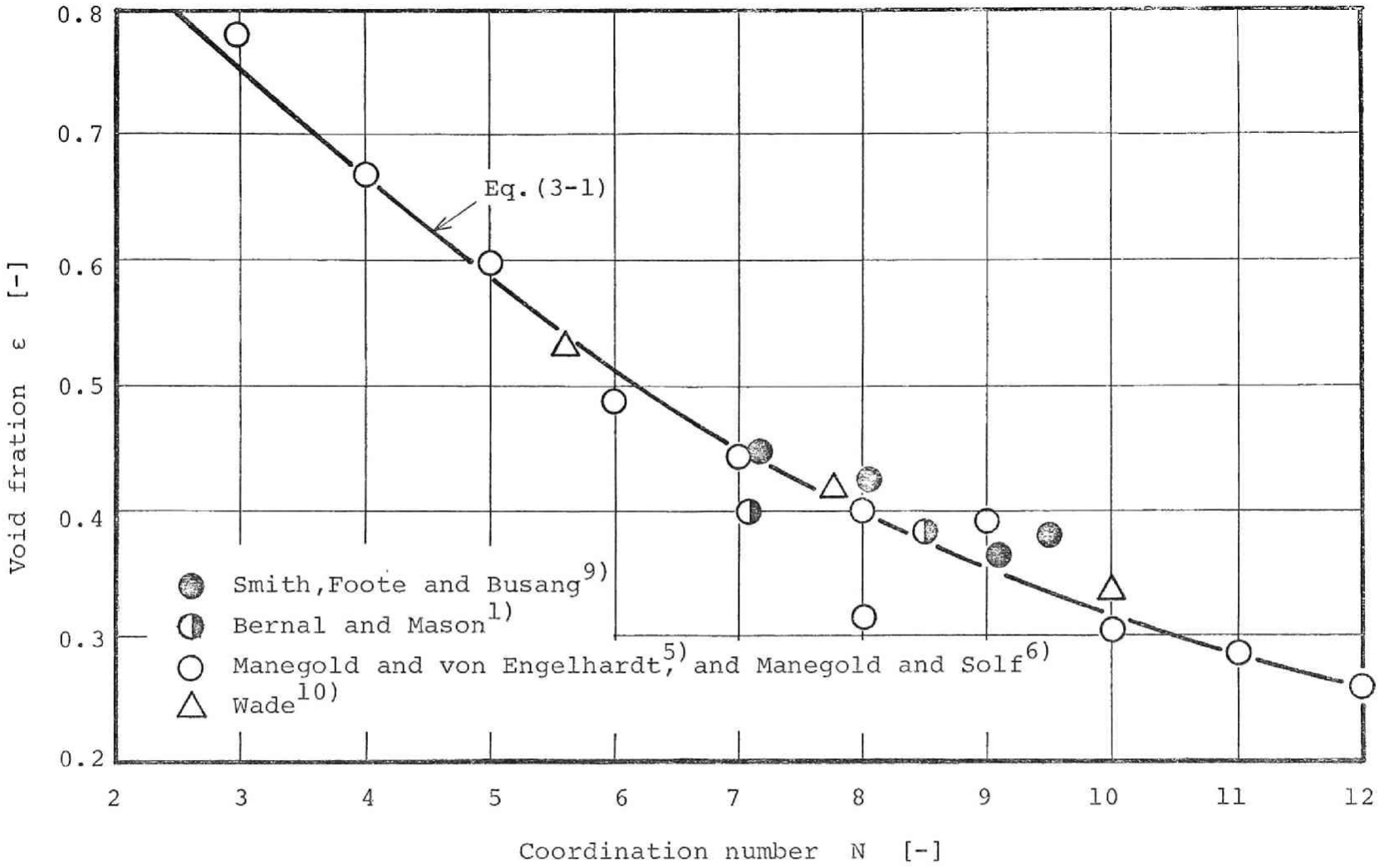

Fig.(3-1) A plot of void fraction against coordination number

From Eq. (3-1), the coordination number N is given explicitly as follows.

$$N = 13.8 - \sqrt{232\,\varepsilon - 57.8} \qquad (3\text{-}2)$$

$$\text{for} \quad \varepsilon \geqq 0.246$$

In the following analysis, Eq. (3-2) is used to give the coordination number for arbitrary void fraction.

1.2 Equivalent number of contact points on hemi-sphere for heat transfer

The contact points, whose number can easily be estimated from Eq. (3-2), randomly locate on the surface of spherical particle. Now let us cut a sphere by the plane, on which there is the center of the sphere and also perpendicular to the macroscopic direction of heat flux. As shown in Fig. (3-2), we denote α as the angle which is made by the line $\overline{OP}$ connecting between the center of sphere "O" and a contact point "P" to that plane.

First of all, we consider that the contact points locating on the surface of hemisphere correspond to how many number of contact point P' locating just on the macroscopic direction of heat transfer at the view point of the contribution for heat transfer.

The following assumptions are postulated for simplifying of calculations.

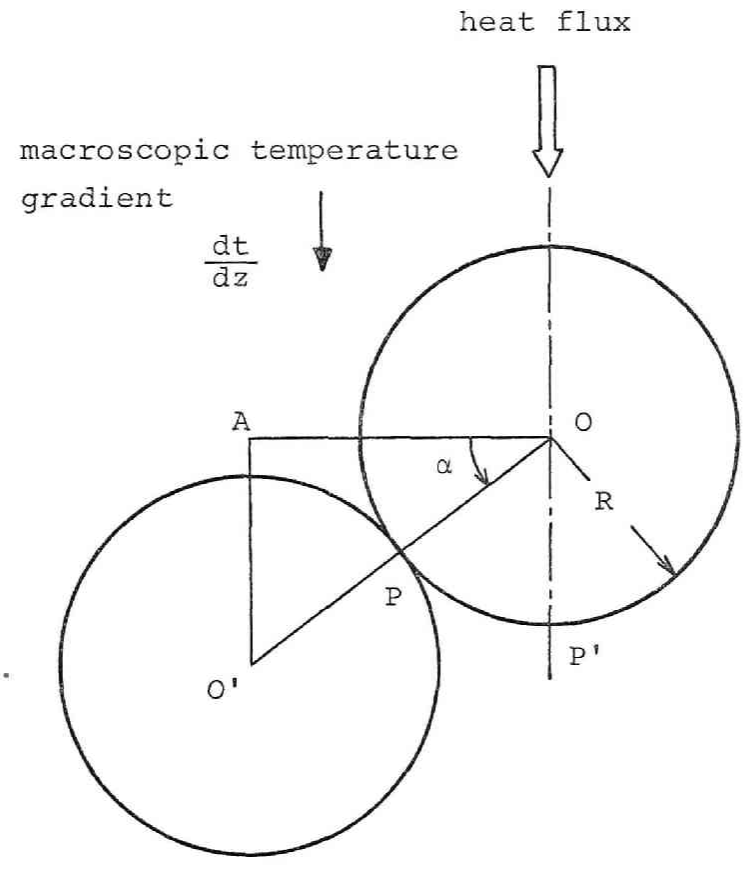

Fig. (3-2) Position of contact point and heat flux

1. The temperature is uniform in the direction perpendicular to the macroscopic direction of heat transfer.
2. Transfer of heat from a shpere to an adjacent sphere through the contact point can be substantially reduced to that from the center of the particle to the one of the adjacent along the line between them.

From these assumptions we can assume that the temperature gradient along the line $\overline{OO'}$ becomes $\sin\alpha \cdot dt/dz$ where dt/dz means the gradient along the macroscopic direction. Further, the displacement from the center O to the center O' is equivalent to the displacement of $2R \cdot \sin\alpha$ along the macroscopic direction. Therefore finally we can assume that the heat flux through a point P having an (inclinating) angle of α corresponds to "$\sin^2\alpha$" times of that at the point P'.

Now further we postulate the two assumptions as follows.

3. The probability of contact point to locate on the surface is uniform everywhere.
4. The contact points have the independent contributions for heat transfer each other.

Then the number of contact points per unit surface area of shpere is given as $N/4\pi R^2$. The surface element corresponds to an angle element $d\alpha$ is $2\pi R^2 \cdot \cos\alpha \cdot d\alpha$. Consequently the effective number of contact points on hemi-sphere based on the contribution of heat transfer is given by Eq. (3-3).

$$n = \int_0^{\frac{\pi}{2}} \sin^2\alpha \ (N/4\pi R^2) \ 2\pi R^2 \cos\alpha \ d\alpha$$

$$= \frac{N}{6} \qquad (3\text{-}3)$$

1.3 Heat flux through a contact point

When the effect of radiation and contact thermal resistance at contact point are negligible, the heat flux near a contact point was given by Kunii and Smith[4] assuming it to be unidirectional, as follows. (cf. Fig. (3-3))

$$q = \int_0^{\theta_0} dq = \pi R k_f \Delta t \left(\frac{\kappa}{\kappa - 1}\right)^2 [\ln\{\kappa - (\kappa - 1)\cos\theta_0\}$$

$$- \left(\frac{\kappa - 1}{\kappa}\right)(1 - \cos\theta_0)] \qquad (3\text{-}4)$$

where the area possessed exclusively by one contact point and across which heat flows is assumed to be 1/n of the cross-sectional area of sphere, and therefore, in Fig. (3-3), the angle θ_0 which is the upper bound of integration for heat heat flux is given as Eq. (3-5).

$$\begin{aligned} \theta_0 &= \mathrm{Sin}^{-1}(\sqrt{1/n}) \ : \ n \geqq 1 \\ &= \pi/2 \qquad\qquad : \ n < 1 \end{aligned} \qquad (3\text{-}5)$$

As the heat flux per a sphere is nq, so the effective thermal conductivity of solid part, k_{es}, is

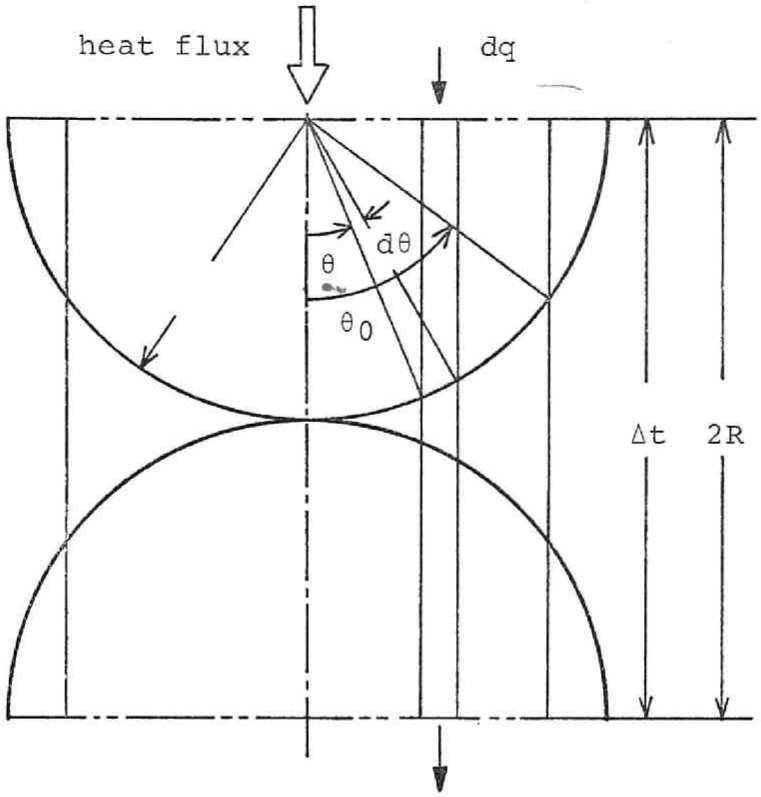

Fig. (3-3) Heat transfer model near a contact point

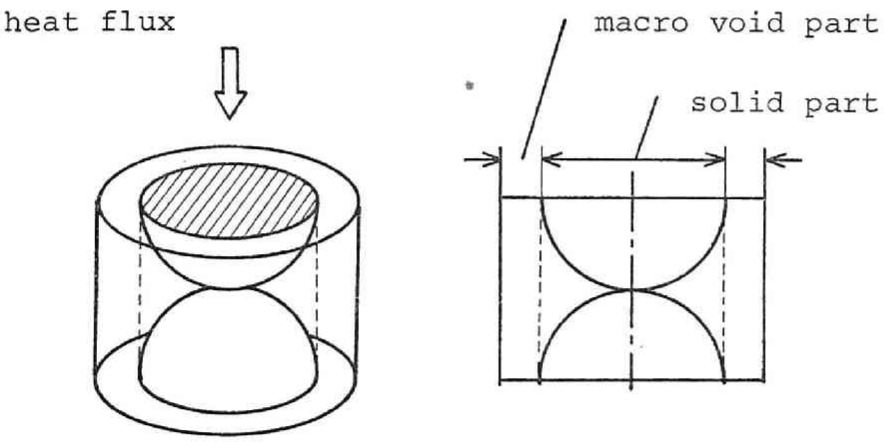

Fig. (3-4) Unit cell of packed bed

$$k_{es} = \frac{nq}{\pi R^2}\frac{\Delta L}{\Delta t} = \frac{2RnK\ \pi Rk_f\Delta t}{\pi R^2\Delta t} = 2nk_fK \tag{3-6}$$

where

$$K = \left(\frac{\kappa}{\kappa - 1}\right)^2\left[\ln\{\kappa - (\kappa - 1)\cos\theta_0\} - \left(\frac{\kappa - 1}{\kappa}\right)(1 - \cos\theta_0)\right] \tag{3-7}$$

1.4 Unit cell of packed bed

In the calculation of effective number of contact points, the position P' in Fig. (3-2) was chosen as the standard position, so the cylinder, which consists of the solid part and the macro void part as shown in Fig. (3-4), can be assumed as the unit cell.

$$\begin{aligned}&\text{Volume of the solid part} = 2\pi R^3\\ &\text{Volume of the spheres in the solid part} = \frac{4}{3}\pi R^3\end{aligned} \tag{3-8}$$

The void fraction of the solid part in the cell is 1/3. Therefore the equivalent areas of the solid part and the macro void part across which heat flows are given as follows respectively.

$$\begin{aligned}&\text{at}\quad \varepsilon \geq 1/3 \quad : \quad [\text{SOLID}] = 3(1 - \varepsilon)/2\\ &\qquad\qquad\qquad\quad\ \ [\text{VOID}] = (3\varepsilon - 1)/2\\ &\text{at}\quad \varepsilon < 1/3 \quad : \quad [\text{SOLID}] = 1\\ &\qquad\qquad\qquad\quad\ \ [\text{VOID}] = 0\end{aligned} \tag{3-9}$$

1.5 Predicting formula of effective thermal conductivity

The apparent heat flux through the bed is the sum of the flux through the solid part and the one through the macro void part. Then the effective thermal conductivity k_e is given as

$$k_e/k_f = [VOID] + 2nK[SOLID]$$
$$= [VOID] + (NK/3)[SOLID] \quad (3\text{-}10)$$

Equation (3-10) is the predicting formula for the bed of spherical particles. Now let us consider the case for the bed of non-spherical particles. The experimental data of the coordination number of non-spherical particles can not be found anywhere, then as the first approximation the coordination number N of non spherical is assumed to be given as

$$N = N'F \quad (3\text{-}11)$$

where N' is the number calculated by Eq. (3-2) supposing it to be spherical and F is a correction factor which must be determined to minimize the deviations between the observed and the predicted conductivities.

In order to satisfy the restriction that Eq. (3-10) always should give $k_e/k_f = 1$ at $k_s/k_f = 1$ regardless the void fraction of bed, the condition of $n \geq 1$, or $N \geq 6$, is required taking into account of the behaviors of Eq. (3-8)

and (3-10). As the void fraction which gives n = 1 is 0.51 for spherical particles (or 0.55 for non-spherical because F = 1.1 of Eq. (3-11) gives the best fit as described below in detail), Eq. (3-10) can be rewritten as follows;

		Spherical	Non-spherical
$k_e/k_f = \frac{NK}{3}$	:	$\varepsilon \leqq \frac{1}{3}$	$\varepsilon \leqq \frac{1}{3}$
$= \frac{3\varepsilon - 1}{2} + \frac{NK(1 - \varepsilon)}{2}$	:	$\frac{1}{3} < \varepsilon < 0.51$	$\frac{1}{3} < \varepsilon < 0.55$
$= \frac{3\varepsilon - 1}{2} + 3K(1 - \varepsilon)$	:	$\varepsilon \geqq 0.51$	$\varepsilon \geqq 0.55$

(3-12)

2. Discussion and Consideration

The representative formula to predict the effective thermal conductivity which have been proposed are as follows;

Schumann & Voss[8)]

$$\frac{k_e}{k_f} = \varepsilon^3 + \frac{(1 - \varepsilon^3)\kappa}{1 - p(\kappa - 1)}\{1 - \frac{p(1 + p)(\kappa - 1)}{1 - p(\kappa - 1)}\ln(\frac{1 + p}{\kappa p})\}$$

$$\text{where} \quad \varepsilon = p(1 + p)\ln(\frac{1 + p}{p}) - p \qquad (3\text{-}13)$$

Kunii & Smith[4)]

$$\frac{k_e}{k_f} = \varepsilon + \frac{1 - \varepsilon}{\phi + 2/(3\kappa)}$$

where $\phi = \frac{\sin^2\theta_0}{2nK} - \frac{2}{3\kappa}$

$\sin^2\theta_0 = 1/n$

loose packing $\varepsilon = 0.476$ ..... $n = 1.5$

closed packing $\varepsilon = 0.260$ ..... $n = 4\sqrt{3}$

(3-14)

Krupiczka[3)]

$$\frac{k_e}{k_f} = \kappa^A - 0.0248 \cdot \ln\kappa$$

where $A = 0.280 - 0.329 \cdot \ln\varepsilon$

(3-15)

Zehner & Schlünder[13)]

$$\frac{k_e}{k_f} = 1 - \sqrt{1 - \varepsilon} + \sqrt{1 - \varepsilon}\,\frac{2\kappa^2}{B + \kappa}\left\{\frac{B(\kappa - 1)}{(\kappa - B)^2}\ln\kappa - \frac{B + 1}{2\kappa} - \frac{B - 1}{\kappa - B}\right\}$$

where $B = C\left(\frac{1 - \varepsilon}{\varepsilon}\right)^{10/9}$

C = 1.25 : sphere

1.4 : crushed particle

2.5 : raschig ring

(3-16)

The calculated standard deviations between the observed and the predicted by the four formulas above and Eq. (3-12) are listed in Table (3-1), with the 158 observed data collected by Krupiczka having the void fractions above 0.250. The formula of Schumann and Voss has the worst deviation of 35.8%, and Eq. (3-12) postulating F = 1.1 has the best of 23.8%. But the differences among the formulas except for Eq. (3-13) are relatively small.

However when the accuracy of predicting formula is examined, we must take into account of that all of the observed conductivity, the void fraction and conductivity of solid which is measured or estimated have inherently considerable errors respectively. If the standard deviation of observed conductivity caused by these inherent errors is considerably large, the differences in accuracy of prediction do not appear distinctly in the differences of the standard deviations between the observed and the predicted conductivities by the different formulas. Consequently even the small differences might be a basis to persist the superiority of the predicting formula.

When the correction factor F is equal to 1.1, the deviation becomes minimum. Figure (3-5) shows the comparison of examples between the observed and the predicted conductivities (calculated) by the five formulas. As seen in the figure, the formula of Schumann & Voss makes considerably under-estimation, but the others predict relatively well. The comparison of the predicted conductivities by the formulas at the void fraction of 0.395 which is the one of

Table (3-1) Comparison of standard deviations of prediction errors

Schumann & Voss[8]		35.8 %
Kunii & Smith[4]		24.6 %
Krupiczka[3]		24.3 %
Zehner & Schlunder[13]		24.4 %
present work	F = 1.0	24.1 %
	F = 1.1	23.7 %

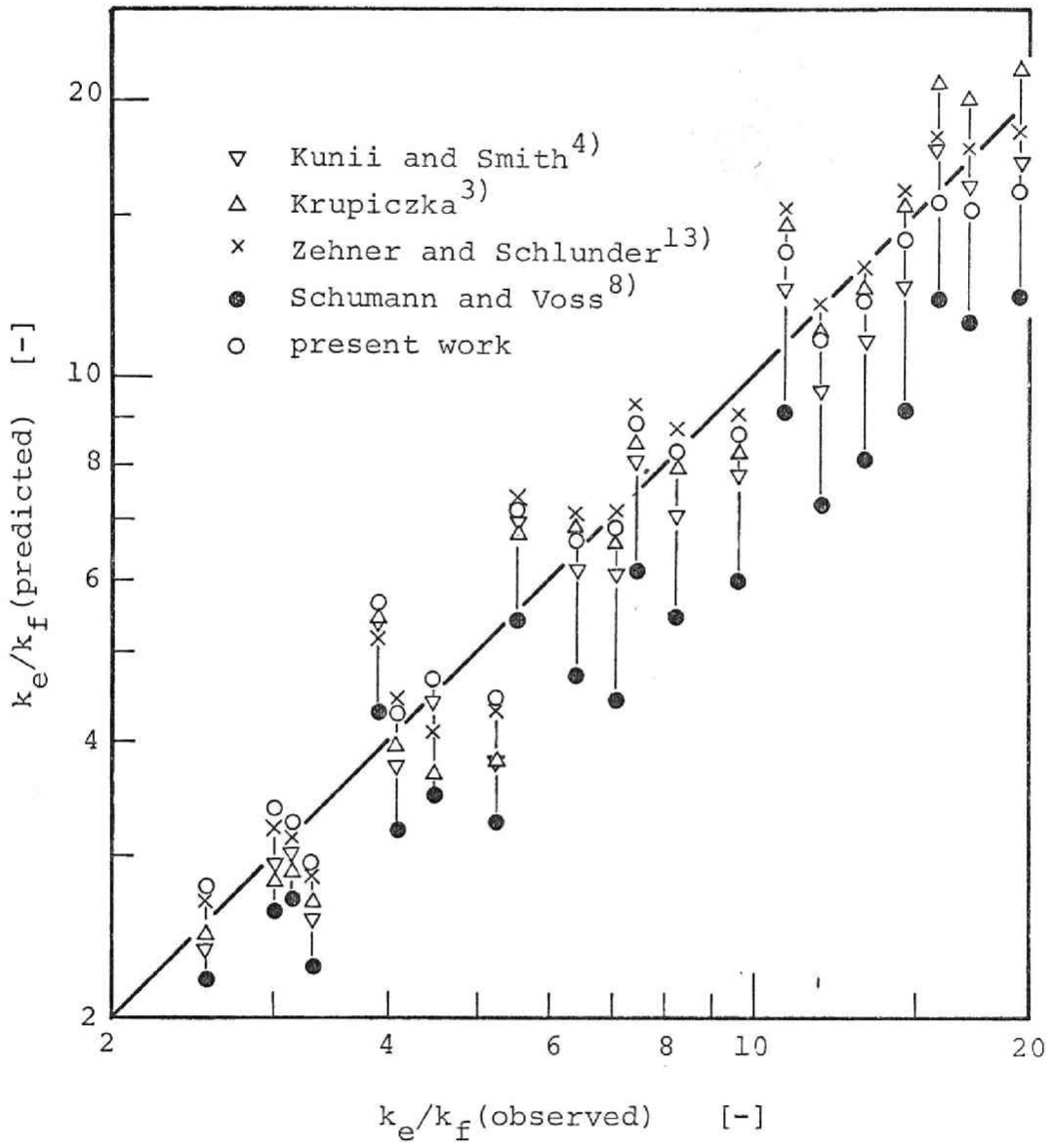

Fig. (3-5) Comparison of predicted and observed data

orthorhombic packing is shown in Fig. (3-6), and the conductivities predicted by Eq. (3-12) at various void fraction and various κ are shown in Fig. (3-7).

Conclusion

1. A predicting fromula, Eq. (3-12), for the effective thermal conductivities of beds, based on the effective number of contact points around a particle for random packing, was proposed.
2. By comparing Eq. (3-12) to the other formulas proposed by several workers, it was shown that the present formula gives the best fit to the observed conductivities collected by Krupiczka.
3. It was given graphically the effective thermal conductivities of beds for various ratios of solid and fluid conductivities and void fractions.

Nomenclature

F = correction factor for coordination number of non-spherical particles in Eq. (3-11) [-]

K = given by Eq. (3-7) [-]

k_e = effective thermal conductivity of bed [kcal/m·hr·°C]

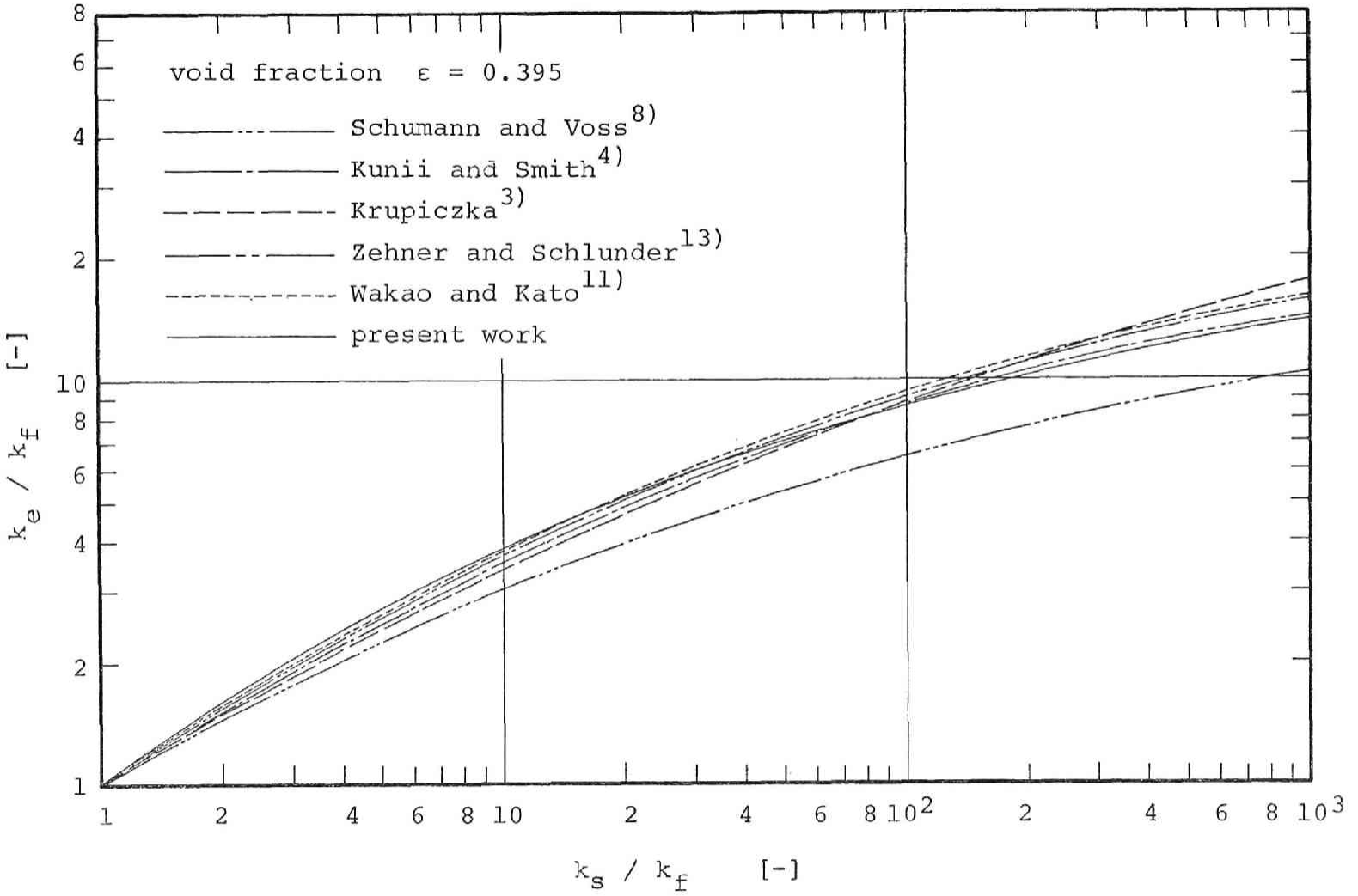

Fig. (3-6) Comparison of various predicting formulas

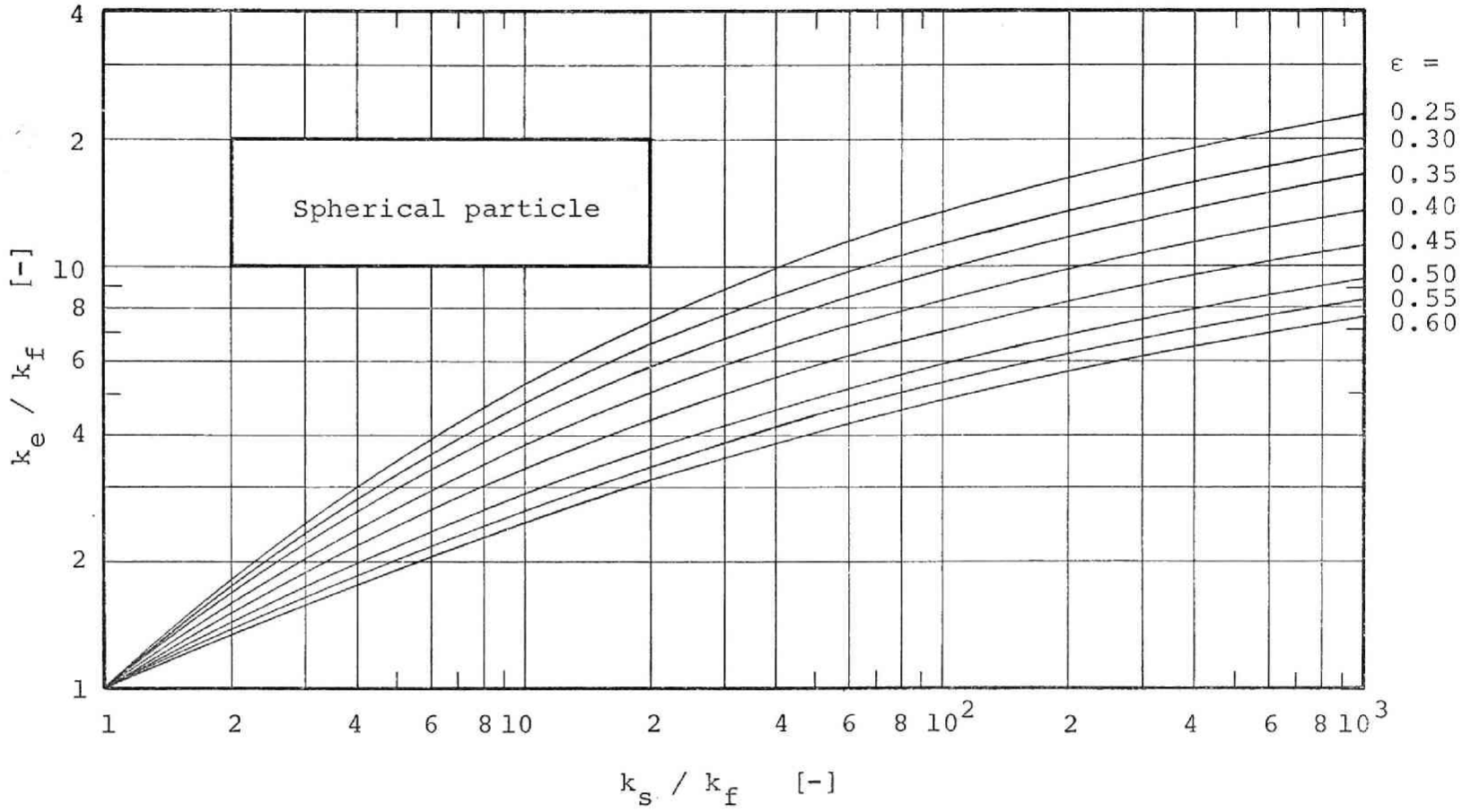

Fig. (3-7)-1 Predicted effective thermal conductivity of packed bed of spherical particles

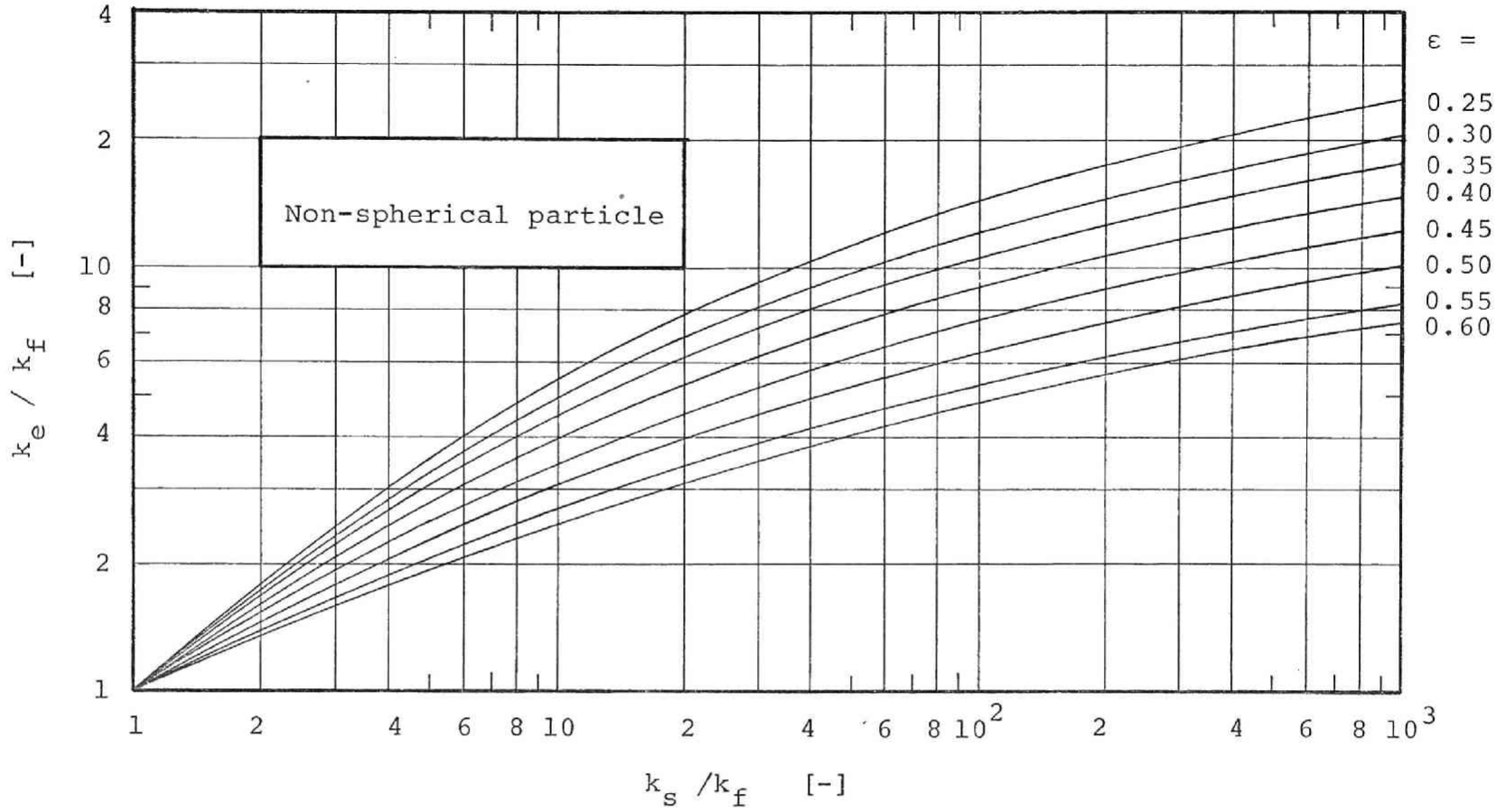

Fig. (3-7)-2 Predicted effective thermal conductivity of packed bed of non-spherical particles

k_{es} = apparent thermal conductivity of solid part [kcal/m·hr·°C]

k_f = thermal conductivity of fluid [kcal/m·hr·°C]

k_s = thermal conductivity of solid [kcal/m·hr·°C]

L = length [m]

N = coordination number of packed bed [-]

N' = coordination number of non-spherical particle calculated by Eq. (3-2) supposing it ' ' spherical [-]

n = effective number of contact points on hemi-sphere [-]

q = heat flux near a contact point [kcal/m^2 hr]

R = radius of sphere [m]

t = temperature [°C]

Z = length [m]

α = inclination angle of contact point [radian]

ε = void fraction of bed [-]

κ = k_s/k_f [-]

θ = angle [radian]

θ_0 = upper bound of angle θ, given by Eq. (3-5) [radian]

Literature Cited

1) Bernal, J. D. and Mason J.: Nature, 188, 910 (1960)

2) Deissler, R. G. and J. S. Boegli: Trans. Amer. Soc. Mech. Eng., 80, 1417 (1958)

3) Krupiczka, R.: Int. Chem. Eng., 7, 122 (1967)

4) Kunii, D. and J. M. Smith: A. I. Ch. E. Journal, 6, 71 (1960)

5) Manegold, E. and von Engelhardt, W.: Kolloid Z., 62, 285 (1933)

6) Manegold, E., R. Hofmann and K. Solf: Kolloid Z., 56, 142 (1931)

7) Ridgway, K. and K. J. Tarbuck: Brit. Chem. Eng., 12, 384 (1967)

8) Schumann, T. E. W. and V. Voss: Fuel, 13, 249 (1934)

9) Smith, W. O., P. D. Foote and P. F. Busang: Phys. Rev., 34 (2nd series), 1271 (1929)

10) Wade, W. H.: J. Chem. Phys., 69, 322 (1965)

11) Wakao, N. and K. Kato: J. Chem. Eng. Japan, 2, 25, (1969)

12) Yagi, S. and D. Kunii: A. I. Ch. E. Journal, 3, 373 (1957)

13) Zehner, P. and E. U. Schlünder: Chem. Ing. Tech., 42, 933 (1970)

CHAPTER 4

EFFECTIVE THERMAL CONDUCTIVITIES OF WET GRANULAR MATERIALS

Introduction

The prediction of thermal conductivities of wet materials such as sand, soil, solid catalyst and brick etc. is very important for engineering calculations.

A number of studies[6,7,10,17] has been successfully conducted to develope techniques for predicting thermal conductivities of porous materials in dried-up and saturated state with water, both being two-phase dispersed system. On the other hand, there are many studies[2,3,5,8,9,12~16] also on the thermal conductivity of wet material which is a system consisting of three phases, however the prediction methods seem to have some defects and to be unaccomplished. Krischer and Esdorn[5] has proposed a typical formula for prediction which is founded on the assumption that heat is transfered through a system of partially parallel and partially series resistances. The different modes of heat transfer considered in their model are

(1) Conduction of heat through solid, water and air.

(2) Enthalpy transfer by an evaporation - diffusion -

- condensation process of water.

Even though their model has been applied to correlate experimental results in many works[2,8,9,16] after them, it is somewhat incovenient for practical use because it has the two parameters to be determined experimentally.

The purpose of the present study is therefore to establish a new method to predict the effective conductivity of wet beds of granular material without any experimental parameters except the void fraction, water content and thermal properties of each phases. The extension of the prediction formula for the two-phase system proposed in previous chapter has been carried out succesively for this purpose, providing the particles of bed were spherical and uniform in size.

1. Derivation of Prediction Formula

1.1 Water configurations retained in beds of granular materials

Although configuration of retained water in bed must be considered as an stochastic phenomena, the quantitative expression of it seems almost impossible. Then in order to simplify the analysis, the rather bold assumptions described below have been postulated.

An angle θ made at the center of particle by wedge

water held around a contact point of two spherical particles, as shown in Fig. (4-1), has been defined as a measure showing the amount of a wedge water. If all of the wedge water in a bed uniformly increase, the pairs of wedge waters adjoining each other become to coalesce just at a certain angle θ_c which is dependent only on the packing mode regardless the diameter of particle and the surface tension of water provided that the particles are fine. After θ reaches θ_c, the void space near contact point may be considered to be suddenly filled up with water as the water content increases. On the other hand, when a higher suction pressure than the entry suction pressure, which is defined as the minimum pressure to remove the water out from the saturated bed with water, is applied, the water is suddenly removed out just to the extent that the angle θ of wedge waters is equal to θ_c. Based on these considerations, the state of retained water can be expressed as follows;

(1) Increasing process of water content : As the macroscopic water content of bed Φ increases gradually from zero, the wedge waters increase uniformly up to θ_c at which Φ is Φ_c, and thereafter they do not increase anymore, but voids saturated with water begin to appear and increase in number up to whole voids to be saturated.

(2) Decreasing process of water content : As Φ decreases from saturated state, saturated voids disappear one after another leaving the wedge water whose θ is equal to θ_c. After all of the saturated voids disappear completely the wedge waters begin to decrease in volume uniformly.

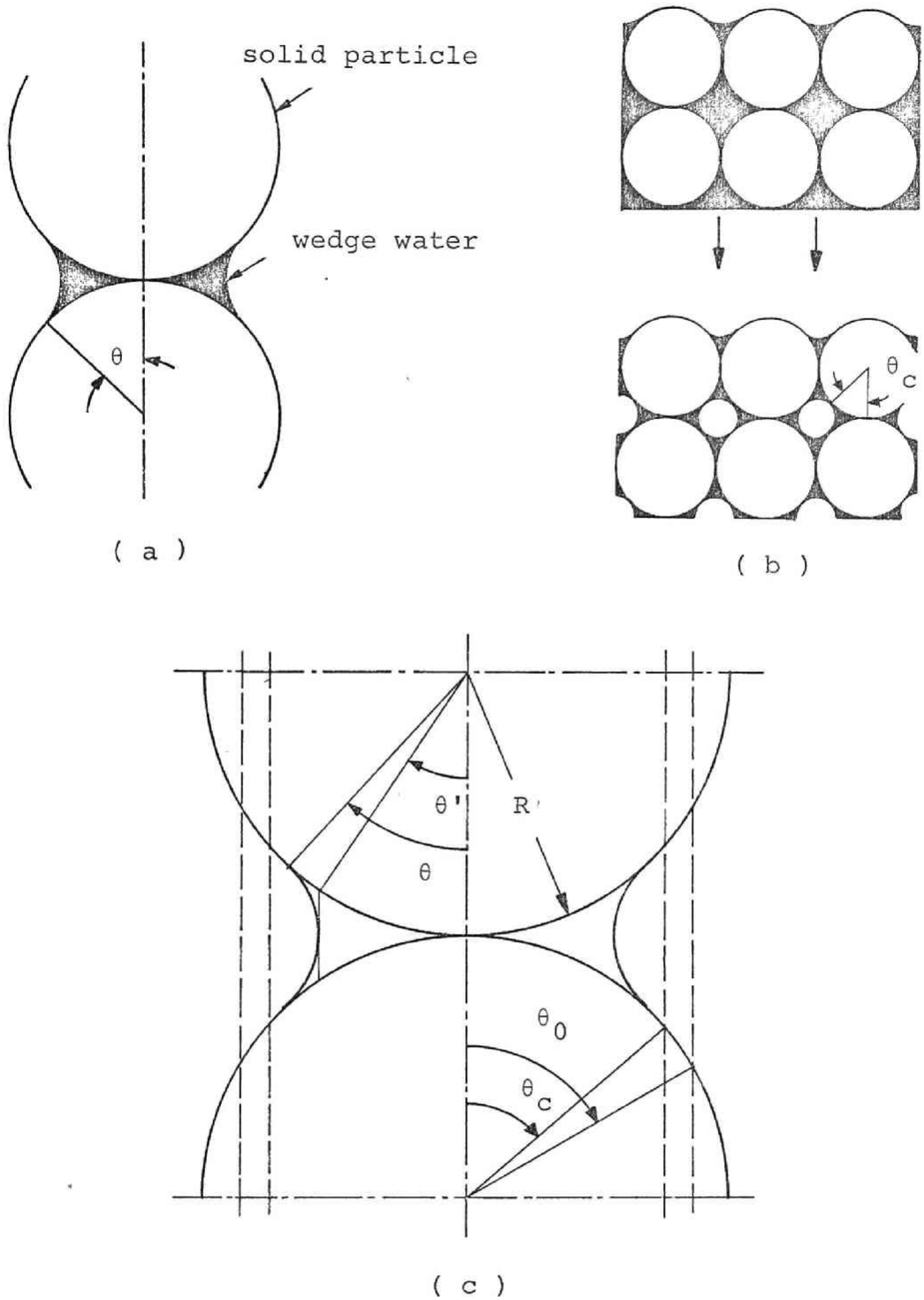

Fig. (4-1) Wedge water held around a contact point

With these assumptions, we can specify the configurations of water in beds through the whole range of water content.

1.2 Relationship between angle θ and water content Φ

When the periphery of the cross section of wedge water is assumed to be circular, the relative volume of wedge water to one of a particle is given as follows (cf. Fig. (4-2))

$$V = (3/2)[(1 - \cos\theta)\{\tan^2\theta + (\sec\theta - 1)^2 - (1 - \cos\theta)^2/3\} - \tan\theta(\sec\theta - 1)^2 \cdot (\sin\theta\cdot\cos\theta + \pi/2 - \theta) - (1 - \cos\theta)^2(2 + \cos\theta)/3] \quad (4\text{-}1)$$

Therefore if the number of contact point per a particle is N, the degree of relative saturation of void with water ψ is

$$\psi = NV(1 - \varepsilon)/(2\varepsilon) \quad (4\text{-}2)$$

where N can be calculated by Eq. (4-3) proposed for spherical particles by Ridgway and Tarbuck[10,11] (cf. Fig. (4-3));

$$N_{spherical} = 13.84 - \sqrt{232\varepsilon - 57.8} \quad (\varepsilon \geqq 0.246) \quad (4\text{-}3)$$

In the case of non-spherical particles[10] (cf. Fig. (4-3)),

$$N_{non\text{-}spherical} = 1.1 \cdot N_{spherical} \quad (4\text{-}4)$$

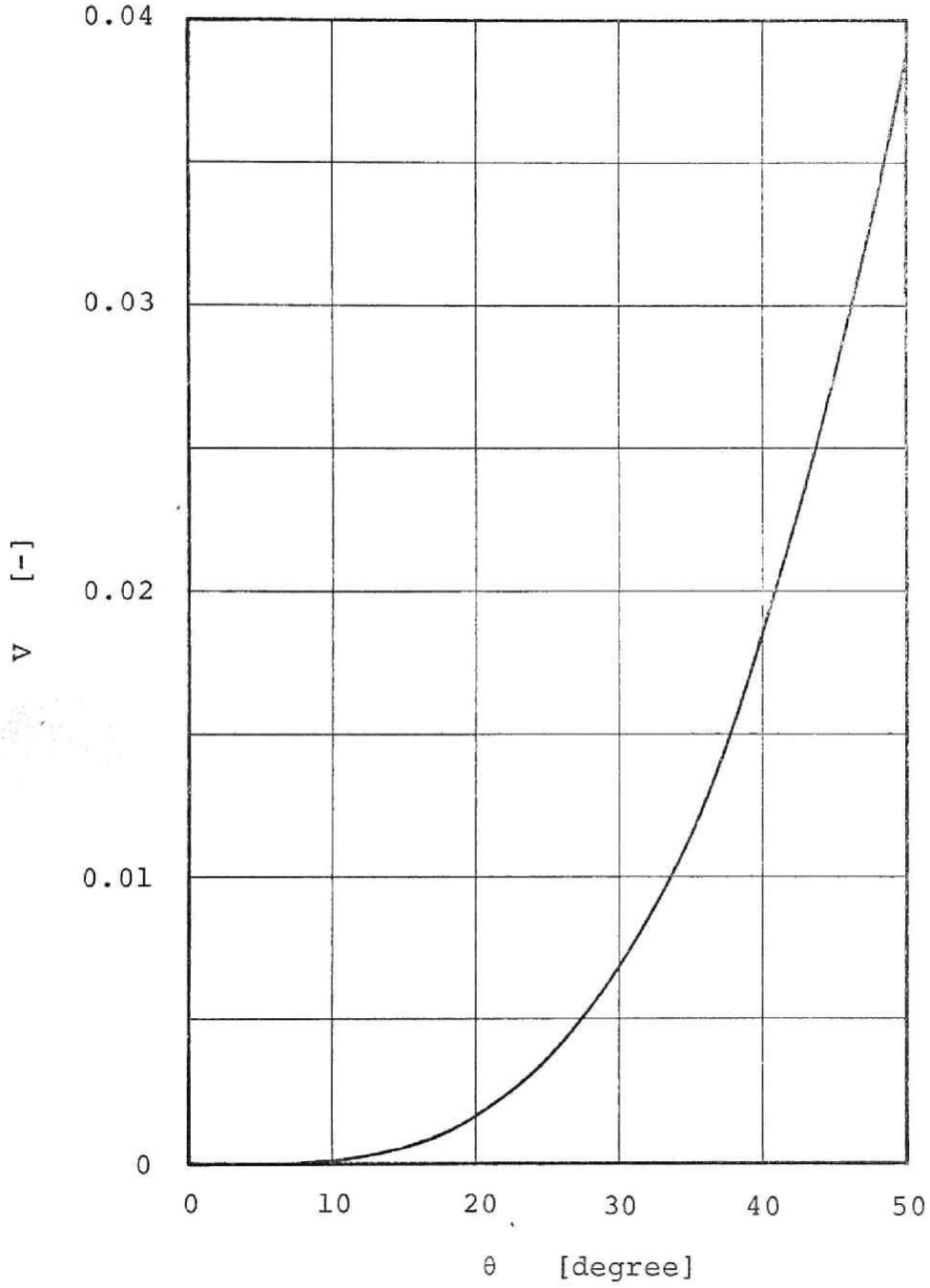

Fig. (4-2) V vs. θ

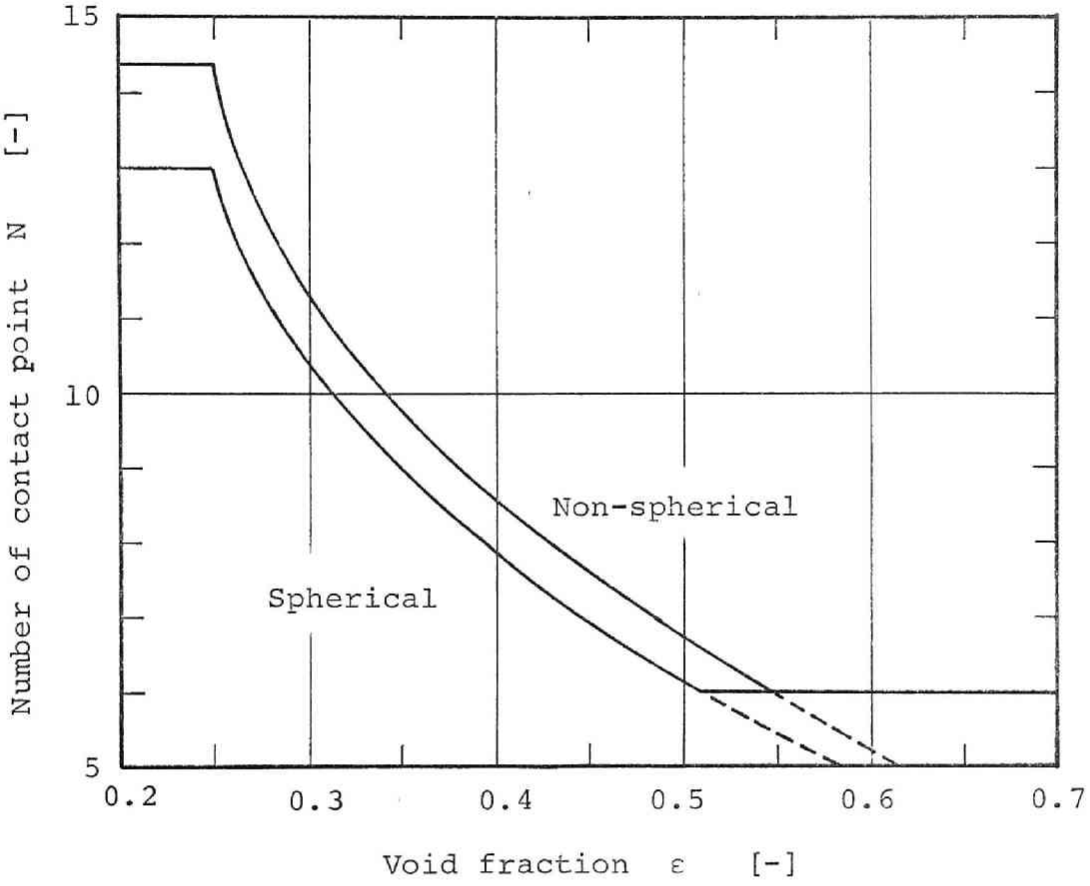

Fig. (4-3) Number of contact point vs. void fraction

As the next problem, let us consider the coalescing angle θ_c. The angle θ' defined in Fig. (4-1) can be represented as the function of θ (cf. Fig. (4-4)).

$$\theta' = \mathrm{Sin}^{-1}(\tan\theta + 1 - \sec\theta) \tag{4-5}$$

Because the rigorous expression of θ_c which is a function of N seems to be impossible, the following assumption was made for simplicity. The cross-sectional area possessed exclusively by one critical wedge water, when it is evaluated at the throat of wedge water as $\pi R^2 \sin^2\theta_c'$, is postulated to be one - "N/2"th of one of a sphere πR^2. Therefore (cf. Fig. (4-5)),

$$\theta_c' = \mathrm{Sin}^{-1}\sqrt{2/N} \tag{4-6}$$

While the theoretical θ_c is 45° for the cubic and 30° for the orthrhombic packing, the calculated from Eqs. (4-6) and (4-5) are 44.5° and 29.3° respectively. Consequently because the critical water content Φ_c is equal to ψ_c obtained from Eqs. (4-6), (4-2) and (4-1), the relationship between the water content of bed Φ and the configuration of wedge waters is expressed as follows;

(i) $0 < \Phi < \Phi_c \ (= \psi_c)$:

$$\psi = \Phi \tag{4-7}$$

θ and θ' can be obtained from ψ by Eqs. (4-1), (4-2) and (4-5).

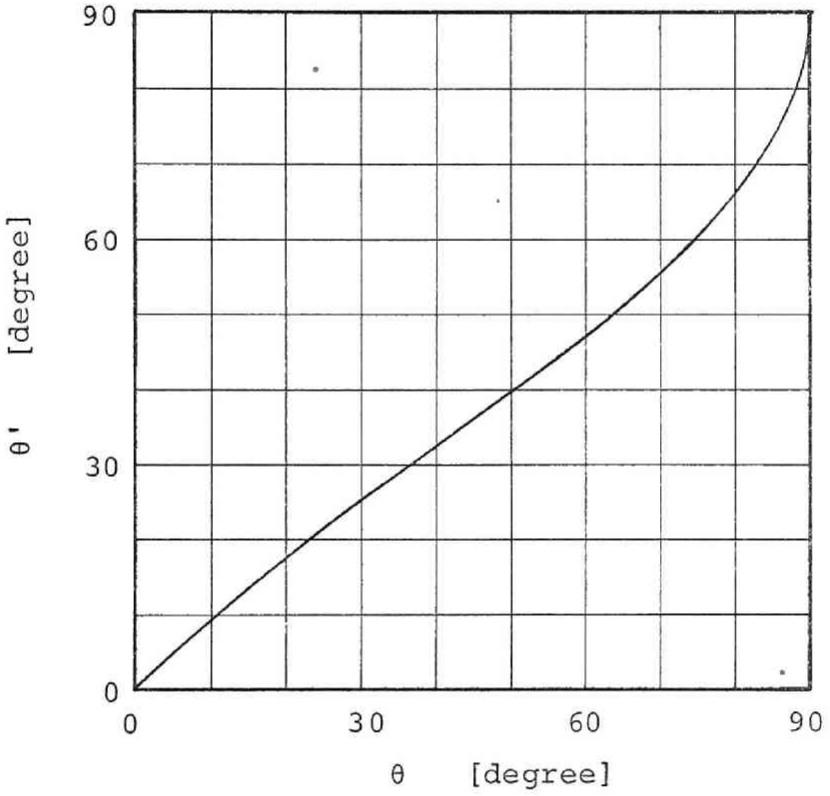

Fig. (4-4) θ' vs. θ

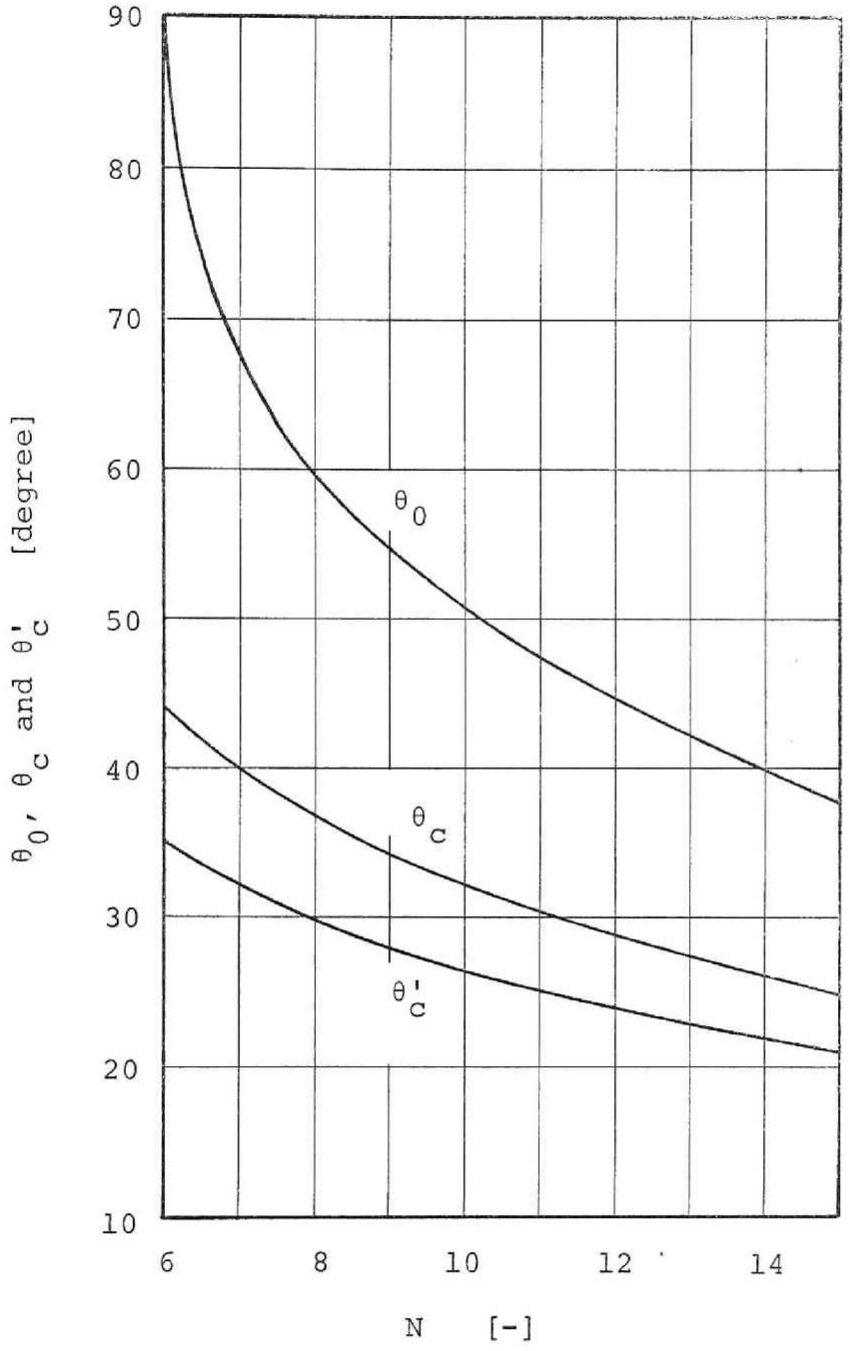

Fig. (4-5) θ_0, θ_c and θ'_c vs. N

(ii) $\Phi_c < \Phi < 1.0$:

$$\Phi = a\psi_c + (1 - a) \tag{4-8}$$

where

$$a = \frac{\text{number of wedge waters in critical state.}}{\text{number of contact point in saturated state.}}$$

From Eq. (4-8);

$$a = (1 - \Phi)/(1 - \psi_c) \tag{4-9}$$

1.3 Modeling of heat transfer near a contact point

Let us consider the mechanisms of heat transfer at a moderate low temperature in beds of wet spherical particles, where there are no convection of fluid and radiative transfer. It is necessary for the present case to take into account of not only the conductive heat transfer through solid, liquid and gas, but also the enthalpy transfer accompanied with the water vapor diffusion. The calculating procedures proposed in the previous chapter has been successfully applied to analyse the present mechanisms.

In Fig. (4-1) showing a cross section of two particles in contact with each other it has been assumed that the heat transfer occurs in the vertical direction by the following mechanisms;

(1) Heat transfer through the solid part.

a. Conduction through solid, liquid which is wedge water and solid;

The heat flux q_a by mechanism "a" per a contact point is

$$q_a = \int_0^{\theta'} dq_a = \pi R k_l K_l \Delta t \tag{4-10}$$

where

$$\kappa_l = k_s/k_l$$

$$K_l = \left(\frac{\kappa_l}{\kappa_l - 1}\right)^2 [\ln\{\kappa_l - (\kappa_l - 1)\cos\theta'\} - \frac{\kappa_l - 1}{\kappa_l}(1 - \cos\theta')] \tag{4-11}$$

as described in the previous chapter.

b. Conduction through solid, enthalpy transfer through gas around wedge water and conduction through solid;

$$q_b = \int_{\theta'}^{\theta} dq_b = \pi R(k_g + k_d) K_d \Delta t \tag{4-12}$$

where

$$\kappa_d = k_s/(k_d + k_g)$$

$$K_d = \left(\frac{\kappa_d}{\kappa_d - 1}\right)^2 [\ln\{\frac{\kappa_d - (\kappa_d - 1)\cos\theta}{\kappa_d - (\kappa_d - 1)\cos\theta'}\} - \frac{\kappa_d - 1}{\kappa_d}(\cos\theta' - \cos\theta)] \tag{4-13}$$

$$k_d = \frac{M_v D_v p_T r_l}{R_v T(p_T - p_s)} \frac{dp_s}{dt} \tag{4-14}$$

c. Conduction through solid, gas and solid;

$$q_c = \int_{\theta}^{\theta_0} dq_c = \pi R k_g K_g \Delta t \tag{4-15}$$

where

$$\kappa_g = k_s/k_g$$

$$K_g = \left(\frac{\kappa_g}{\kappa_g - 1}\right)^2 \left[\ln\left\{\frac{\kappa_g - (\kappa_g - 1)\cos\theta_0}{\kappa_g - (\kappa_g - 1)\cos\theta}\right\} - \frac{\kappa_g - 1}{\kappa_g}(\cos\theta - \cos\theta_0)\right] \tag{4-16}$$

The heat transfer area possessed exclusively by one contact point has been assumed to be one - "n"th of the cross section of particle, and n is the effective number of contact point for heat transfer defined as n = N/6 in the previous chapter. Then the angle θ_0 determining the above area is given as follows (cf. Fig. (4-5));

$$\begin{aligned} \theta_0 &= \mathrm{Sin}^{-1}\sqrt{1/n} \quad \text{for} \quad n > 1 \\ &= \pi/2 \qquad\qquad \text{for} \quad n \leq 1 \end{aligned} \tag{4-17}$$

According to the previous chapter, the unit cell of bed is given as the cylinder consisting of the solid and the macro void part as shown in Fig. (3-4), and the equivalent areas of the parts are given by

$$\begin{aligned} & & \varepsilon \geq 1/3 & & \varepsilon < 1/3 \\ [\mathrm{SOLID}] &= 3(1 - \varepsilon)/2 & \text{or} & & 1 \\ [\mathrm{VOID}] &= (3\varepsilon - 1)/2 & \text{or} & & 0 \end{aligned} \tag{4-18}$$

Consequently the contribution of the solid part to the effective conductivity k_e is

$$(k_e)_S = (N/3)\ [SOLID]\ \{k_l K_l + (k_g + k_d)K_d + k_g K_g\} \tag{4-19}$$

where the condition of $N \geq 6$ should be satisfied, regardless the void fraction of bed, according to the previous chapter. The void fraction which gives N = 6 is 0.51 for spherical or 0.55 for non-spherical particle.

(2) Heat transfer through the macro void part

d. Conduction through gas in macro void space;

The contribution of this mechanism to k_e is

$$(k_e)_{VG} = k_g\ [VOID] \tag{4-20}$$

e. Enthalpy transfer through void space;

As ψ_c is about 0.2 at most, the influence of wedge water on the void space is neglected and the contribution of enthalpy transfer is

$$(k_e)_{VE} = \varepsilon^{1.5} k_d \tag{4-21}$$

where as the tortuosity factor for diffusion in bed $1/\sqrt{\varepsilon}$ evaluated by Bruggemann[1] is adopted.

1.4 Prediction formula of effective thermal conductivity

As a result of above considerations, the effective thermal conductivity is given as follows;

$$k_e = (k_e)_{VE} + (k_e)_{VG} + (k_e)_S \tag{4-22}$$

(i) $\Phi \leqq \Phi_c$

	Spherical	Non-spherical
$k_e = \varepsilon^{1.5} k_d + N k_g K/3$	$\varepsilon \leqq 1/3$	$\varepsilon \leqq 1/3$
$k_e = \varepsilon^{1.5} k_d + k_g(3\varepsilon - 1)/2 + N k_g K(1 - \varepsilon)/2$	$1/3 < \varepsilon < 0.51$	$1/3 < \varepsilon < 0.55$
$k_e = \varepsilon^{1.5} k_d + k_g(3\varepsilon - 1)/2 + 3 k_g K(1 - \varepsilon)$	$\varepsilon \geqq 0.51$	$\varepsilon \geqq 0.55$

(4-23)

where

$$K = (k_l/k_g)K_l + (k_g + k_d)K_d/k_g + K_g \tag{4-24}$$

(ii) $\Phi > \Phi_c$

$$k_e = a(k_e)_{crit} + (1 - a)(k_e)_{sat} \tag{4-25}$$

where $(k_e)_{crit}$ and $(k_e)_{sat}$ [10] are the conductivities at $\Phi = \Phi_c$ and $\Phi = 1.0$ (saturated state) respectively, and "a" can be obtained from Eq. (4-9).

2. Measurement of Effective Thermal Conductivity of Bed of Wet Granular Material

The ordinary stationary method and the transient method were applied to measure conductivities for high and low water contents respectively.

The apparatus of stationary method used is shown schematically in Fig. (4-6). Two glass plates (150 mm^{ϕ} x 10 mm^{t}) were used as the standard plates, and on the under plate a thin ring of Bakelite having 10 mm in height was fixed with adhesive and was served as the container of sample bed. A perforated bronze plate (3 mm^{t}) which had about 26% open area and the holes of 2 mm^{ϕ} was laid on the container. Further a sheet of filter paper, which was being fed with water by dipping its corners into water in test tubes set by the side of the container, was laid on the perforated plate to prevent the drying up of the upper part of bed which might bring considerable errors on the measurement. The lower heating plate was served to control the temperature difference across the bed within about 1°C. The assembly shown in Fig. (4-6) was set in the box maintained at the same temperature as the bed. The measuring procedures was in ordinary manner.

The apparatus for the transient method is shown in Fig. (4-7). The electric heating plate was a thin mica plate, wound by 300 $\mu\phi$ Constantan wire, which was sandwiched in between two aluminum plates (50 mm x 50 mm x 0.5 mm^{t}). The termocouples were placed on the upper and lower surface

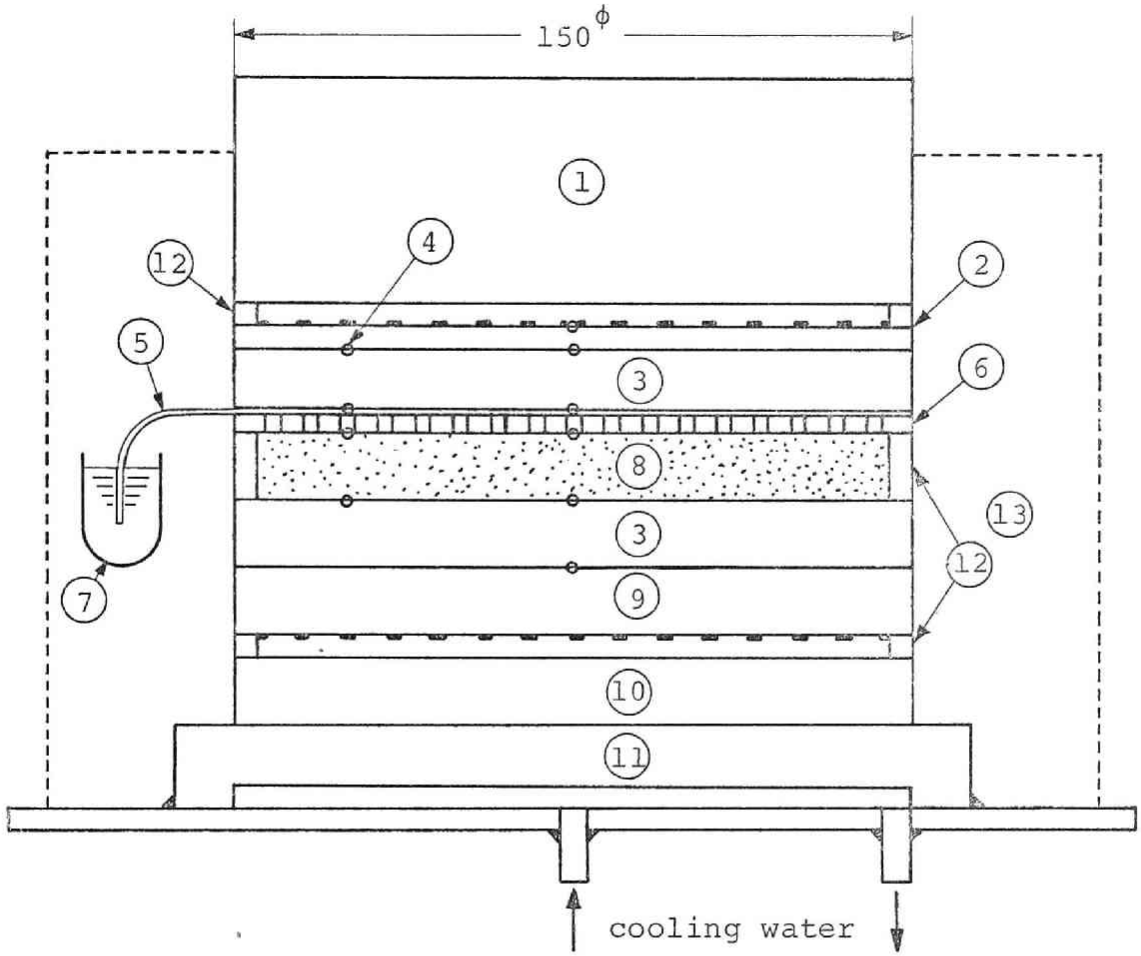

1. weight for pressing down
2. electric heating plate (copper plate 4 mm^{t})
3. standard glass plate (10 mm^{t})
4. copper-constantan thermo-couples (80μ$^{\phi}$)
5. filter paper
6. perforated plate (3 mm^{t}, 2 mm$^{\phi}$ hole)
7. water container
8. sample bed (10 mm^{t})
9. electric heating plate (copper plate 10 mm^{t})
10. bakelite plate (10 mm^{t})
11. cooling plate (170 mm$^{\phi}$ x 12 mm^{t})
12. bakelite rings (150 mm$^{\phi}$)
13. foamed polystyrene

Fig. (4-6) Measuring apparatus for stationary method

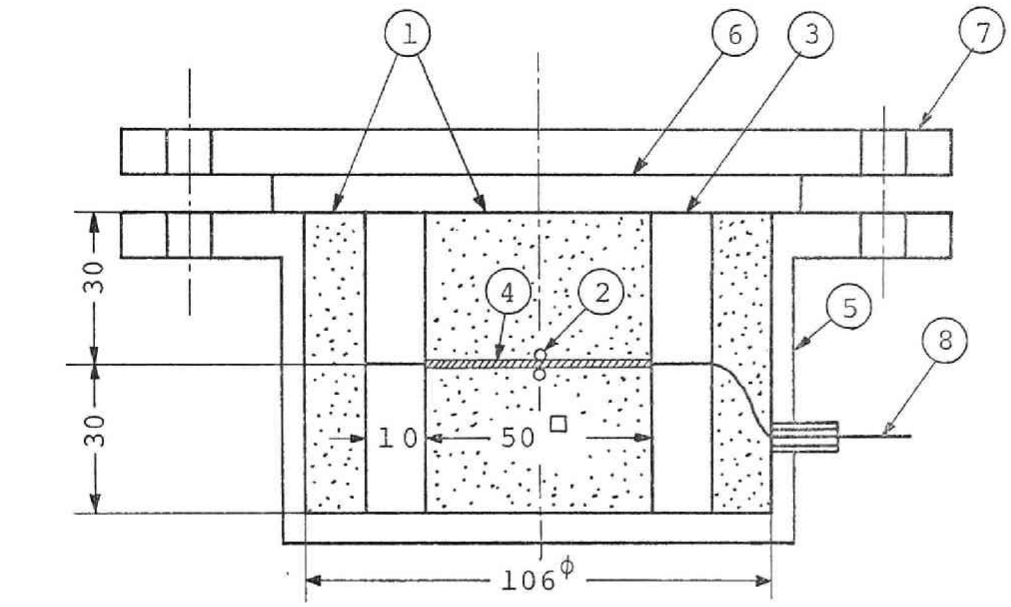

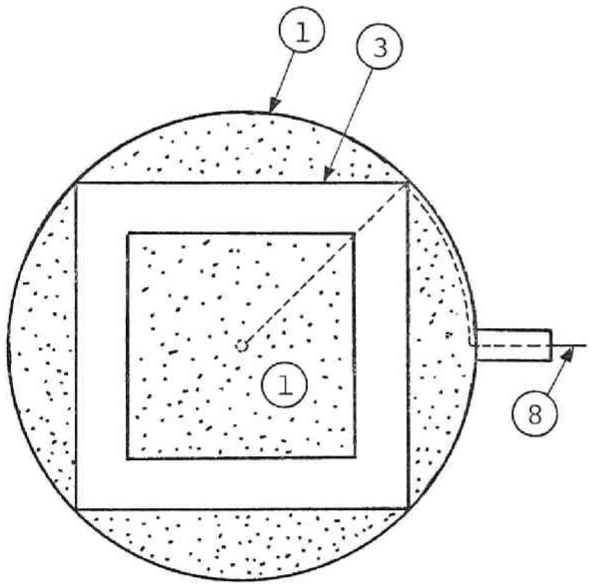

1. sample bed
2. copper-constantan thermo-couples (80μ$^{\phi}$)
3. foamed polystyrene
4. electric heating plate (aluminium plate)
5. container (stainless steel)
6. covering plate (stainless steel)
7. flange (stainless steel)
8. lead wire of thermo-couples

Fig. (4-7) Measuring apparatus for transient method

of it. After the temperature across the sample bed became in uniform, the heater was switched on and the surface temperatures were recorded continuously. The surface temperature t_s is given as follows;

$$t_s = 2q_0 \sqrt{\tau/(k_e \rho C_p \pi)} + t_0 \qquad (4\text{-}26)$$

where t_0 is the initial temperature of bed. Therefore the conductivity k_e were obtained from the gradient of $\Delta t_s = t_s - t_0$ to $\tau^{1/2}$.

As the samples, glass bead (80 ∿ 100#) and sand (100 ∿ 150#) were used. The true thermal conductivity of the sand used was extrapolately decided by the method proposed by Koya and Kunii[4] from the data on the saturated states with ethanol and water, and as the one of glass bead the observed values on the plate made of the same glass were adopted. The void fraction of sample bed was determined from its volume, dried weight and the true density of material.

3. Comparison between Observed and Predicted Conductivity

Figures (4-8) and (4-9) show the comparisons of the observed conductivities by several workers with the predicted at low temperatures where the effect of enthalpy transfer caused by vapor diffusion may be neglected. The predicted results seem to be in good agreement with the

Key	System	ε	Data No.
○ ———	crushed marble - water[15]	0.492	1
◐ ——·——	crushed slate - water[15]	0.528	2
◑ ——··——	crushed glass - water[15]	0.544	3
● -------	sand - water[12]	0.42	4

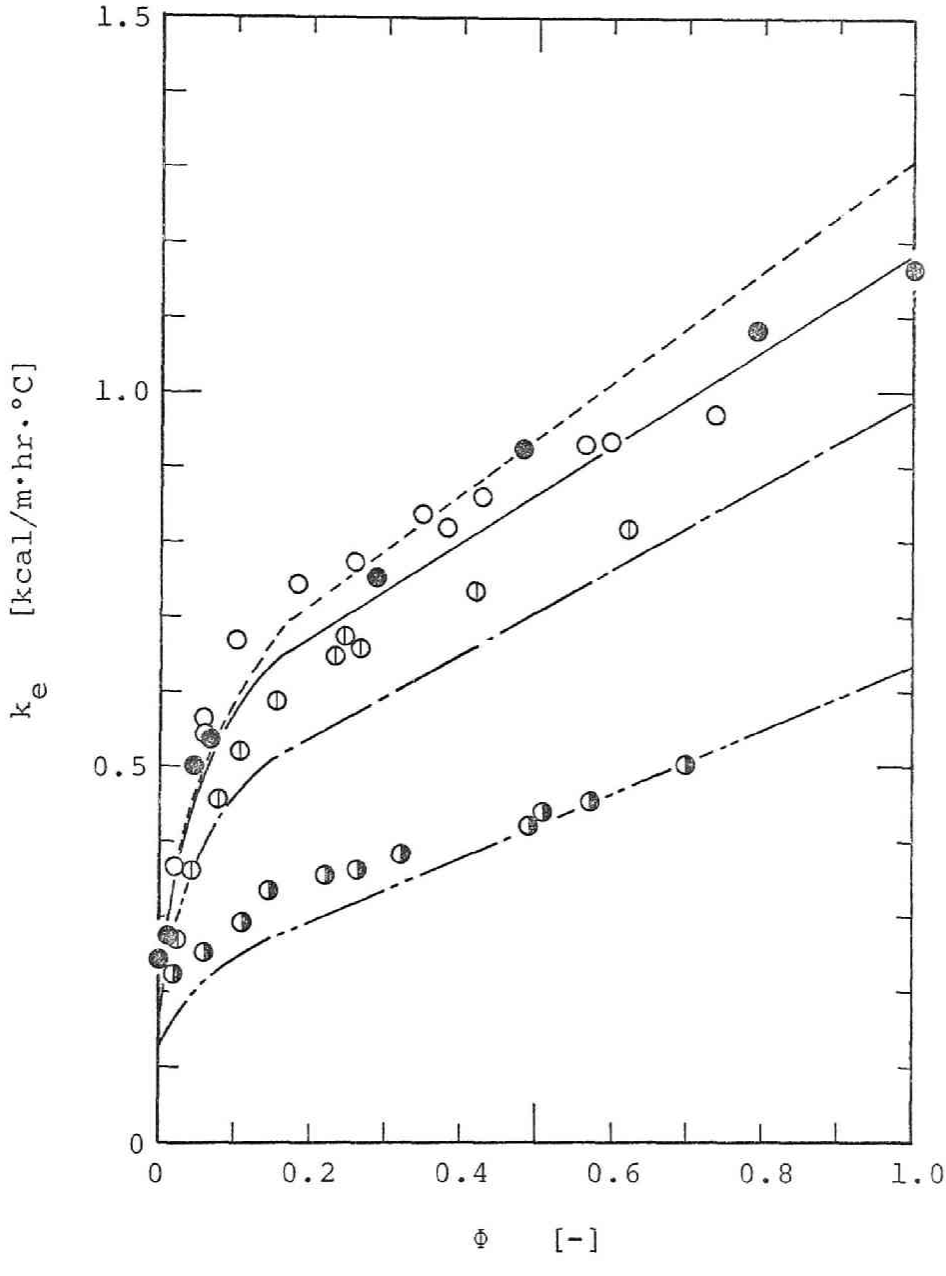

Fig. (4-8) Comparisons of observed and predicted conductivities (no enthalpy transfer effect)

Key	System	ε	Data No.
○ ———	crushed glass - castor oil[3)]	0.453	5
◐ ——·——	crushed glass - water[3)]	0.530	6
◑ ——··——	quarz sand - castor oil[3)]	0.454	7
● -------	quarz sand - water[3)]	0.501	8

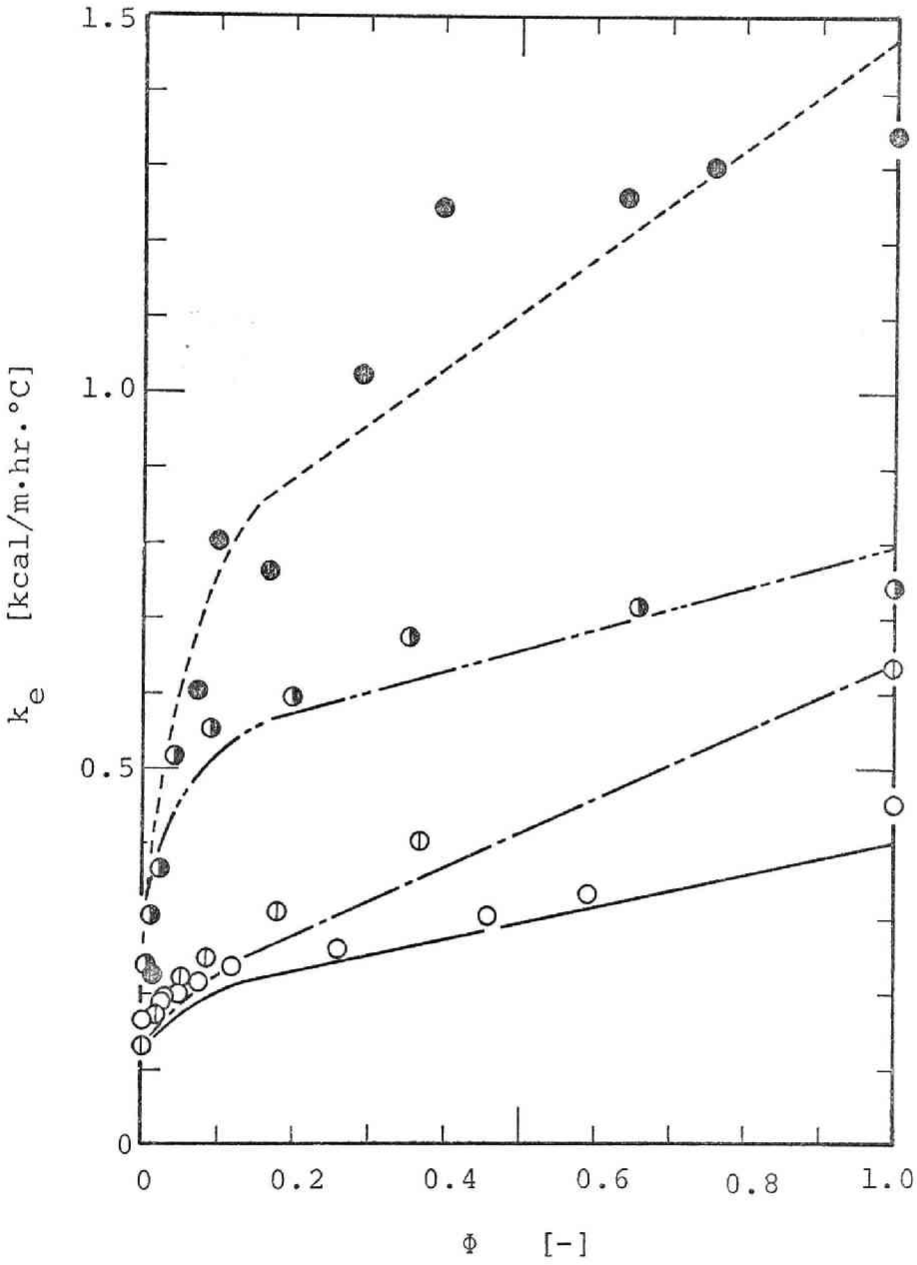

Fig. (4-9) Comparisons of observed and predicted conductivities (no enthalpy transfer effect)

observed over the whole range of water content. The experimental conditions and properties used in the prediction are listed up in Table (4-1). The values of k_s, k_g and k_l used for the prediction were taken from the published papers.

The comparisons of the case of relatively high temperature where the effect of enthalpy transfer must be taken into account for are shown in Figs. (4-10) ∿ (4-15). Figures (4-10) and (4-11) are concerned with the data obtained in the present work and Figs. (4-12) ∿ (4-15) are the data of Yamakawa et al.[16]. By comparing with the case of low temperature, there are relatively large discrepancies between the observed and predicted perhaps because there might be some imperfections on the measuring apparatus. In the present work, the continuous feeding water from the filter paper might disturb to attain the temperature equilibrium across the sample bed or the rearrangement of liquid has occured by vapor diffusion. However, in spite of the defections described above, the experimental points are seen to follow the predicted trend within the deviation of ±25%. Finally it can be concluded that the simplified model proposed in the present work is adequate to predict the effective thermal conductivities of beds of wet granular materials.

Table (4-1)-1 Physical properties of beds

Data No.	System	Particle dia. [cm]	ε [-]	Temp. [°C]	k_s [kcal /m·hr°C]	k_l [kcal /m·hr°C]	k_g [kcal /m·hr°C]	k_d [kcal /m·hr°C]
1	crushed marble ∿water[15]	0.035	0.492	26	2.50	0.520	0.022	0.0802
2	crushed slate ∿water[15]	0.035	0.528	26	2.00	0.520	0.022	0.0802
3	crushed glass ∿water[15]	0.035	0.544	26	0.80	0.520	0.022	0.0802
4	sand ∿ water[12]	< 0.165	0.42	18	2.30	0.520	0.022	0.050
5	crushed glass ∿castor oil[3]	0.141	0.453	14	0.821	0.155	0.022	0.000
6	crushed glass ∿water[3]	0.0252	0.530	14	0.821	0.503	0.022	0.0364
7	quarz sand ∿castor oil[3]	0.100	0.454	14	4.50	0.155	0.022	0.000
8	quarz sand ∿water[3]	0.141	0.501	14	4.50	0.503	0.022	0.0364
9	glass beads ∿water[16]	0.0147 ∿0.0295	0.375	40	0.869	0.540	0.0237	0.166
				55	0.881	0.557	0.0250	0.362
				65	0.889	0.568	0.0255	0.613
				78	0.900	0.578	0.0261	1.29
10	glass beads ∿ethanol[16]	0.0147 ∿0.0295	0.355	7	0.843	0.158	0.0215	0.0318
				30	0.861	0.155	0.0230	0.124

Table (4-1)-2 Physical properties of beds

Data No.	System	Particle dia. [cm]	ε [-]	Temp. [°C]	k_s [kcal /m·hr·°C]	k_l [kcal /m·hr·°C]	k_g [kcal /m·hr·°C]	k_d [kcal /m·hr·°C]
10	glass beads ∿ ethanol[16]	0.0147 ∿ 0.0295	0.355	40	0.869	0.154	0.0237	0.215
				50	0.877	0.153	0.0243	0.410
11	crushed marble ∿ water[16]	0.0210 ∿ 0.0417	0.395	7	2.61	0.484	0.0215	0.0257
				40	2.43	0.540	0.0237	0.166
				55	2.34	0.557	0.0250	0.362
				65	2.29	0.568	0.0255	0.612
				78	2.22	0.578	0.0261	1.29
12	crushed marble ∿ ethanol[16]	0.0210 ∿ 0.0417	0.395	7	2.61	0.158	0.0215	0.0318
				30	2.48	0.155	0.0230	0.124
				40	2.43	0.154	0.0237	0.215
				50	2.37	0.153	0.0243	0.410
				60	2.32	0.153	0.0252	0.801
				70	2.26	0.152	0.0261	1.99
				75	2.33	0.151	0.0265	6.72

Table (4-1)-3 Physical properties of beds

Data No.	System	Particle dia. [cm]	ε [-]	Temp. [°C]	k_s [kcal /m·hr°C]	k_l [kcal /m·hr°C]	k_g [kcal /m·hr°C]	k_d [kcal /m·hr°C]
13	Tottori sand ∿ water (present work)	0.0104 ∿ 0.0147	0.480	30	5.84	0.526	0.0230	0.100
				50	5.84	0.552	0.0243	0.280
				70	5.84	0.572	0.0256	0.806
14	glass beads ∿ water (present work)	0.0147 ∿ 0.0175	0.395	30	0.809	0.526	0.0230	0.100
				50	0.828	0.552	0.0243	0.280
				70	0.846	0.572	0.0256	0.806

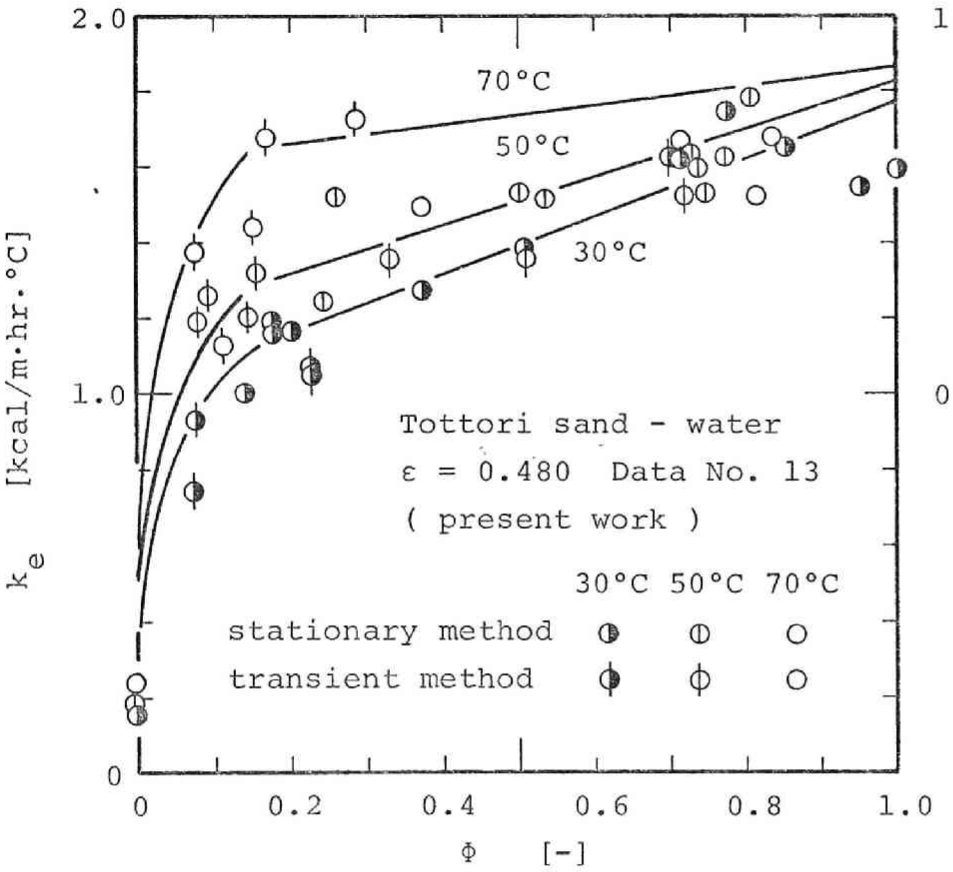

Fig. (4-10) Comparisons of observed and predicted conductivities (enthalpy transfer effect)

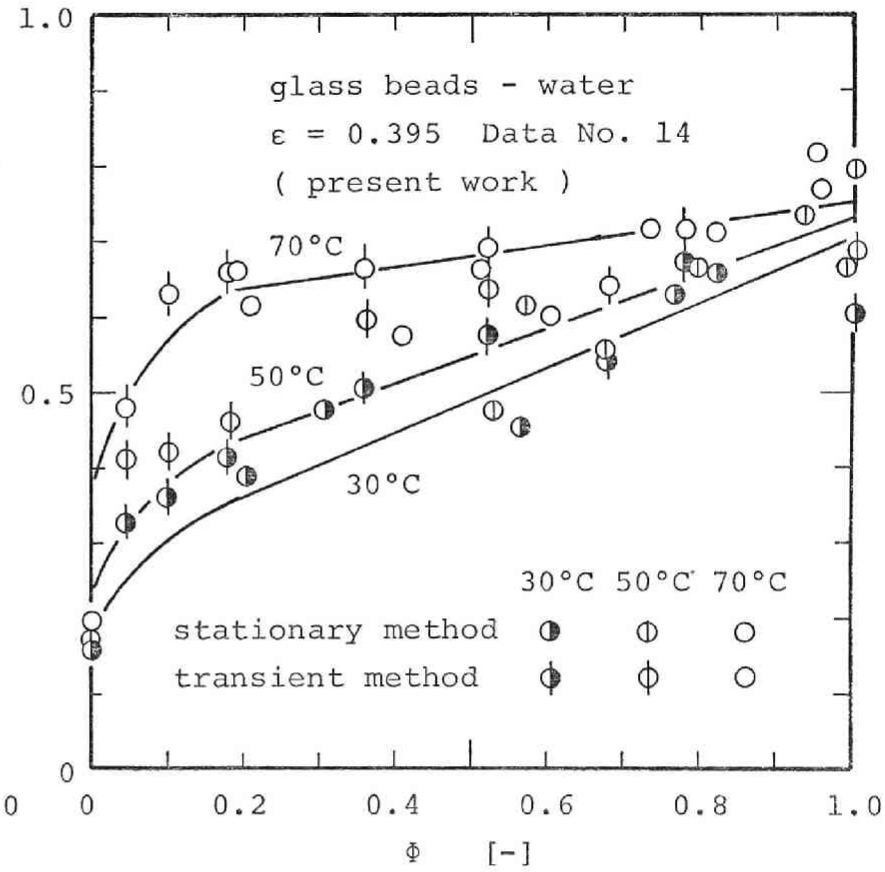

Fig. (4-11) Comparisons of observed and predicted conductivities (enthalpy transfer effect)

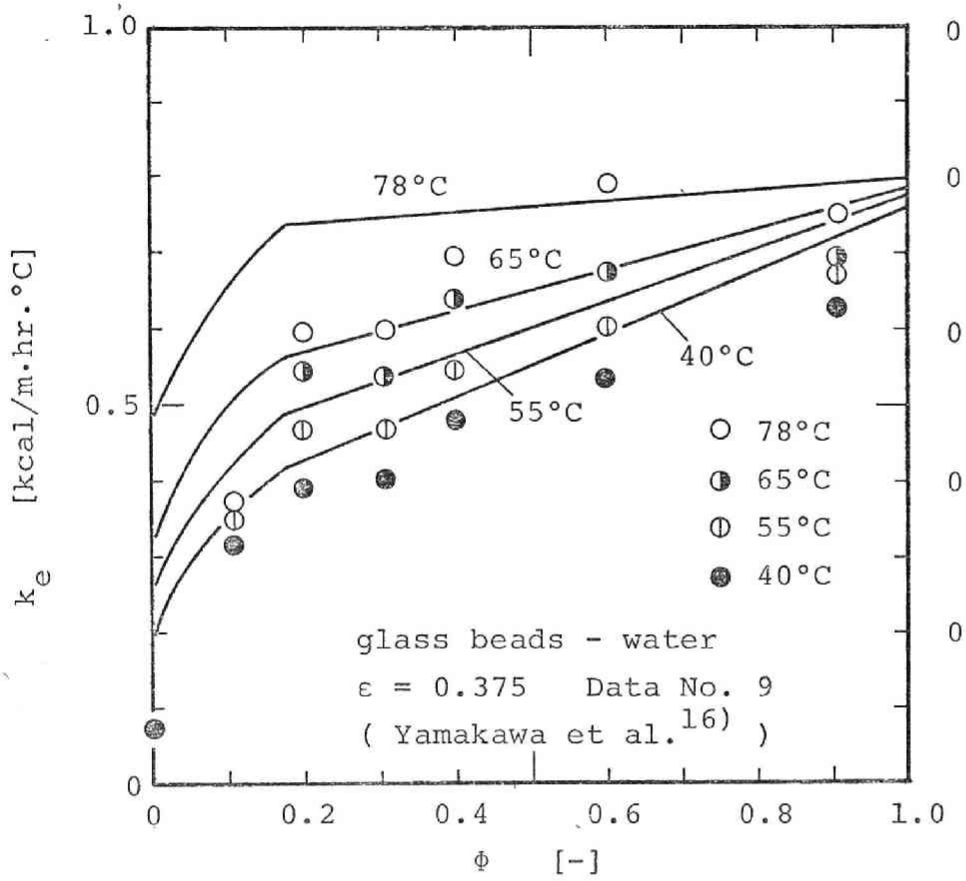

Fig. (4-12) Comparisons of observed and predicted conductivities (enthalpy transfer effect)

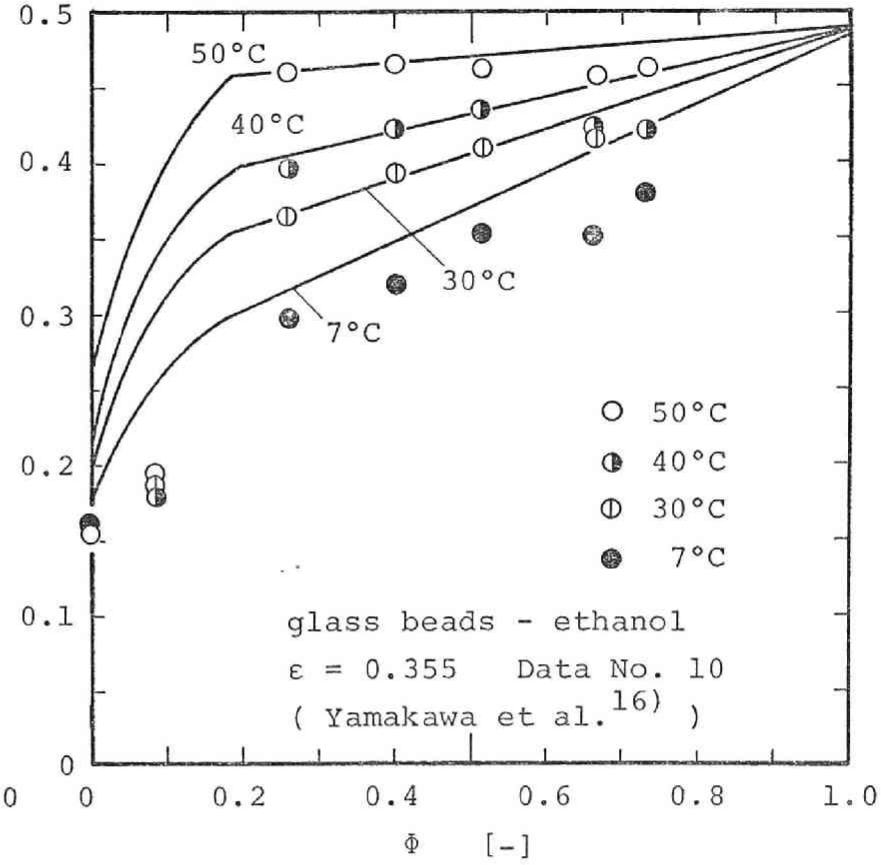

Fig. (4-13) Comparisons of observed and predicted conductivities (enthalpy transfer effect)

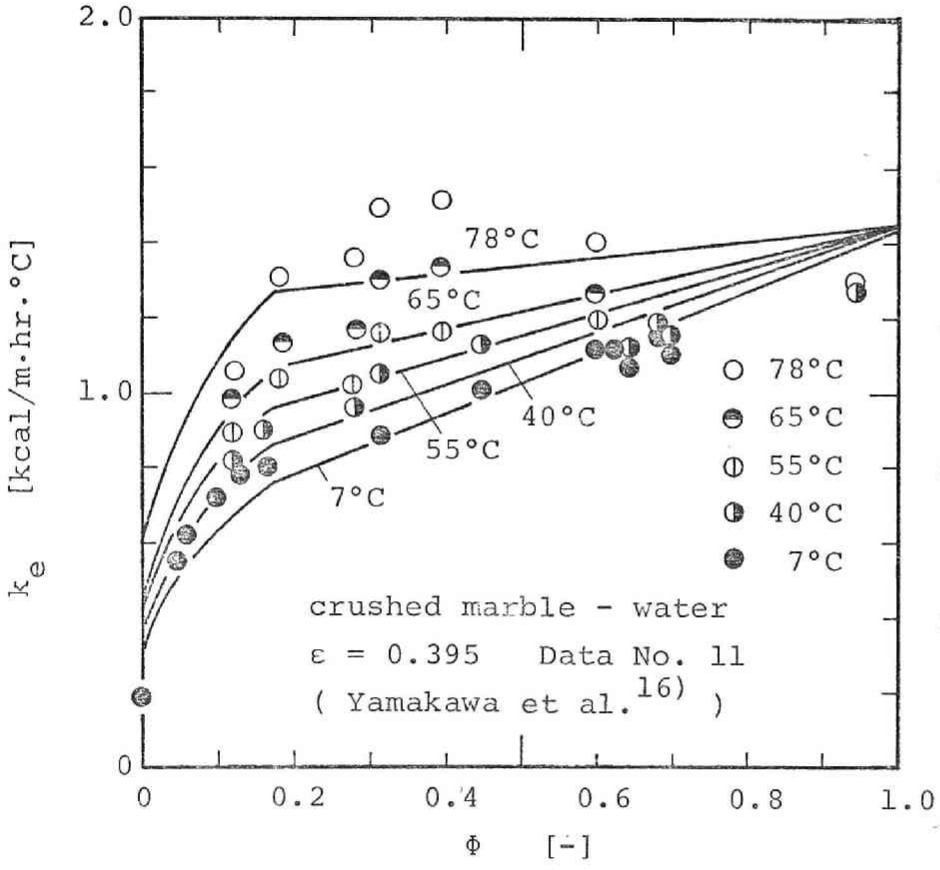

Fig. (4-14) Comparisons of observed and predicted conductivities (enthalpy transfer effect)

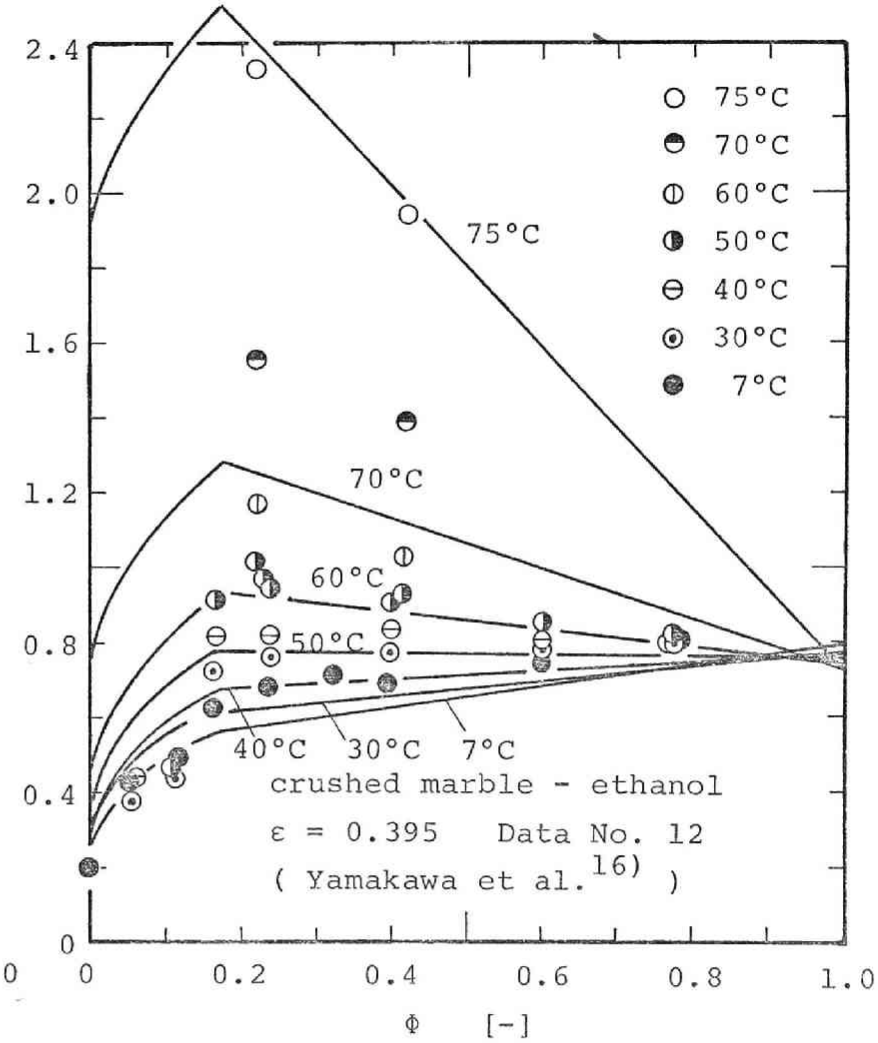

Fig. (4-15) Comparisons of observed and predicted conductivities (enthalpy transfer effect)

Conclusion

On the configurations of water retained in beds of wet granular materials, the simplified model was proposed.

Based on the model, the extension of the prediction formula proposed in the previous chapter for the two-phase systems, those are the states dried up and saturated with liquid was successfully carried out to give the prediction formula for the effective thermal conductivities of beds of wet granular materials. The formula proposed could be said to be adequate to predict the effective conductivity in comparison the predicted with the observed values.

Nomenclature

a = $\frac{\text{(number of wedge waters in critical state)}}{\text{(number of contact point in saturated state)}}$ [-]

C_p = heat capacity of bed [kcal/kg °C]

D_v = diffusion coefficient of vapor in air [m^2/hr]

k = thermal conductivity [kcal/m hr °C]

k_e = effective thermal conductivity [kcal/m hr °C]

M_v = molecular weight of diffusing vapor [kg/kg-mol]

N = number of contact point per a particle [-]

n = effective number of contact point per hemi-sphere [-]

p_T = total pressure [mmHg]

p_S = saturated vapor pressure of liquid [mmHg]

q = heat transfer rate [kcal/hr]

q_0 = heat flux at the surface of heating plate [kcal/m^2 hr]

R = radius of sphere [m]

R_v = gas constant of vapor : 8.314×10^7 [kcal/°K kg-mol]

r_l = heat of vaporization [kcal/kg]

T = absolute temperature [°K]

t = temperature [°C]

V = (volume of a wedge water)/(volume of a sphere) [-]

ε = void fraction of bed [-]

θ = angle [degree or radian]

ρ = apparent density of bed [kg/m^3-bed]

τ = time [hr]

Φ = water content of bed (averaged degree of saturation with liquid based on the voids) [-]

ψ = degree of saturation of a void [-]

(suffix)

c = wedge water at coalescing angle

crit. = critical state on wedge water

d = vapor diffusion

g = air or gas

l = water or liquid

S = surface

s = solid

sat. = saturated state

Literature Cited

1) Bruggemann, D. A. G.: Ann. Phys., 24, 636 (1935)

2) Herminge, L.: Tappi, 44, 570 (1961)

3) Kimura, M.: Kagaku Kogaku (Chem. Eng., Japan), 23, 502 (1959)

4) Koya, T. and D. Kunii: Kagaku Kogaku (Chem. Eng., Japan), 35, 887 (1971)

5) Krischer, O. and H. Esdorn: V. D. I. Forsch., 22, 1 (1956)

6) Krupiczka, R.: Int. Chem. Eng., 7, 122 (1967)

7) Kunii, D. and J. M. Smith: A. I. Ch. E.Journal, 6, 71 (1960)

8) Morita, Y.: J. of J. S. M. E., 63, 1177 (1960)

9) Nissan, A. H., D. Hansen and J. L. Walker: Chem. Eng. Progr. Symposium Series, 59, 114 (1963)

10) Okazaki, M., S. Yamamoto and R. Toei: unpublished

11) Ridgway, K. and K. J. Tarbuck: Brit. Chem. Eng., 12, 384 (1967)

12) Saito, T. and O. Okagaki: J. of J. S. M. E., 62, 741 (1951)

13) Sugawara, A.: Ōyōbutsuri, 30, 899 (1961)

14) Tanazawa, Y.: J. of J. S. M. E., 38, 207 (1935)

15) Tanazawa, Y.: Trans. of J. S. M. E., 2, 352 (1936)

16) Yamakawa, N., Y. Sasaki, T. Okada and S. Ohtani: Kagaku Kogaku (Chem. Eng. Japan), 36, 1342 (1972)

17) Zehner, P. and E. O. Schlünder: Chem. Ing. Tech., 42, 933 (1970)

CHAPTER 5

DRYING MECHANISM OF A CAPILLARY POROUS SOLID

Introduction

It is important to investigate the drying process of capillary porous solids from the view point of transport phenomena, because the drying of those plays a very important part in drying technique. During the past thirty years a considerable amount of research has been directed toward evaluating the drying rate of various materials. Luikov[3] and his coworkers have theoretically done the phenomenological treatment of simultaneous heat and mass transfer in capillary porous solids, and given a plenty of the experimental datum on the drying process. Krischer and Mahler[2] have studied also the drying mechanism of capillary porous solids. They examined the water transfer coefficient, κ, during the constant drying rate period, but did not intend to study the falling rate period. In order to evaluate a drying time, the quantitative analysis on the falling rate period is more important than the constant rate period.

According to the generally accepted picture for the drying mechanism of capillary porous solids, water in the solid is fed to the surface by capillarity and evaporates

there, during constant rate period. As long as the surface is wet with water, this constant rate period contiunes. At the end of this period the rate of drying begins to decrease, and at this time the surface itself is almost dried up. The average moisture content of the solid at this time has been termed the "critical moisture content", and is governed by the conditions of stream of drying air and the water transfer coefficient. It seems that the internal evaporation of water does not practically take place until the falling rate period begins. During the falling rate period, the vapor transfer through the solid plays an important roll as well as the water transfer. But there have been many problems unsolved yet in this field.

In this work, the results of an experimental study of drying process on a capillary porous solid are reported, and a new simple mathematical model to represent the mechanism of drying is proposed. An unglazed pottery made chiefly of Al_2O_3 having a considerable good thermal conductivity was used as a sample.

1. Experimental Apparatus and Procedures

Hot air having a constant humidity and temperature flowed through the wooden test duct being one hundred and twenty millimeters in breadth and seventy in height. Two perfectly wetted samples, which were square columns of

unglazed pottery being 30 mm by 44 mm and 100 mm high, were inserted on the under surface of the duct, and were dried from the upper surface of them. The one of two was served to take the water content distributions and the other the temperature, and both of them were measured at moderate time intervals. The pore distribution curve of the sample observed by mercury porosimeter and the physical properties are shown in Fig. (5-1).

2. Determination of Local Water Content

The electric capacitance method using high frequency alternative current which has been adopted by Mahler[2] was taken to measure local water contents of the drying sample. The principle of this method is that an apparent dielectric constant of a porous material is a function of water content. The electric conductivity of water increases a great deal when small inpurities are present, but the dielectric constant scarcely changes.

The basic circuit used is shown in Fig. (5-2), where the porous solid containing water is simulated by a parallel circuit composed of a capacitance C_x and a resistance R_x, on account of the conductivity effect of the solid. In Fig. (5-2), the impedances between "a" and "c", and between "a" and "b" are respectively

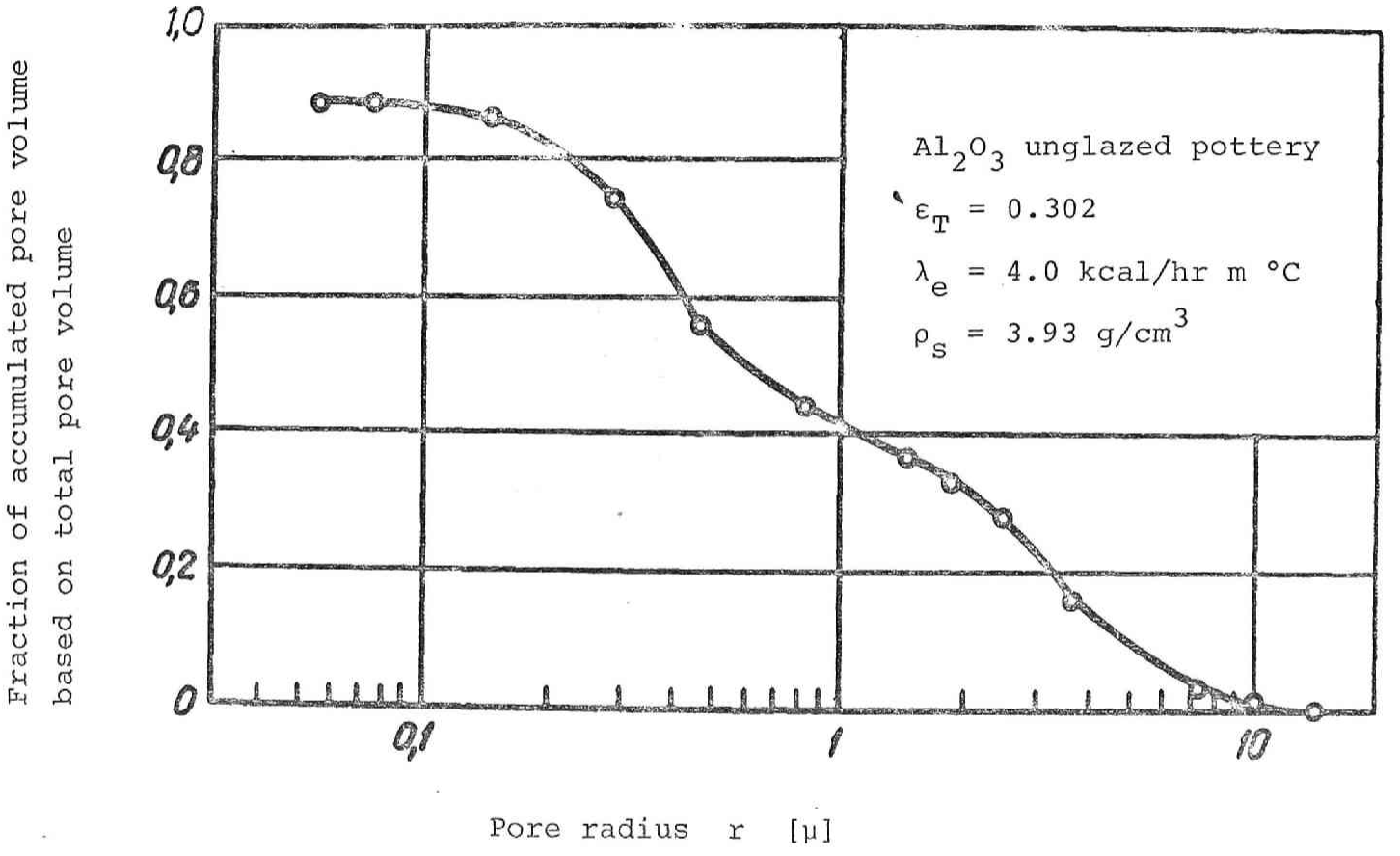

Fig. (5-1) Distribution curve of pore radius

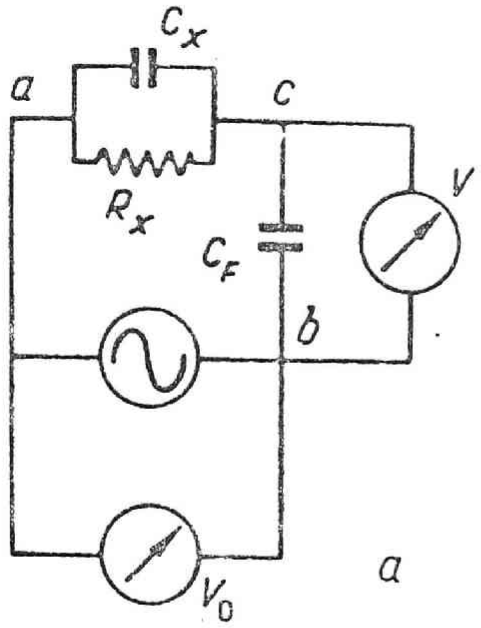

Fig. (5-2) Basic circuit

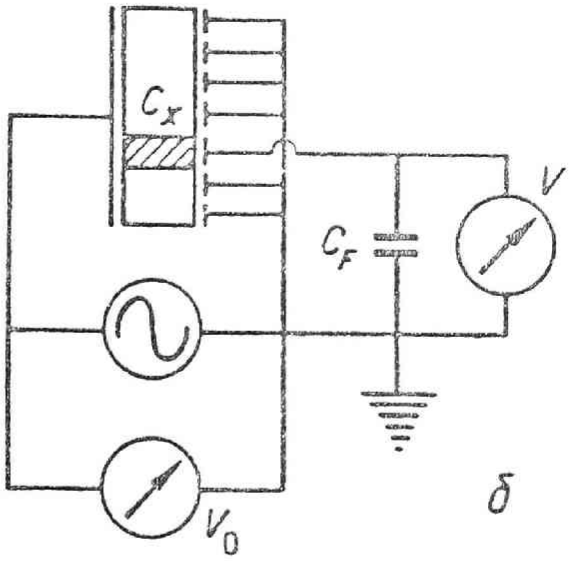

Fig. (5-3) Measuring circuit

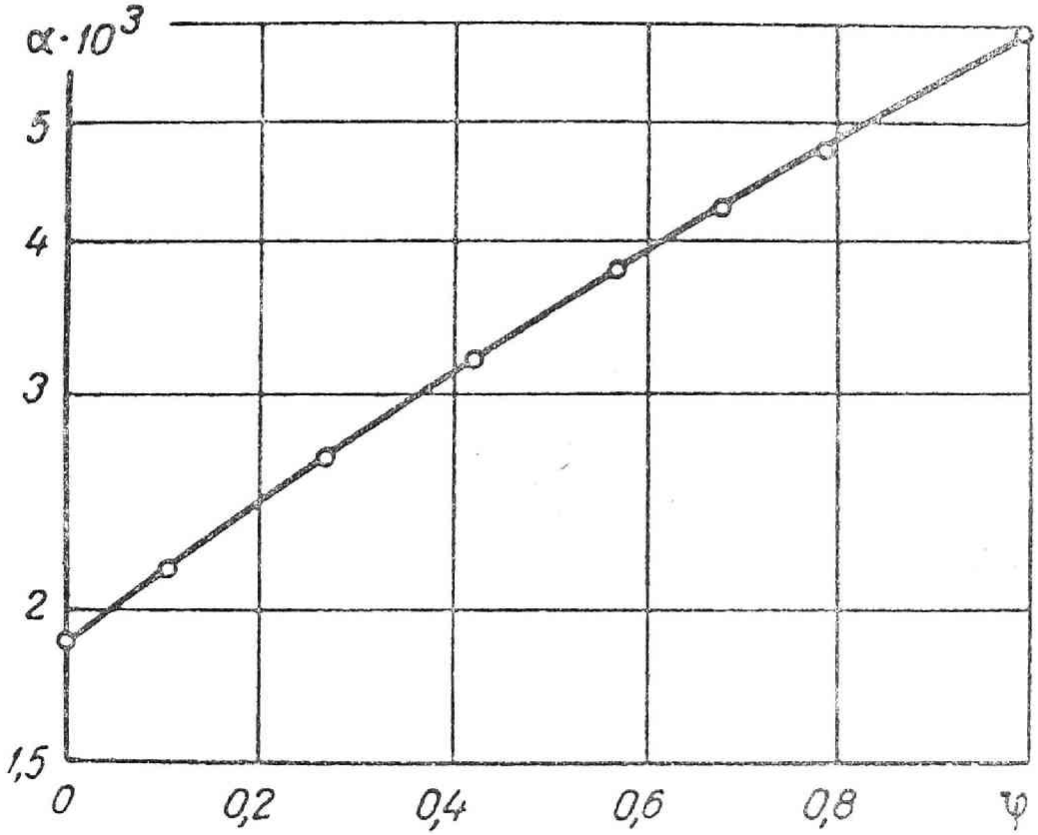

Fig. (5-4) α vs. ψ relation curve

$$\dot{Z}_{ac} = \frac{1}{\frac{1}{\dot{Z}_{R_x}} + \frac{1}{\dot{Z}_{C_x}}} = \frac{R_x}{1 - j\omega C_x R_x} \tag{5-1}$$

and

$$\dot{Z}_{ab} = \dot{Z}_{ac} + \dot{Z}_{bc} = \frac{R_x}{1 - j\omega C_x R_x} - \frac{1}{j\omega C_F} \tag{5-2}$$

The total current flowing through the sample is

$$\dot{I} = \frac{V_0}{\dot{Z}_{ab}} \tag{5-3}$$

then the voltage V to be measured between "c" and "b" is given as

$$\dot{V} = \dot{I}\dot{Z}_{bc} = \frac{\dot{Z}_{bc}}{\dot{Z}_{ab}} V_0 = \frac{1 - j\omega C_x R_x}{1 - j\omega R_x (C_F + C_x)} \tag{5-4}$$

and thus

$$V = \frac{\sqrt{\{\beta^2 + \alpha(\alpha + 1)\}^2 + \beta^2}}{\beta^2 + (\alpha + 1)^2} V_0 \tag{5-5}$$

where

$$\alpha = \frac{C_x}{C_F}, \quad \beta = \frac{1}{\omega C_F R_x} \tag{5-6), (5-7}$$

Using the values of V measured at the two frequencies, ω_1 and ω_2, we can calculate C_x and R_x from Eq. (5-5) separatively. ω_1 and ω_2 were five and ten Mega-Cycles. The measuring circuit used in the present experiment is shown in Fig. (5-3). Eighteen brass plates, each being 44 mm in breadth, 5 mm in height and 0.5 mm in thickness, were placed one above the other on the one side of the sample. One plate being 44 mm in breadth and 99 mm in height was placed on the other side.

These plates were fastened by epoxy resin and served as electrodes. C_F was far larger than C_x, so the electric flux lines through the sample could be expected to be parallel. Then it may be said that this method has a fairly good precision for the determination of local water content. An example of $\alpha \sim \psi$ relation curve of an electrode obtained in this experiment is shown in Fig. (5-4). By using the $\alpha \sim \psi$ relation curve for each electrode, the local water content of the sample can be measured continuously. This method also is applicable to beds of granular or powdered materials.

3. Experimental Results and Discussions

3.1 Constant drying rate period

The water distribution curves observed are shown in Fig. (5-5). Fig. (5-6) is the characteristic drying rate curve calculated from Fig. (5-5).

The liquid water transfer coefficient κ is defined as follows:

$$G = -\rho_w \varepsilon_T \kappa \frac{d\psi}{dx} \tag{5-8}$$

Assuming that the evaporation of water occurs only at the surface of sample during the constant rate period, the following equation is obtained:

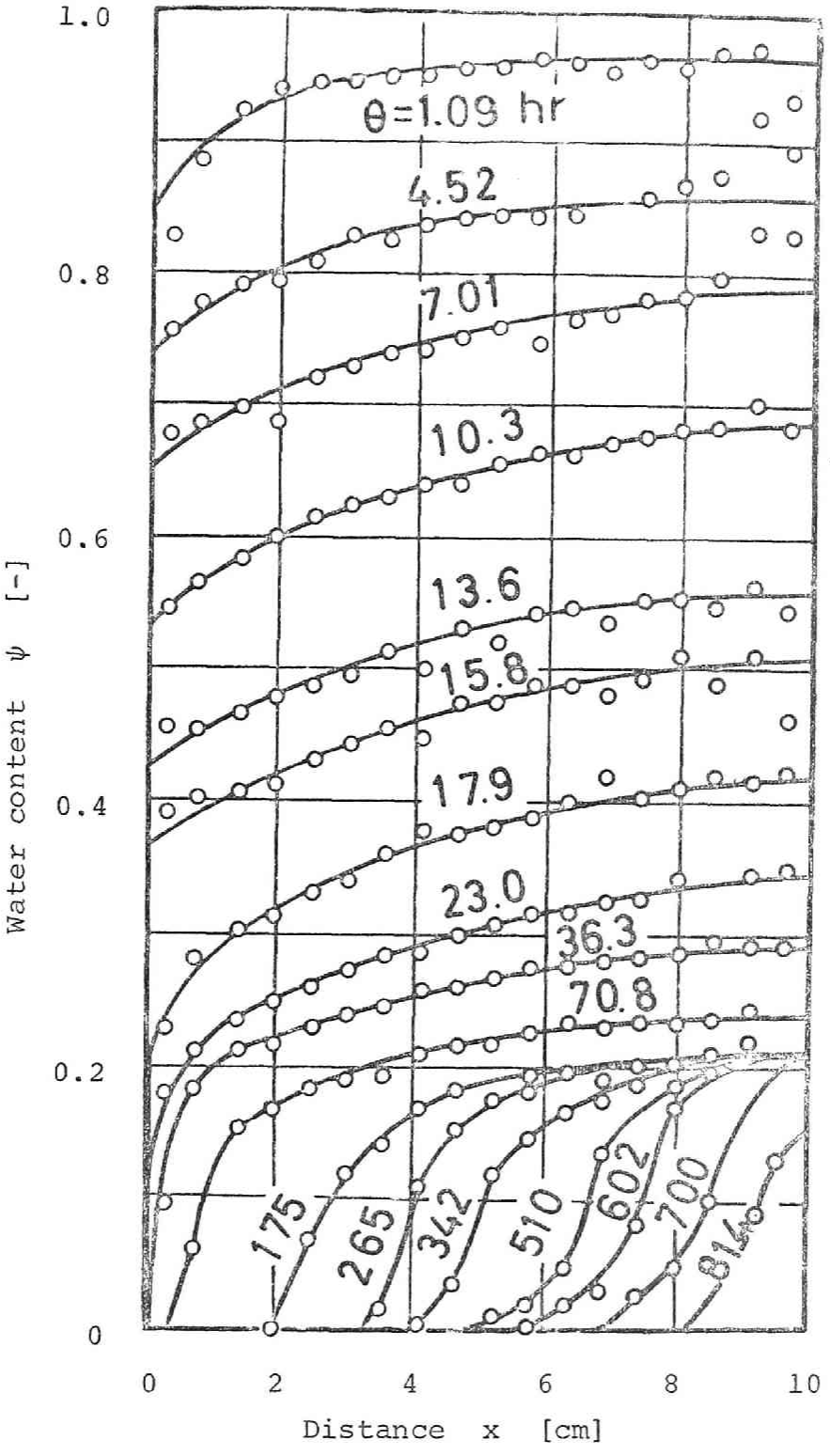

Fig. (5-5) Observed distributions of water content

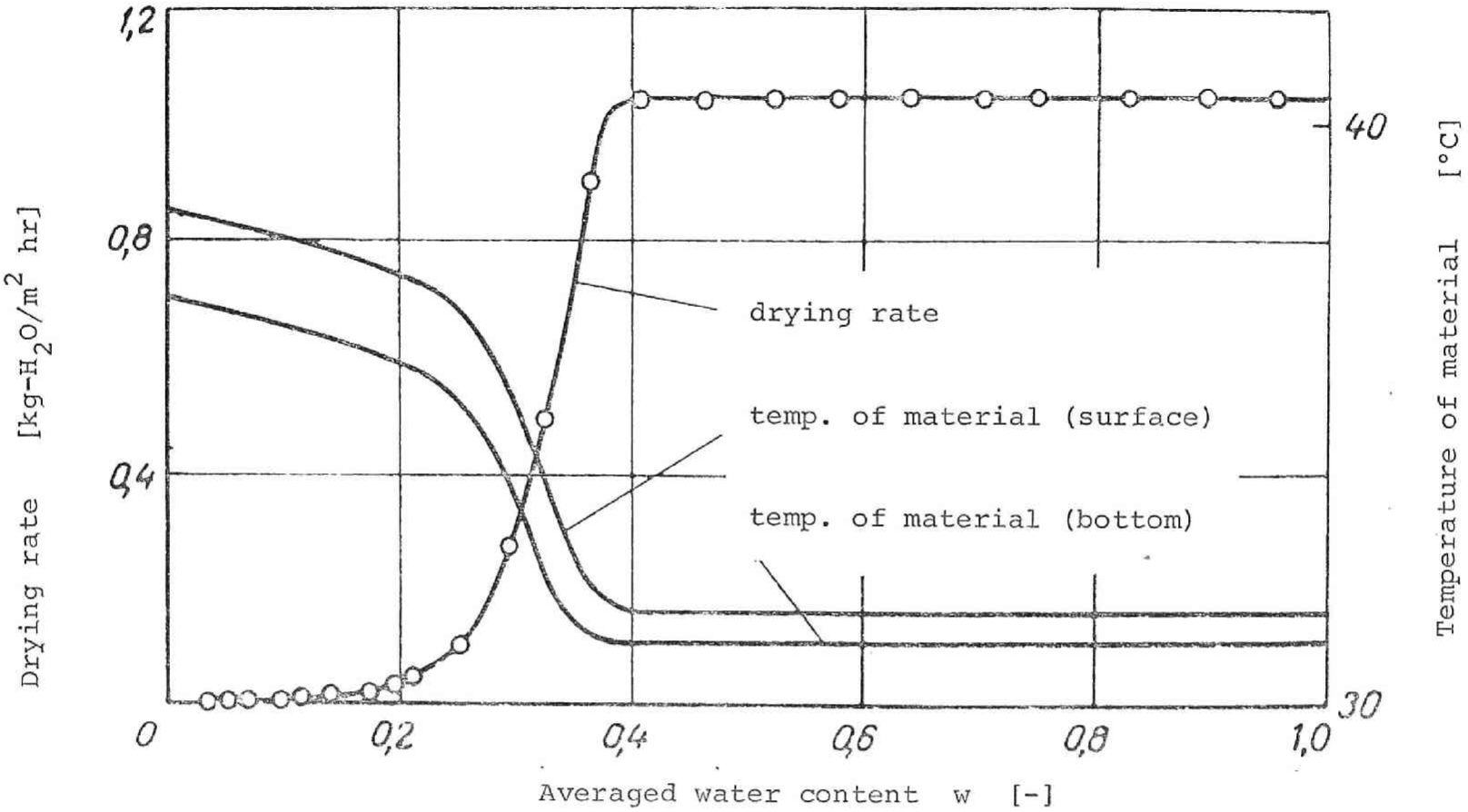

Drying conditions (hot air) : velocity = 10.5 m/sec temperature = 41.6 °C
humidity = 0.0182 kg-H_2O/kg-dry air

Fig. (5-6) Drying characteristic curve

$$\frac{\partial}{\partial\theta} = \frac{\partial}{\partial x}(\kappa\frac{\partial\psi}{\partial x}) \tag{5-9}$$

Integrating Eq. (5-9) from x_1, to L;

$$\int_{x_1}^{L}(\frac{\partial\psi}{\partial\theta})dx = \frac{\partial}{\partial\theta}\int_{x_1}^{L}\psi dx = [\kappa\frac{\partial\psi}{\partial x}]_{x_1}^{L} = -\kappa\frac{\partial\psi}{\partial x}\Big|_{x_1} \tag{5-10}$$

Thus

$$\kappa = -\frac{\partial}{\partial\theta}\int_{x_1}^{L}\psi dx/\frac{\partial\psi}{\partial x}\Big|_{x_1} \tag{5-11}$$

Values of κ which were calculated by using the experimental data in Eq. (5-11) are shown in Fig. (5-7). The values of κ drop over 200% as the water content drops from 0.95 to 0.85. It remains essentially constant for the water contents between 0.4 and 0.7, and drops sharply at the lower water contents. It is of interest that the Krischer's results show similar status. Krischer[1] has applied his model to calculation of κ.

3.2 Critical water content

As shown in Fig. (5-5) and (5-6), water content distribution corresponding to the critical water content w_c is roughly the one when θ equals to 18 hours. At this time the water content at the surface is about 0.21 and is named ψ_c. It seems reasonable to assume that there is funicular water at $\psi > \psi_c$, and all water is in the pendular state at $\psi \leq \psi_c$. Consequently the surface water content becomes zero as soon

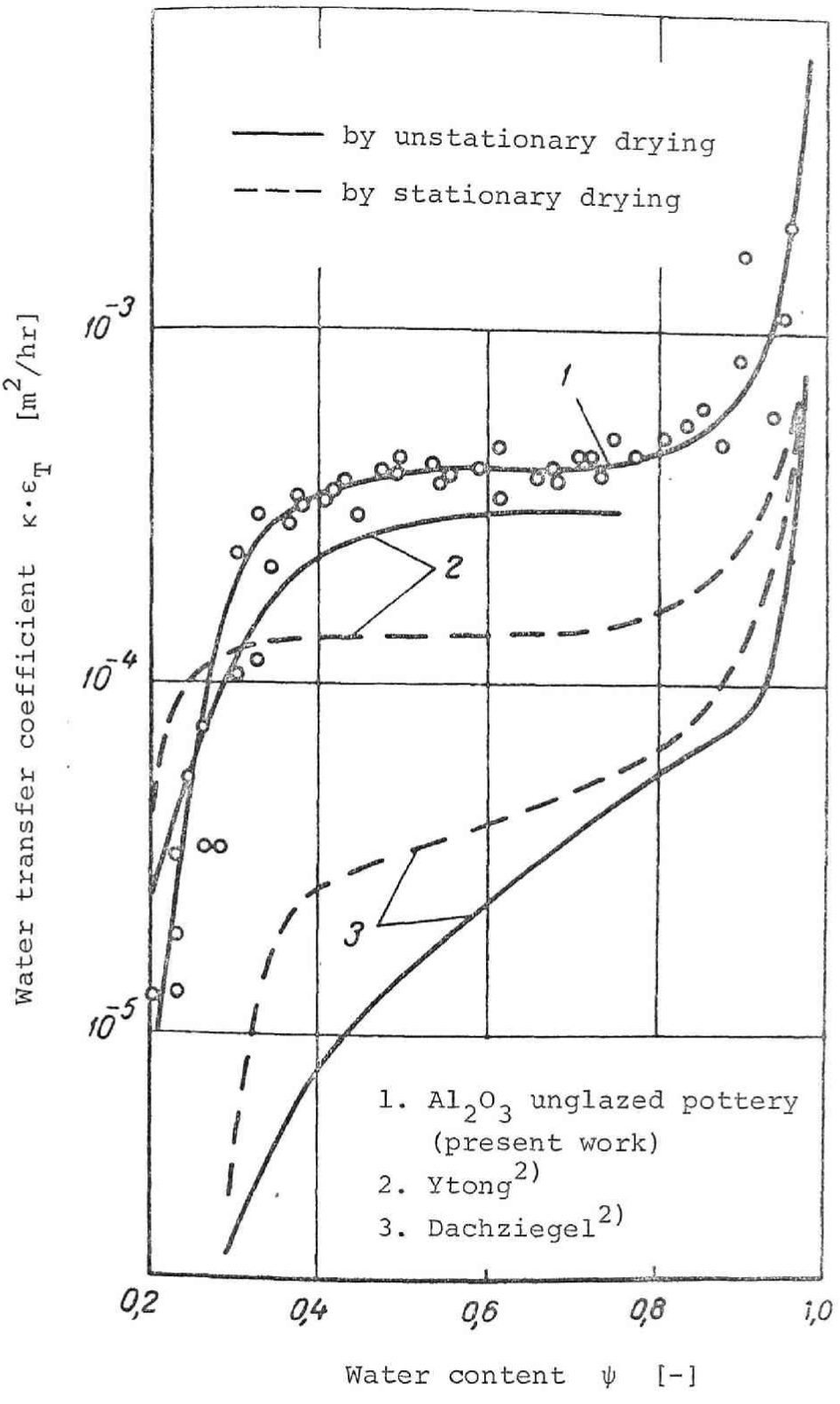

Fig. (5-7) Observed water transfer coefficient κ vs. water content ψ

as it reaches ψ_c, and the falling drying rate period begins at this instant.

3.3 Falling drying rate period

As mentioned above, the moisture transfer during the constant drying rate period is caused by the flow of water through the capillary porous solid. However during the falling drying rate period, drying is caused by the flow of water and vapor, or only by the flow of vapor at the last stage.

As shown in Fig. (5-5) and (5-6), the temperature increases of the surface and the bottom were less than 1°C, and the difference between the temperature of surface and bottom was less than 2°C, after θ = 40 hr. Therefore the drying process during the falling drying rate period in this experiment can be assumed to be an isothermal process.

From the fact that the temperature of the sample is constant during the constant drying rate period and ψ_s is approximately equal to ψ_c at w_c, it may be assumed for simplicity that water transfer occurs at $\psi > \psi_c$, and vapor transfer or internal evaporation occurs at $\psi \leqq \psi_c$, as shown in Fig. (5-8). Generally speaking, the falling drying rate is substantially determined by the resistance of the vapor transfer in the porous solid.

Fig. (5-8) shows a schematic model proposed for the drying mechanism. The solid is separated into three zones,

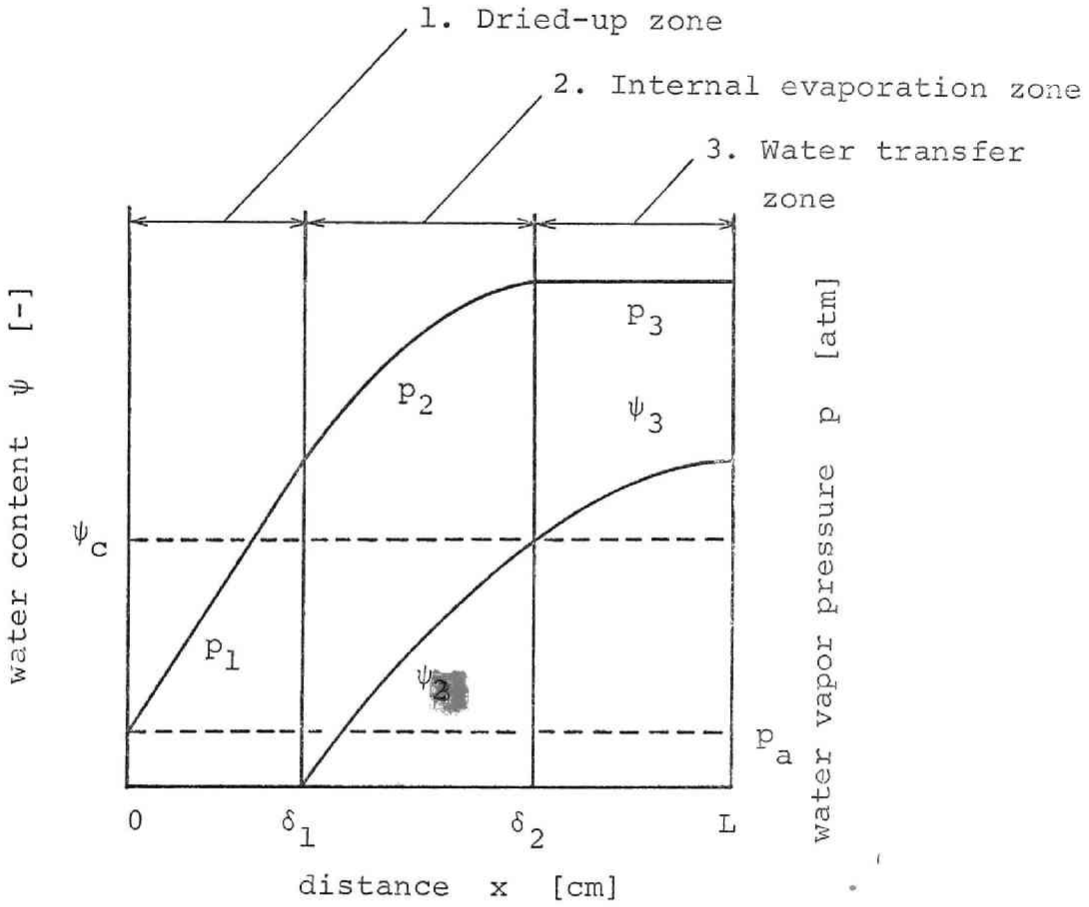

Fig. (5-8) Distributions of water content and water vapor pressure

i. e. the dried-up zone, the internal evaporation zone and the water transfer zone.

Dried-up zone $(0 \leq x < \delta_1)$

The vapor transfer only occurs in this zone, thus we obtain the following equation;

$$\varepsilon_T \frac{\partial p_1}{\partial \theta} = \frac{D'_v}{\mu_1} \frac{\partial^2 p_1}{\partial x^2} \tag{5-12}$$

where

$$D'_v = \frac{D_v \pi}{(\pi - p)_{lm}} = \frac{D_v \pi}{(p_{air})_{lm}} \tag{5-13}$$

The value of the term of left hand side in Eq. (5-12) is generally far smaller than that of right hand side, then it may be taken to be **nearly** equal to zero.

Internal evaporation zone $(\delta_1 \leq x < \delta_2)$

Assuming that the vapor transfer is caused by the partial pressure gradient of water vapor, the following equation is obtained;

$$\frac{\varepsilon M}{RT_{av}} \frac{\partial p_2}{\partial \theta} = \frac{D'_v M}{\mu_1 RT_{av}} \frac{\partial^2 p_2}{\partial x^2} + [\text{internal evaporation rate}] \tag{5-14}$$

The internal evaporation rate is estimated as follows. The schematic model for capillary porous solid is shown in Fig. (5-9). The funicular water is held in primary pores and the

1. Primary pore
2. Secondary pore
3. Funicular water
4. Pendular water

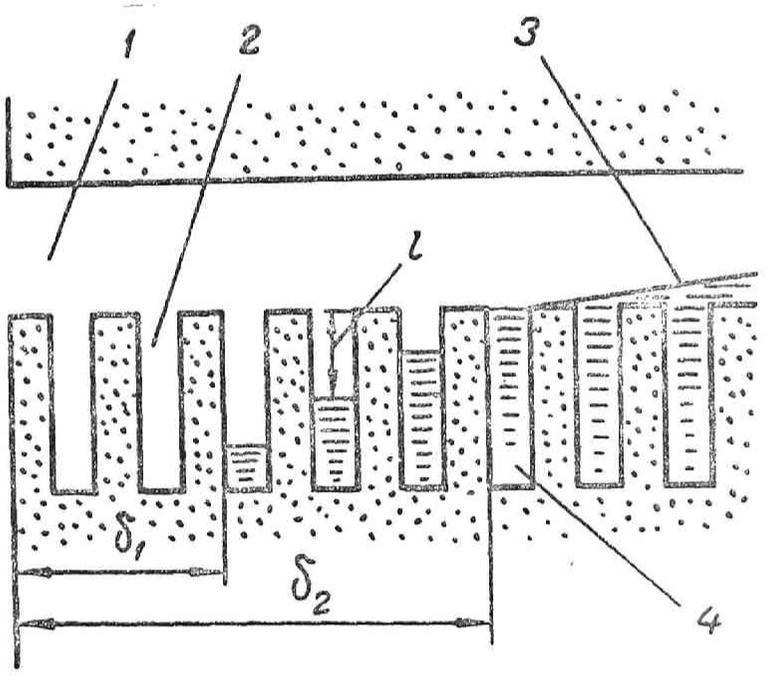

Fig. (5-9) Schematic configuration of water in pores (Falling drying rate period)

pendular water in secondary pores. The former can flow through the primary pores, but the latter cannot flow and can only be removed by evaporation and vapor transfer in pores. Then we assume that the water content at which all the secondary pores are filled with water corresponds with ψ_c. At a place where the water content is smaller than ψ_c, evaporation of water and vapor transfer occurs only and water transfer scarcely happens. On the other hand, water transfer predominates over at a place where the water content is larger than ψ_c.

At the secondary pores in Fig. (5-9) it is assumed that the length l is proportional to $(\psi_c - \psi_2)$, and the resistance of internal evaporation in the secondary pore is proportional to l. Therefore,

$$[\text{internal evaporation rate}] = \frac{k'}{\psi_c - \psi_2}(p_s - p_2) \qquad (5\text{-}15)$$

Substituting Eq. (5-15) into Eq. (5-14);

$$\frac{\varepsilon M}{RT_{av}} \frac{\partial p_2}{\partial \theta} = \frac{D_v' M}{\mu_l RT_{av}} \frac{\partial^2 p_2}{\partial x^2} + \frac{k'}{\psi_c - \psi_2}(p_s - p_2) \qquad (5\text{-}16)$$

$$-\varepsilon_T \rho_w \frac{\partial \psi_2}{\partial \theta} = \frac{k'}{\psi_c - \psi_2}(p_s - p_2) \qquad (5\text{-}17)$$

The value of the term of left hand side in Eq. (5-16) is far smaller than that of right hand side in this case, then it may be neglected.

Water transfer zone $(\delta_2 \leqq x \leqq L)$

At the early stage of the falling drying rate period, water transfer occurs in the inner part of the sample where $\psi_3 \geqq \psi_c$, so the following equation should be applied to this zone.

$$\frac{\partial \psi_3}{\partial \theta} = \frac{\partial}{\partial x}(\kappa \frac{\partial \psi_3}{\partial x}) \tag{5-18}$$

The initial and boundary conditions for Eqs. (5-12) ~ (5-18) are as follows.

Initial conditions:

$$\text{at} \quad \theta = 0; \quad \psi_3 = \psi_{crit}(x), \tag{5-19}$$

$$\delta_1 = \delta_2 = 0 \tag{5-20}$$

$\psi_{crit}(x)$ can be decided from Eq. (5-8) and Fig. (5-7) where $\psi_s = \psi_c$.

Boundary conditions:

$$\text{at} \quad x = 0; \quad \frac{D'_v M}{\mu_1 R T_{av}} \frac{\partial p_1}{\partial x} = k_g (p_1 - p_a) \tag{5-21}$$

$$\psi_1 = 0 \tag{5-22}$$

$$\text{at} \quad x = \delta_1; \quad p_1 = p_2, \tag{5-23}$$

$$\frac{\partial p_1}{\partial x} = \frac{\partial p_2}{\partial x}, \tag{5-24}$$

$$\psi_2 = 0 \tag{5-25}$$

$$\text{at} \quad x = \delta_2; \quad \frac{D'_v M}{\mu_1 R T_{av}} \frac{\partial p_2}{\partial x} = \varepsilon_T \kappa \rho_w \frac{\partial \psi_3}{\partial x} , \tag{5-26}$$

$$\psi_2 = \psi_3 = \psi_c, \tag{5-27}$$

$$p_2 = p_s \quad (= \text{const.}) \tag{5-28}$$

$$\text{at} \quad x = L; \quad \frac{\partial \psi_3}{\partial x} = 0 \tag{5-29}$$

Solutions of partial differential equations

The set of partial differential equations obtained above is a kind of two points boundary problem and is solved numerically under the following four assumptions.

(1) The terms of left hand side in Eq. (5-12) and (5-16) are neglected.

(2) The water transfer coefficient κ is assumed to be constant.

(3) The term of internal evaporation rate is approximately linearised as follows and k'' and c' are taken as constant;

$$\frac{k'}{\psi_c - \psi_2}(p_s - p_2) \cong k''(\psi_2 + c')(p_s - p_2) \tag{5-30}$$

(4) The boundary condition of the third kind, Eq. (5-21), is approximated as the first kind.

Then the following conversions of variables are performed on Eq. (5-12) ∿ (18).

$$P = \frac{p - p_a}{p_s - p_a}, \quad \Phi = \frac{\psi}{\psi_c}, \quad \xi_1 = \frac{x}{\delta_1}, \quad \xi_2 = \frac{x - \delta_2}{L - \delta_2} \tag{5-31}$$

$$\Delta = \frac{\delta}{L}, \quad C = \frac{c'}{\psi_c}, \quad H = F\theta$$

Where

$$A = \frac{D_v' M}{\mu_1 R T_{av} L^2 k'' \psi_c}, \quad D = \frac{\kappa \rho_w \varepsilon_T}{L^2 k''(p_s - p_a)}, \tag{5-32}$$

$$E = \frac{\mu_1 R T_{av} \rho_w \varepsilon_T \kappa \psi_c}{D_v' M (p_s - p_a)}, \quad F = \frac{k''(p_s - p_a)}{\varepsilon_T \rho_w}$$

Thus the following equations are obtained:

$$0 \leq \xi_1 < 1 ; \quad \frac{\partial^2 P_2}{\partial \xi_1^2} = 0 \tag{5-33}$$

$$0 \leq \xi_2 < 1 ; \quad \frac{A}{(\Delta_2 - \Delta_1)^2} \frac{\partial^2 P_2}{\partial \xi_2^2} + (1 - P_2)(\Phi_2 + C) = 0 \tag{5-34}$$

$$- \frac{\partial \Phi_2}{\partial H} + \frac{1}{\Delta_2 - \Delta_1}\{(1 - \xi_2)\frac{d\Delta_1}{dH} + \xi_2 \frac{d\Delta_2}{dH}\}\frac{\partial \Phi_2}{\partial \xi_2}$$

$$= (1 - P_2)(\Phi_2 + C) \tag{5-35}$$

$$0 \leq \xi_3 < 1 ; \quad \frac{\partial \Phi_3}{\partial H} + \frac{\xi_3 - 1}{1 - \Delta_2} \frac{d\Delta_2}{dH} \frac{\partial \Phi_3}{\partial \xi_3}$$

$$= \frac{D}{(1 - \Delta_2)^2} \frac{\partial^2 \Phi_2}{\partial \xi_3^2} \tag{5-36}$$

In these equations, it is assumed that ε is nearly equal to ε_T, for simplicity.

The initial and boundary conditions are as follows;

at $H = 0$; $\Phi_3 = \Phi_{crit}(\xi_3)$, (5-37)

$\Delta_1 = \Delta_2 = 0$ (5-38)

at $\xi_1 = 1$, $\xi_2 = 0$; $P_1 = P_2$, (5-39)

$\Phi_2 = 0$ (5-40)

$$\frac{1}{\Delta_1}\frac{\partial P_1}{\partial \xi_1} = \frac{1}{\Delta_2 - \Delta_1}\frac{\partial P_2}{\partial \xi_2} \tag{5-41}$$

at $\xi_2 = 1$, $\xi_3 = 0$; $P_2 = 1$, (5-42)

$$\frac{1}{\Delta_2 - \Delta_1}\frac{\partial P_2}{\partial \xi_2} = \frac{E}{1 - \Delta_2}\frac{\partial \Phi_3}{\partial \xi_3}\ , \tag{5-43}$$

$$\frac{\partial \Phi_2}{\partial \xi_2} = 0 \tag{5-44}$$

$\Phi_2 = \Phi_3 = 1$ (5-45)

at $\xi_3 = 1$; $\frac{\partial \Phi_3}{\partial \xi_3} = 0$, (5-46)

$P_3 = 1$ (5-47)

Eq. (5-44) is an additional condition to shift δ_2 smoothly.

The moment method proposed by Yamada[4] was applied to solve this set of equations numerically. This method is composed of the following procedures; We assume the solutions of P and Φ respectively as polynomials of ξ with unknown coefficients which are functions of H, and substitute these polynimials into the set of partial differential equations. Then various integral moments on ξ are obtained

as many as the number of the unknown coefficients, so the new set of first order ordinary differential equations are obtained on these unknown coefficients. Therefore the problem resolves itself to solve this set of differential equations by an appropriate method of numerical calculation.

In the present calculation, the polynomials of second degree on ξ were taken as the approximate solutions for P and Φ.

The calculated solutions of the water content ψ and the partial pressure of water vapor in the sample are shown in Fig. (5-10) and (5-11) respectively. The numerical values used in this calculation are as follows:

$$c' = 0.0473 \ [-] \ , \qquad k'' = 0.935 \ [g/cm^3 atm \ hr]$$
$$T_{av} = 310 \ [°K] \ , \qquad \kappa = 0.233 \ [cm^2/hr]$$
$$\mu_1 = 4.5 \ [-] \ , \qquad \varepsilon_T = 0.30 \ [-]$$

The values of k', then k" and c', are calculated from Fig. (5-5) and Eq. (5-16), (5-17) as

$$k' = \frac{D'_v}{\mu_1 RT_{av}} \frac{\partial^2}{\partial x^2}\{(\psi_c - \psi_2)\frac{\partial \psi_2}{\partial \theta}\} \ / \ (\frac{\partial \psi_2}{\partial \theta}) \qquad (5\text{-}48)$$

Fig. (5-12) shows the calculated relation between drying time and averaged water contents during falling drying rate period to be compared with the observed one. In Fig. (5-10), there are some discrepancies between the calculated and the observed one. However this may be attributed to use the constant values of κ and k', then k" and c'

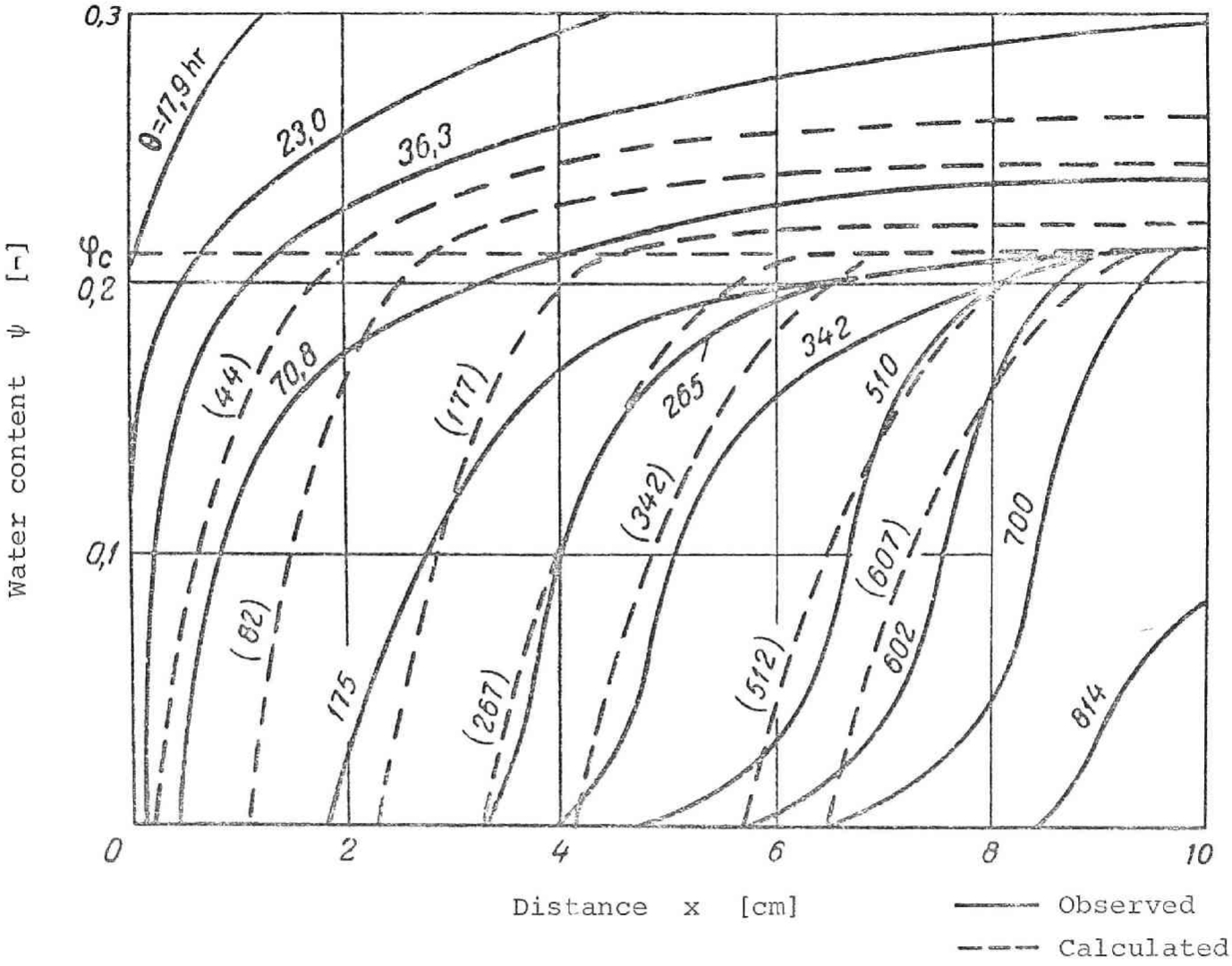

Fig. (5-10) Comparison of observed and calculated distributions of water content

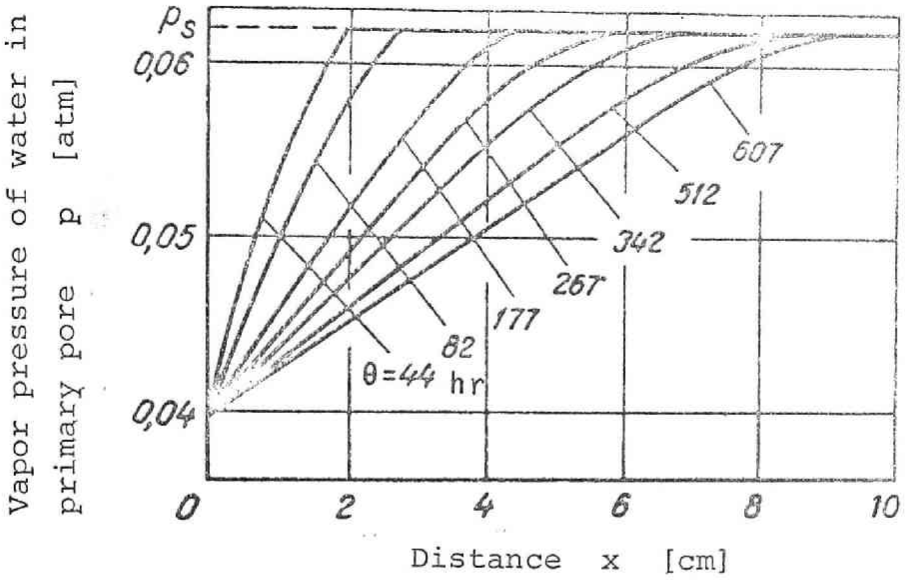

Fig. (5-11) Calculated distribution curves of water vapor pressure

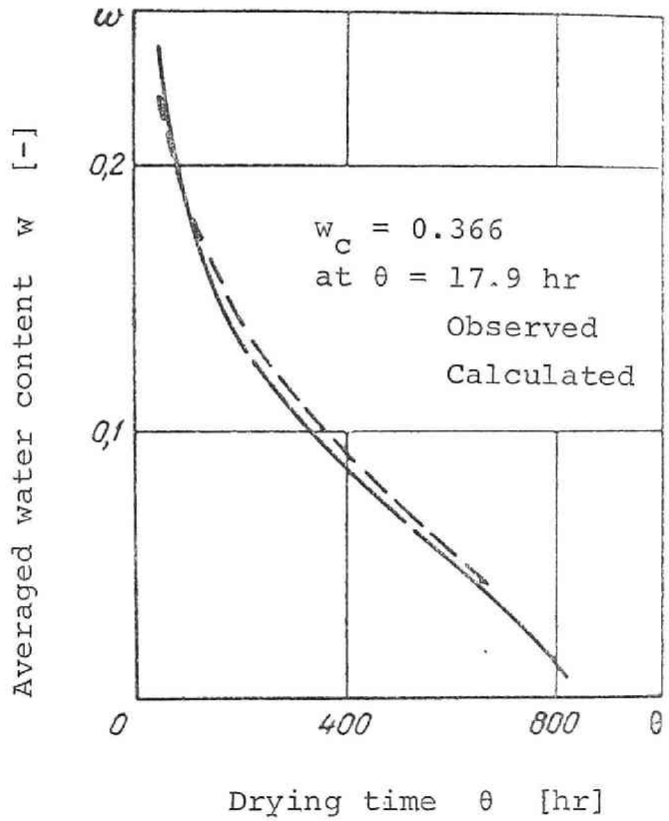

Fig. (5-12) Comparison of observed and calculated averaged water content

which are the values at mid time of falling rate period. At lower water contents the adsorption effects of water might found also.

In spite of considerably rough approximations mentioned above, the calculated ones fairly agree with the observed ones. From thes facts, the model and the calculation procedeures proposed here on the mechanism of drying, then of transfer of water and vapor of a capillary porous solid may be regarded as appropriate.

Conclusion

A solid having fine capillary pores were dried and the water content distributions during the whole drying period were measured by the electric capacitance method, and the mechanism of drying was discussed. A new model for the drying process of capillary porous solid was suggested based on the experimental results for the falling drying rate period.

Nomenclature

c' = constant in Eq. (5-30) [-]

C_x = capacitance of sample [PF]

C_F	= standard capacitance	[PF]
D_v	= diffusivity of water vapor in air	[cm^2/hr]
I	= electric current	[amp]
k'	= internal evaporation coefficient	[$g/cm^3 \cdot atm \cdot hr$]
k"	= constant in Eq. (5-30)	[$g/cm^3 \cdot atm \cdot hr$]
k_g	= mass transfer coefficient	[$g/cm^3 \cdot atm \cdot hr$]
l	= diffusion distance in secondary pore	[cm]
L	= depth of sample	[cm]
M	= molecular weight of water	[g/g-mol]
p	= vapor pressure of water	[atm]
p_a	= vapor pressure of water in drying air	[atm]
p_s	= saturated vapor pressure of water	[atm]
R	= gas constant	[$cm^3 \cdot atm/g\text{-}mol \cdot °K$]
R_x	= electric resistance	[Ω]
r	= pore radius	[μ]
t	= temperature	[°C]
T	= absolute temperature	[°K]
V	= voltage	[V]
w	= average water content	[cm^3-H_2O/cm^3-pore]
w_c	= critical water content	[cm^3-H_2O/cm^3-pore]
x	= distance measured from surface	[cm]
Z	= impedance	[Ω]
δ	= distance measured from surface to moving boundary	[cm]
ε	= porosity	[-]
ε_T	= total porosity	[-]
θ	= time	[hr]
κ	= water transfer coefficient	[m^2/hr], [cm^2/hr]

μ_l = way factor of vapor diffusion through pores[1], $(\mu_l = \mu_{l\ diff}/\varepsilon_T)$ [-]

π = total pressure [atm]

λ_e = thermal conductivity of solid [kcal/hr·m·°C]

ρ_s = true density [g/cm^3]

ρ_w = density of water [g/cm^3].

ψ = local water content; relative volumetric fraction of water to total pore volume [cm^3-H_2O/cm^3-pore]

ψ_{crit} = local water content at w_c [cm^3-H_2O/cm^3-pore]

ψ_c = local critical water content [cm^3-H_2O/cm^3-pore]

ψ_s = local water content at surface [cm^3-H_2O/cm^3-pore]

ω = frequency [1/sec]

Literature Cited

1) Krischer, O.: "Die wissenschaftlichen Grundlagen der Trocknungstechnik", Zweite Auflage, Springer-Verlag, Berlin (1963)

2) Krischer, O. and Mahler, K.: V. D. I-Forsch. Heft 473 (1959)

3) Luikov, A. V.: "Heat and Mass Transfer in Capillary-porous Bodies", Pergamon Press, Oxford (1966)

4) Yamada, H.: Reports of Research Inst. Fluid Eng., Kyushu Univ., Japan, Vol. 6. No. 2. p. 42 (1950)

CHAPTER 6

SUPER-HEATED STEAM DRYING OF POROUS MATERIAL

Section 6-1 Evaporation from a Water Drop in the Stream of Steam-air Mixtures

Introduction

On the liquid evaporation from a free surface of a liquid into the stream of gas, unidirectional diffusion and heat transfer occur through a stagnant gas film outside of the liquid surface. They are classified by the composition of the gas as follows;

i) p_A is far smaller than p_π

There are many studies in such a case. About a single drop evaporation, Frössling[1] and Ranz et al.[2] have presented the experimental formulas of h_c and k_G. These experimental formulas of k_G contain the term of p_{Bm}. But they did not change practically the gas phase compositions in their experiments. Therefore at least, from the view point of the effect of p_{Bm} on k_G, it may be said that these

results are attributed to the formal application of the "Film Theory" for unidirectional diffusion, that is, k_G is proportional to $1/p_{Bm}$.

ii) p_A is equal to p_π

The evaporation of a liquid into the super-heated vapor of its own liquid corresponds to this case. Since the evaporation temperature is very close to the boiling temperature under the surrounding total pressure,[3,4] k_G is too large to take its value by experiment, but h_c can be taken and there have been several reports on the evaporation and drying by super-heated steam from flat pans. Wenzel at al.[4] carried out the studies about super-heated ateam drying and air drying using the same experimental apparatus, and got the results that the value of j_h in the former one was about 20% higher than the latter. Chu et at.[3,5] also gave the experimental equation of j_h for the evaporation and drying from the flat pan by the super-heated vapor and the value of j_h was higher than the Pohlhausen's theoretical equation[6].

iii) p_A is considerably large

This case lies between i) and ii). As the study being consciously changed on p_{Bm}, there has been the one of water evaporation into high humid air using a wetted wall column by Cairns et al.[7] The effect of p_{Bm} on h_c has been found as well as on k_G. After that, Westkaemper et al.[8] and Shulman et al.[9] have carried out similar works. The works

cited above have shown the discrepancy between the "Film Theory" and the experimental results on k_G also.

In this paper, the effects of p_{Bm} on h_c and k_G are discussed, performing the experiments of evaporation from a single drop of water in the wide range of gas phase composition from air to super-heated steam.

1. Heat Transfer Coefficients

1.1 Experimental procedures

The experimental apparatus is shown in Fig. (6-1-1). The steam generator of the wetted wall colmun type with nitre bath jacket (4) was used and water was supplied by a constant rate pump, so the steam was generated at a constant rate. The steam generated was heated up to the appointed temperature in the super-heater (5), and led to the calming section (6) to make the eddies in the stream disappear and then to the convergent nozzle[10] (7) for uniforming the velocity distribution. The stream was flown uniformly through the rest section (8) and condensed out in the condenser (9). In mixing air and steam, air was supplied through the orifice (12) from the top of (4) at constant rate.

The details of the test section are shown in Fig. (6-1-2). A droplet having about one to two millimeters diameter

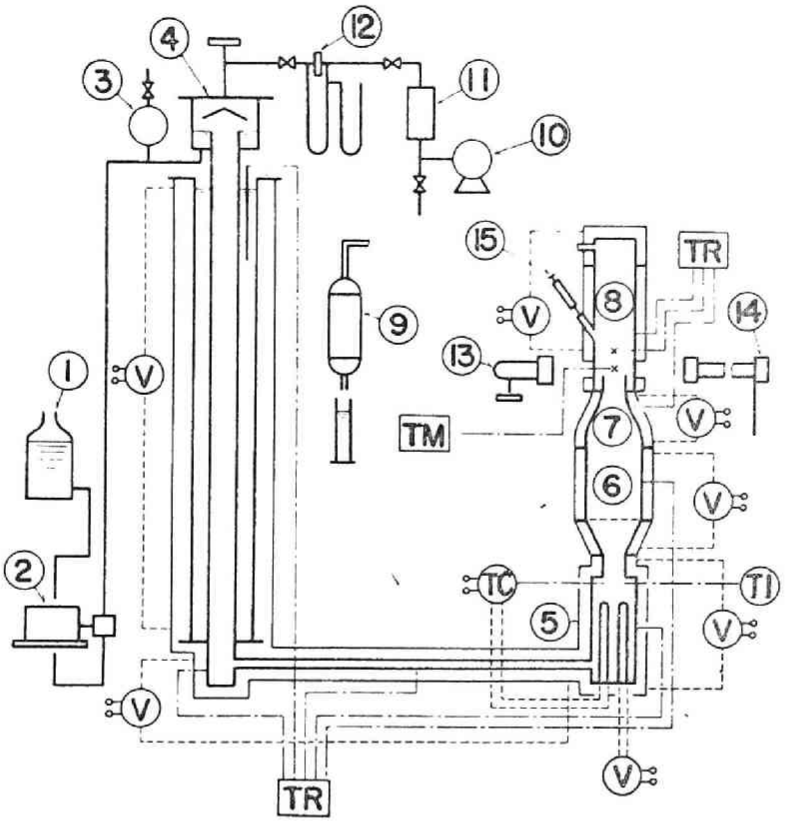

(1) Feed tank
(2) Milton Roy pump
(3) Air chamber
(4) Vapor generator (3" ϕ × 2450, 10 KW nitre bath)
(5) Super heater (4" ϕ × 600, 750 W)
(6) Calming section (160 ϕ × 200)
(7) Convergent nozzle (50 ϕ × 160 ϕ × 220)
(8) Test section (75 ϕ × 250)
(9) Condenser
(10) Rotary blower
(11) Deoiler
(12) Orifice meter
(13) Lamp
(14) Camera
(15) Syringe

TC: Temp. controller
TI: Temp. indicator
TM: Potentiometer
TR: Temp. recorder
V : Voltage adjuster

Fig. (6-1-1) Experimental apparatus

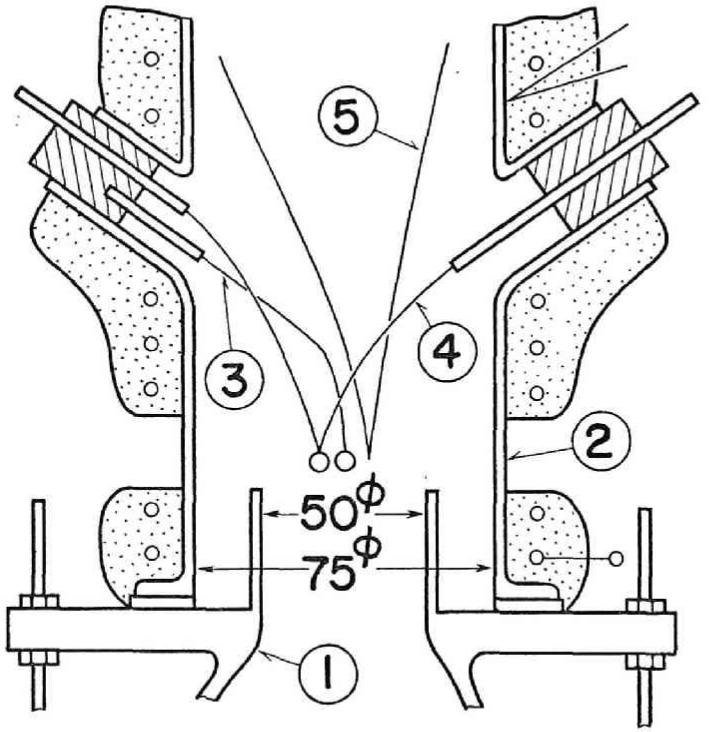

① Convergent nozzle
② Glass tube ($75^{\phi} \times 250$)
③ Fine glass rod ($70^{\mu\phi}$)
④ Thermo couple ($40^{\mu\phi}$, c-c)
⑤ Thermo couple ($300^{\mu\phi}$, c-c)

Fig. (6-1-2) Test section

was suspended at the tail-end of a fine glass rod (3) by using a syringe, in a vertically upward-flowing stream of gas. Evaporation rates were determined by measuring the decrease of the diameter of the droplet on the photograph pictured by a camera at an interval 10 or 15 sec..

The temperature of the drop was measured by the fine thermocouple (4) with which the drop was suspended. (It was estimated that the errors in measuring the temperature of the drop were less than 0.05°C.)

1.2 Transport properties used

Transport properties used for the calculations were cited from the following literatures.

Viscosity

air: D'Ans and Lax[11] steam: Licht and Stechert[12]

mixed gas: Wilke's formula[13]

Thermal conductivity

air: Keyes[14] steam: Kagakukogaku-benran[15]

mixed gas: Lindsay-Bromley's formula[13]

Heat capacity

air: Keyes[14] steam: Landolt-Börnstein[16]

mixed gas: the weighed mean value on molar fractions

1-3 Calculation of heat transfer coefficients

(1) Calculation procedure of heat transfer coefficients

As neglecting the temperature distribution in the drop, the heat balance is taken as follows:

$$-(\rho_l \lambda/A)(dV/d\theta) = q_T = q_c + q_k + q_r \tag{6-1-1}$$

$$q_c = q_T - q_r - q_k = h_c'(t_v - t_l) \tag{6-1-2}$$

$$(1/A)(dV/d\theta) = (1/2)(dD_p/d\theta) \tag{6-1-3}$$

Eqs. (6-1-1) and (6-1-3) give the next equation;

$$h_c' = \frac{(\rho_l \lambda/2)(dD_p/d\theta) + q_r + q_k}{(t_v - t_l)} \tag{6-1-4}$$

Considering the sensible heat increase of the evaporate water vapor across the gas film;[17]

$$h_c = N h_c' \tag{6-1-5}$$

where

$$N = \frac{C_{pA}(t_v - t_l)/\lambda}{\ln\{C_{pA}(t_v - t_l)/\lambda + 1\}} \tag{6-1-6}$$

(2) Radiative heat transfer rate, q_r In this experiment, the wall temperature of the test section, t_s, was adjusted equal to the gas temperature, t_v. Hence q_r was calculated by the following equation;

$$q_r = 1.356 \times 10^{-4}\{(\frac{t_s + 273}{100})^4 - (\frac{t_l + 273}{100})^4\}F_A F_E \tag{6-1-7}$$

F_A was equal to one, because the drop was entirely enclosed with the wall. As the surface area of the drop was far smaller than that of the wall, F_E was estimated to be equal to the emissivity of water, 0.95. At most, q_r was less than 15% of q_T.

(3) Conductive heat transfer rate, q_k The rates of conductive heat transfer to the drop from the fine glass rod and the thermocouple were estimated as follows respectively:

$$q_k = k_k \left(\frac{A_k}{A}\right) \left.\frac{dt_k}{dx}\right|_{x=0} = \frac{\pi r_k^2 k_k \sqrt{\alpha}(t_v - t_l)}{A}$$

$$\alpha = 2h_k/k_k r_k \qquad \text{(see Appendix.)} \qquad (6\text{-}1\text{-}8)$$

The value of h_k was estimated by the literature 18). At most, q_k was less than about 5% of q_T.

(4) The mean diameter of the drop, D_p The typical photographs are shown in Fig. (6-1-3). The arithmetic mean value of the two diameters measured on the directions of the diagonal lines, as shown in Fig. (6-1-4), was used as D_p.

1.4 Experimental results for heat transfer

Experimental conditions were as follows:

$G = 2.52 \times 10^{-2} \sim 12.0 \times 10^{-2}$ g/cm^{2}sec

$t_v = 42 \sim 155$°C

$\Delta t = t_v - t_l = 24 \sim 55$°C

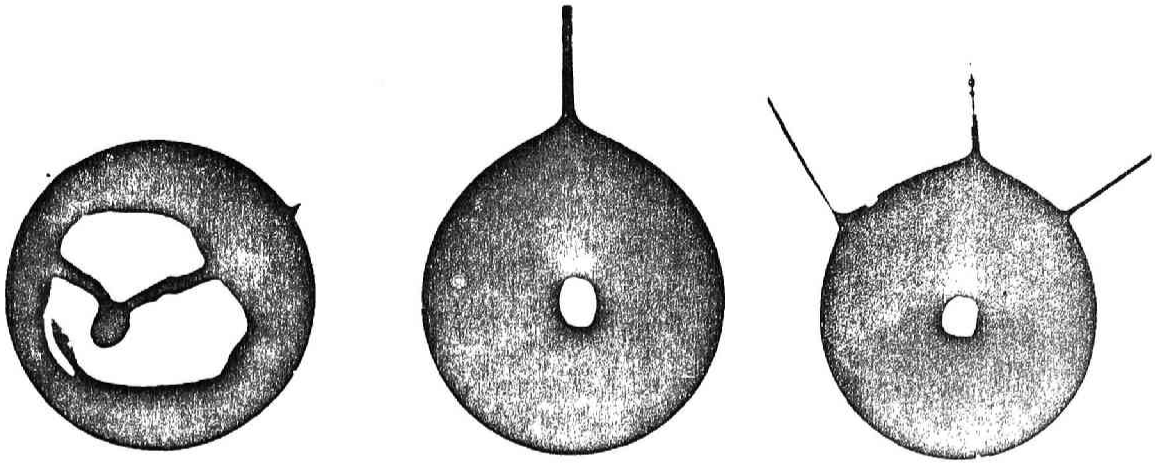

(a) (b) (c)

Fig. (6-1-3) Photographs of water drops

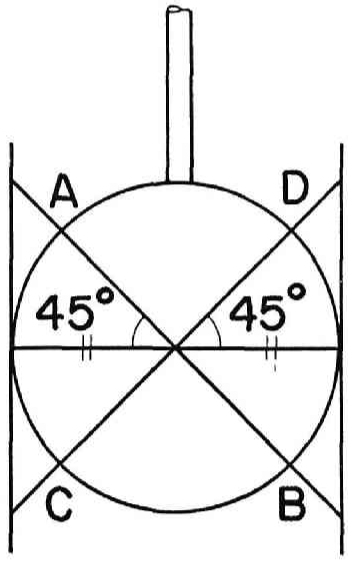

$$\frac{\overline{AB} + \overline{CD}}{2} = D_p$$

Fig. (6-1-4) Diameter of drop

$(p_{B\infty}/p_{\pi}) = 0 \sim 0.98$

$Re_p = 9 \sim 120$

(When there is no notice, mean values in transfer path were used as transport properties in non-dimensional numbers.)

During the evaporation of the drop, t_l was maintained at the constant temperature which might be considered as a sort of the wet bulb temperature decided by the gas phase condition. Of course as the decrease of p_{Bm}, t_l approaches the boiling temperature under the total pressure of the circumference.

In the case of super-heated steam, t_l was equal to the boiling temperature as same as the previous works[3,4]. The boiling of the drop has not been observed. The photographs of the drops suspended with the 40μφ thermo-couple and the fine glass rod are shown in Fig. (6-1-3.a) and (b). The typical experimental results for heat transfer as shown in Table (6-1-1).

The correlation of Nu vs. $Re_p^{1/2}Pr^{1/3}$ obtained in the present work is shown in Fig. (6-1-5). As shown in Fig. (6-1-5), the results have no significant differences with the gas composition, therefore the equation for the correlation in Fig. (6-1-5) was obtained in the full range of gas phase composition ($p_{Bm}/p_{\pi} = 1 \sim 0$) within 15% error as follows:

$$(h_c D_p/k) = 2.0 + 0.65(D_p G/\mu)^{1/2}(C_p \mu/k)^{1/3} \qquad (6\text{-}1\text{-}9)$$

Table (6-1-1) Experimental conditions and data for heat transfer

$p_{B\infty}/p_{\pi}$	$G\times10^2$	t_v	t_l	D_p	$-dD_p/d\theta\times10^4$	$q_T\times10^3$	$q_c\times10^3$	$h_c\times10^3$	Nu	Re_p	Pr
				0.1684	4.33	112	93.0	2.02	5.56	31.0	1.02
				0.1549	4.53	117	98	2.12	5.37	28.5	"
0	2.52	147.1	100.0	0.1411	4.87	126	106	2.29	5.28	26.0	"
				0.1260	5.23	135	114	2.46	5.06	23.2	"
				0.1099	5.57	144	121	2.61	4.69	20.2	"
				0.1618	4.30	112	98	2.89	7.69	90.5	0.998
				0.1527	4.80	124	110	3.26	8.19	85.4	"
0.05	7.68	133.9	99.7	0.1429	5.00	130	115	3.40	7.99	79.9	"
				0.1328	5.10	132	117	3.46	7.56	74.3	"
				0.1225	5.05	131	115	3.40	6.89	68.9	"
				0.1671	5.30	138	124	3.34	8.73	116	0.926
				0.1509	5.80	152	136	3.67	8.66	104	"
0.20	10.39	132.7	95.0	0.1322	6.10	159	143	3.85	7.96	91.8	"
				0.1127	7.15	187	169	4.54	8.00	78.0	"
				0.0901	8.20	215	192	5.17	7.29	62.3	"
				0.1577	4.20	111	99	3.06	7.26	66.2	0.849
				0.1492	4.15	110	98	3.01	6.76	62.6	"
0.40	6.94	118.3	85.4	0.1408	4.35	115	103	3.16	6.70	59.1	"
				0.1318	4.60	122	109	3.35	6.65	55.3	"
				0.1223	4.60	122	108	3.33	6.13	51.2	"
				0.1592	1.83	53.5	48.5	2.04	5.18	34.3	0.699
				0.1513	1.83	53.5	48.1	2.03	4.90	32.6	"
0.98	3.96	42.1	18.1	0.1425	2.07	60.5	54.7	2.30	5.23	30.7	"
				0.1328	2.20	64.3	57.9	2.44	5.17	28.6	"
				0.1223	2.33	68.1	60.8	2.56	5.00	26.3	"

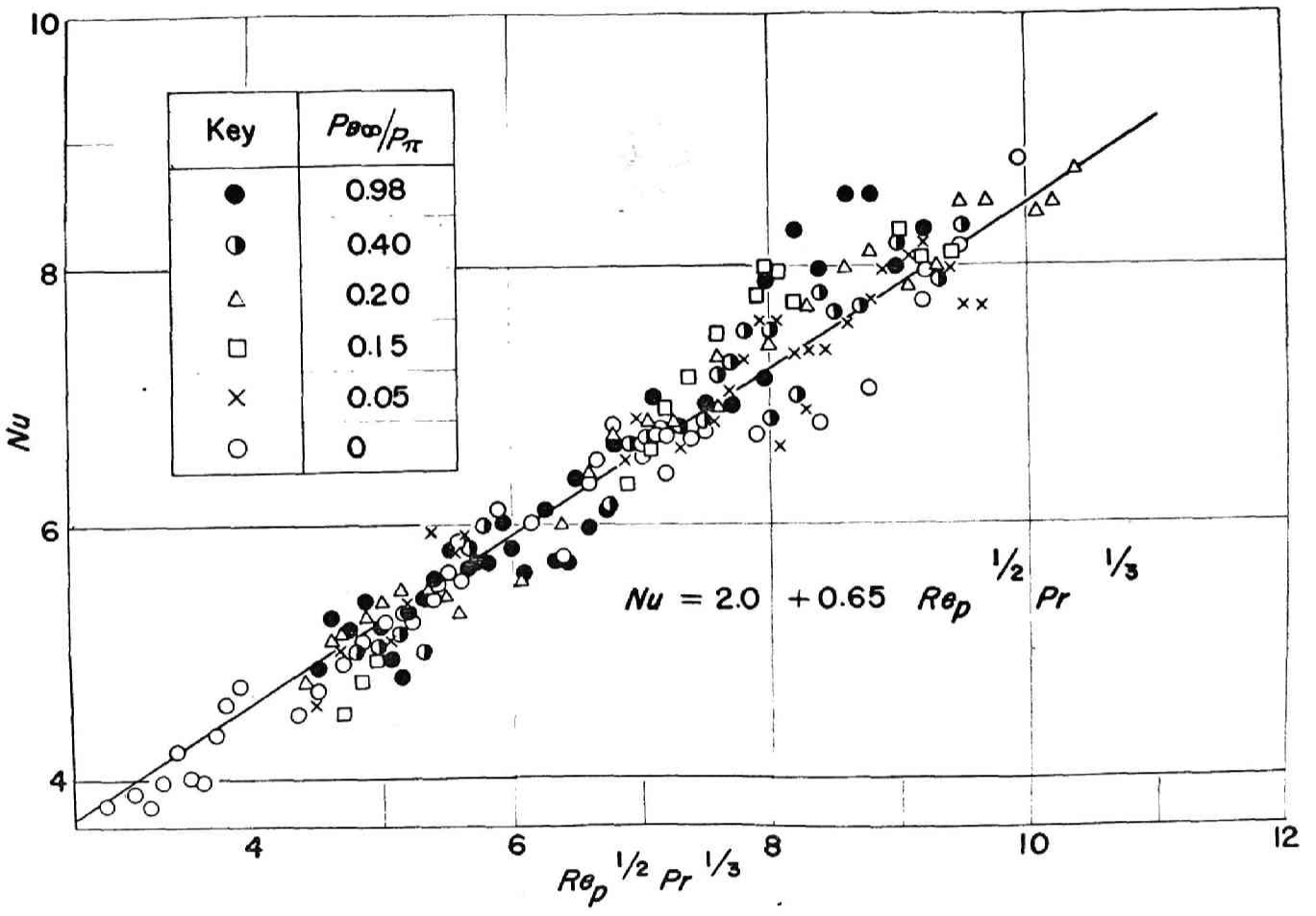

Fig. (6-1-5) Correlation of Nu vs. $Re_p^{1/2}Pr^{1/3}$

2. Mass Transfer Coefficients

2.1 Experimental procedures

The precision of the measuring data was demanded more severely in the determination of mass transfer coefficient than in the one of heat transfer coefficient. For this sake, the junction of the fine thermo-couple was fixed about one millimeter below the tail-end of the fine glass rod. The drop was suspended with both, as the junction of the thermo-couple should be surely placed in the drop.

(Some error was produced by heat conduction through thermo-couple in temperature measurement, but was negligible when the junction of the thermo-couple was submerged about 1 mm into the drop. (Fig. (6-1-3.c))

The compositions of gases were obtained by analysis of the sample gas directly sucked from the test section. The water vapor was caught out in the P_2O_5-tube and the volume of the air dried up was measured by the method of replacement with salt-saturated water. (It was estimated that the errors in the analysis of the compositions of the gases were less than 0.2%.)

2.2 Transport properties used

The diffusivity of water vapor in air that was calcula-

ted by Ranz et al.[2] based on the literature 19) was used.

2.3 Calculation of mass transfer coefficients

The mass balance is taken as follows:

$$-(\rho_l/M_A A)(dV/d\theta) = k_G(p_{A0} - p_{A\infty}) \qquad (6\text{-}1\text{-}10)$$

From Eqs. (6-1-3) and (6-1-10), k_G was calculated by Eq. (6-1-11).

$$k_G = -\frac{\rho_l}{2M_A(p_{A0} - p_{A\infty})}\left(\frac{dD_p}{d\theta}\right) \qquad (6\text{-}1\text{-}11)$$

The effect of mass transfer rate on k_G[20] was 0.9% at most on this case, therefore no correction was done.

2.4 Experimental results for mass transfer

Experimental conditions were as follows:

$G = 3.96 \times 10^{-2} \sim 12.0 \times 10^{-2}$ g/cm^{2}sec

$t_v = 42 \sim 142$°C

$\Delta p = p_{A0} - p_{A\infty} = 12.0 \sim 24.9$ mmHg

$(p_{Bm}/p_\pi) = 0.38 \sim 0.98$

$Re_p = 9 \sim 120$

The typical experimental results for mass transfer are shown

Table (6-1-2) Experimental conditions and data for mass transfer

p_{Bm}/p_{π}	$G\times10^2$	t_v	t_l	Δp	D_p	$-dD_p/d\theta \times10^4$	$k_G\times10^7$	Sh	$Sh(\frac{p_{Bm}}{p_{\pi}})^{-0.20}$	Re_p	Sc
					0.2124	6.80	12.0	6.15	7.45	87.9	0.630
					0.2052	6.90	12.1	6.02	7.29	84.8	"
0.384	6.96	141.6	87.56	15.3	0.1986	6.85	12.1	5.79	7.01	82.1	"
					0.1915	7.08	12.5	5.76	6.98	79.2	"
					0.1485	6.95	12.2	5.44	6.59	76.3	"
					0.1806	7.90	9.52	5.95	6.72	75.7	0.630
					0.1726	8.15	9.81	5.87	6.63	72.3	"
0.546	7.55	141.6	80.33	22.4	0.1643	8.55	10.3	5.86	6.61	68.9	"
					0.1555	8.65	10.4	5.61	6.33	65.3	"
					0.1470	8.75	10.6	5.36	6.05	61.6	"
					0.1981	6.05	6.60	5.58	6.97	81.5	0.636
					0.1920	6.15	6.71	6.47	6.86	78.9	"
0.746	7.82	120.2	66.84	24.9	0.1858	6.30	6.88	6.41	6.79	76.4	"
					0.1794	6.60	7.20	6.47	6.86	73.8	"
					0.1726	6.90	7.53	6.52	6.91	70.9	"
					0.1682	3.13	5.44	6.72	6.74	71.0	0.665
					0.1553	3.73	5.79	6.61	6.63	65.5	"
0.982	8.17	62.0	30.2	15.9	0.1416	3.57	6.21	6.45	6.47	59.7	"
					0.1267	3.88	6.75	6.28	6.30	53.4	"
					0.1106	4.15	7.21	5.87	5.89	46.5	"

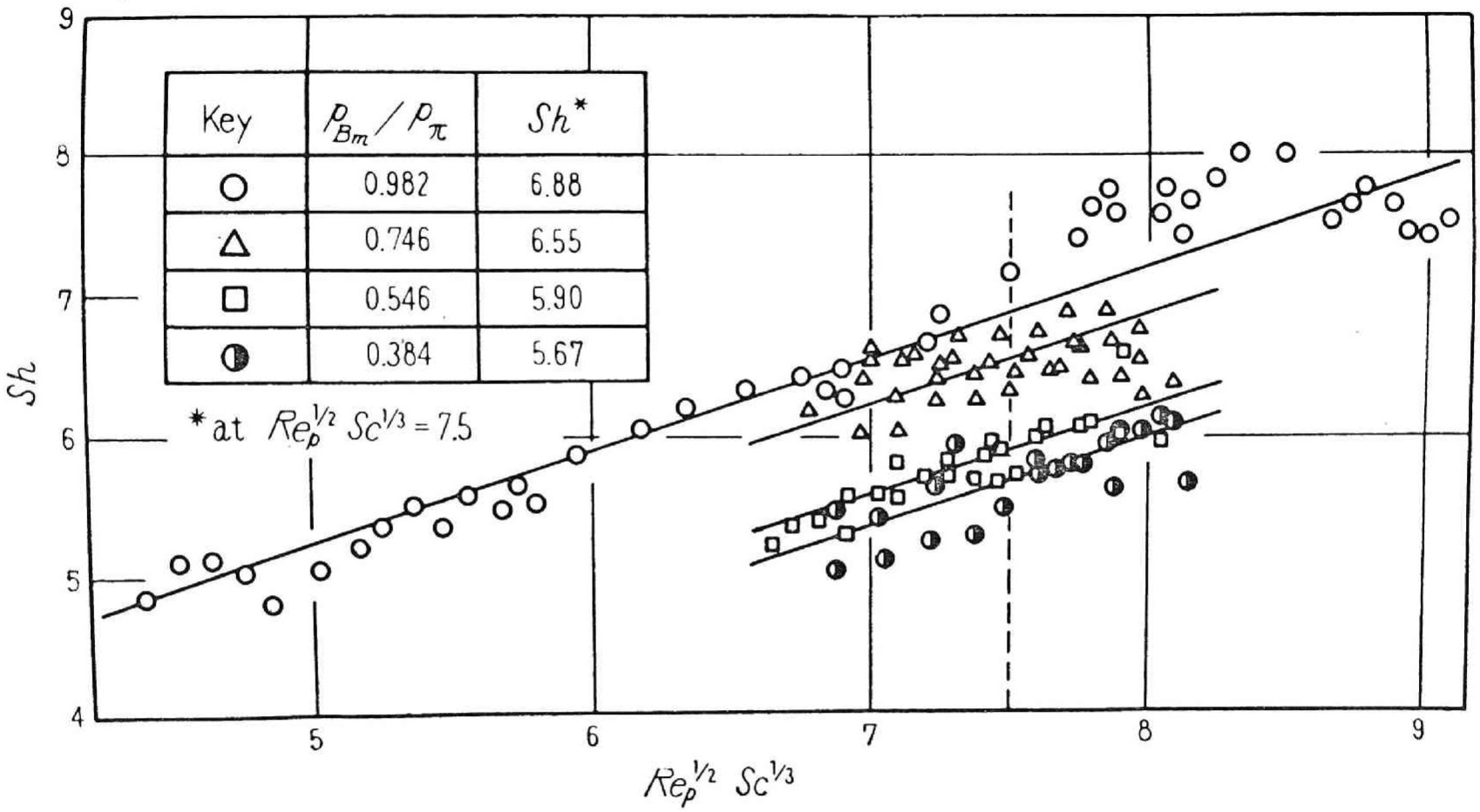

Fig. (6-1-6) Correlation of Sh vs. $Re_p^{1/2}Sc^{1/3}$

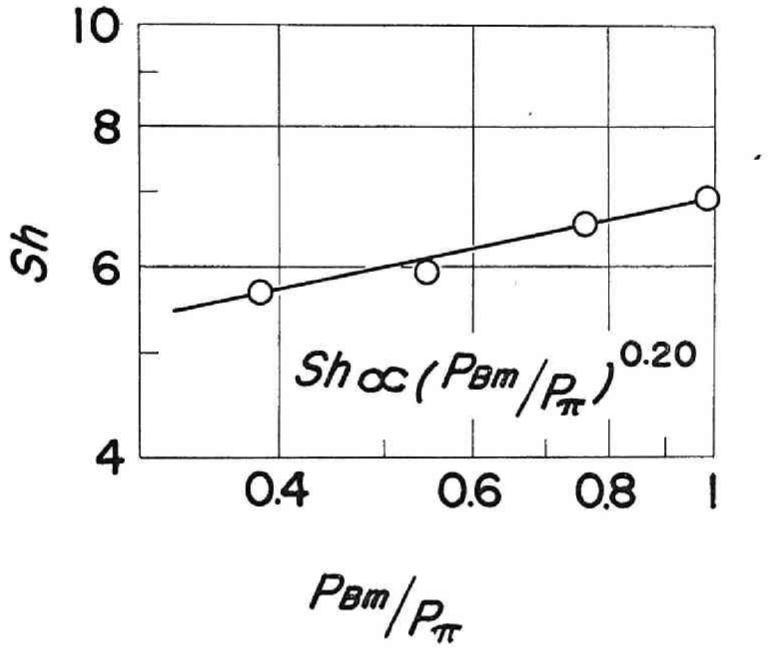

Fig. (6-1-7) Correlation of Sh vs. p_{Bm}/p_{π}

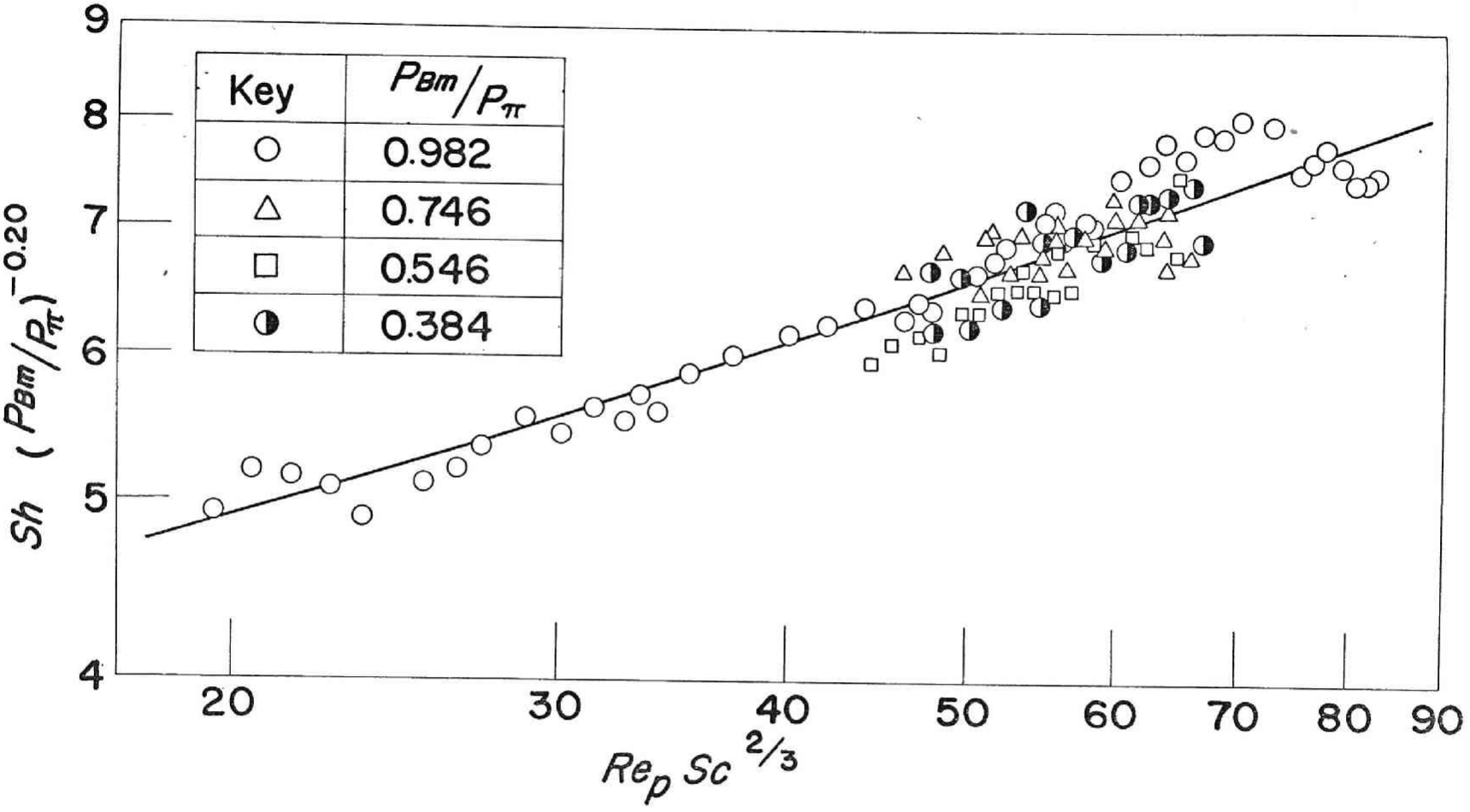

Fig. (6-1-8) Correlation of $Sh(p_{Bm}/p_{\pi})^{-0.20}$ vs. $Re_p Sc^{2/3}$

in Table (6-1-2). The correlation of Sh vs. $Re_p^{1/2}Sc^{1/3}$ obtained in the present work is shown in Fig. (6-1-6). It is shown that as the decrease of p_{Bm}/p_π, the values of Sh corresponding to the same value of $Re_p^{1/2}Sc^{1/3}$ decrease. The values of Sh at $Re_p^{1/2}Sc^{1/3} = 7.5$ are plotted in Fig. (6-1-7), and it may be said that Sh is proportional to $(p_{Bm}/p_\pi)^{0.20}$. The correlation of $Sh(p_{Bm}/p_\pi)^{-0.20}$ vs. Re_pSc $Re_pSc^{2/3}$ is shown in Fig. (6-1-8). Then the following equation was obtained within ±15% error.

$$\left(\frac{k_G M_m D_p p_{Bm}}{\rho D_v}\right)\left(\frac{p_{Bm}}{p_\pi}\right)^{-0.20} = 2.0 + 0.65\left(\frac{D_p G}{\mu}\right)^{1/2}\left(\frac{\mu}{\rho D_v}\right)^{1/3} \qquad (6\text{-}1\text{-}12)$$

3. Comparison with Previous Works

About the heat transfer coefficient h_c, there has been no influence of composition of gas on Nu and the equation for Nu obtained in the present work agreed practically with the one of Ranz et al.[2] Hence these results do not agree with the one of Cairns et al.[7] who have observed the effect of (p_{Bm}/p_π) on Nu. The present result differs from the one of Wenzel et al.[4] also, by which there was difference between super-heated steam and air.

About the mass transfer coefficient k_G, the value of k_G was in proportion to $(p_{Bm}/p_\pi)^{-0.8}$ in the present work. The previous works are summarized in Table (6-1-3) from the

Table (6-1-3) Effects of partial pressure of non-diffusional component on mass transfer coefficient

Author	System	p_{Bm}/p_{π}	n*
Film theory			1
Hanks & McAdams[21]	Ammonia-air (Absorption)	0.35-0.94	1
Hinchley & Himus[22]	Water-air (Evaporation)	0.55-0.99	1
			0
Wade[23]	Water, acetone, benzene-air (Evaporation)	0.68-0.99	1
			0
Boelter, et al.[24]	Water-air (Evaporation)	0.5-0.99	0.75
Gilliland & Sherwood[25]	Water, solvent-air (Evaporation)	0.7-0.99	1
Cairns & Roper[7]	Water-air (Evaporation)	0.15-0.97	0.83
Westkaemper[8]	Tetrachloromethane-air (Evaporation)	0.30-1.0	(0.83)
Shulman & Delany[9]	Tetrachloromethane-air (Evaporation)	0.10-0.50	2/3
This work	Water-air (Evaporation)	0.38-0.98	0.80

* n : $k_G \propto p_{Bm}^{-n}$

view point of the effect of p_{Bm} on k_G. The experiments by Hanks et al.[21], Hinchley et al.[22], Wade[23], Boelter et al.[24] were not carried out for the purpose of investigation the effect of p_{Bm}, and these results have been rearranged by Cairns et al.[7], Hence may not have a high reliability. The work of Gilliland et al.[25] had no wide variation of p_{Bm} and the effect of p_{Bm} on k_G may not be so correct also. Cairns et al.[7] have obtained experimentally the results that $h_c \propto (p_{Bm}/p_\pi)^{-0.27}$ and n = 0.83 for k_G, in Table (6-1-3). Shulman et al.[9] have obtained that n = 2/3 for k_G using the packed column. The present result shows fairly good agreement with their results.

From Eqs. (6-1-9) and (6-1-12), the analogy between heat and mass transfer can be obtained. These two equations are shown on Fig. (6-1-9) and the results by previous workers for a single sphere are plotted on the same figure. The equations obtained in the present work show good agreement with those data for the wide range of $Re_p Pr^{2/3}$ or $Re_p Sc^{2/3}$.

Conclusion

For the purpose of determining the effects of the partial pressure of non-diffusional component on heat and mass transfer coefficients, the evaporations from a single water drop in the stream of super-heated steam and various steam-air mixtures were investigated experimentally. The

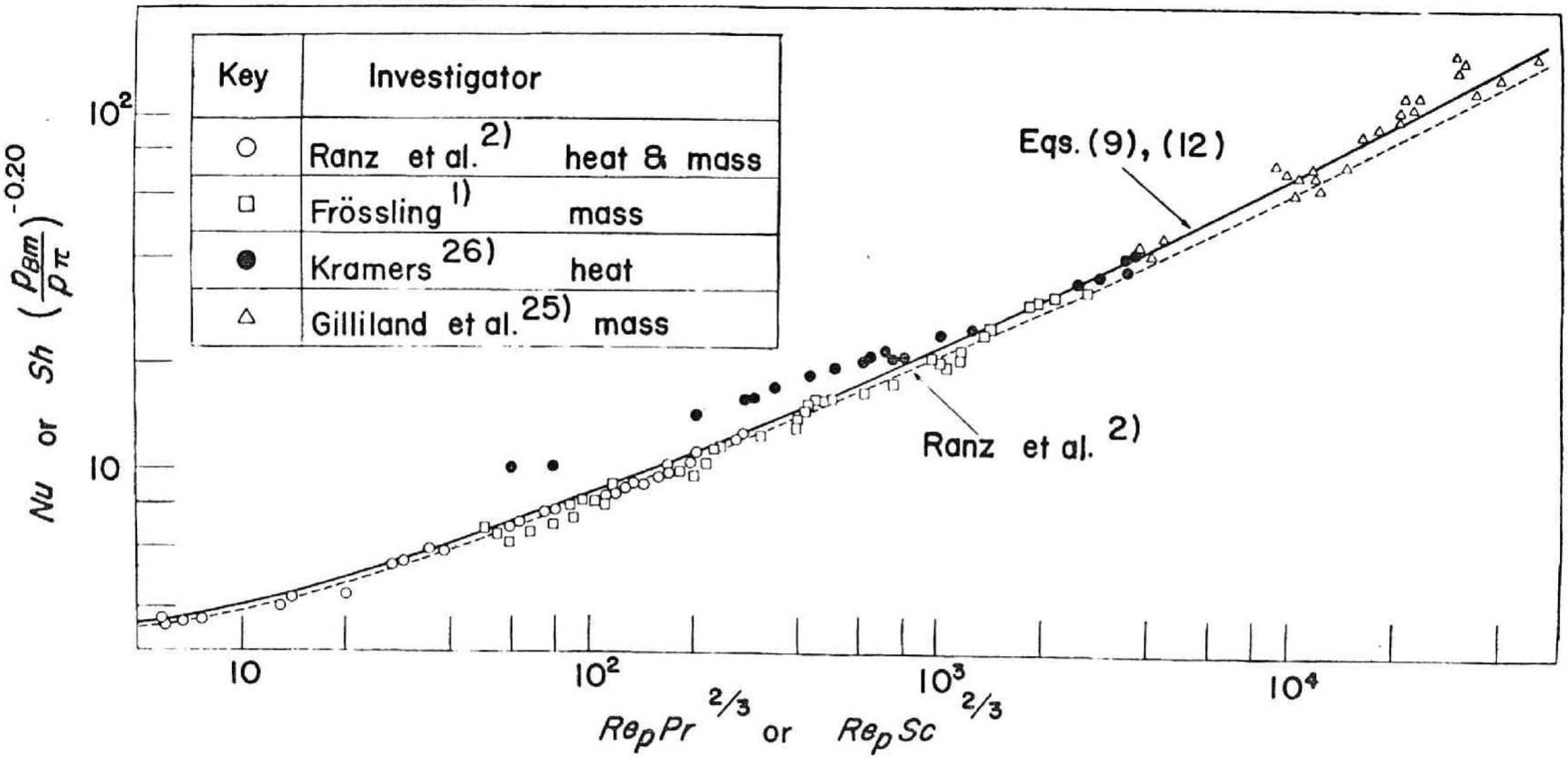

Fig. (6-1-9) Comparison of Eqs.(6-1-9) and (6-1-12) with other works

heat and mass transfer coefficients were calculated from the evaporation rates, and Eqs. (6-1-9) and (6-1-12) were obtained.

Appendix

The schematic look of a fine glass rod submerged into a water drop is shown in Fig. (6-1-A). The following assumptions may be permitted for this case.
(i) The length of the rod is infinite. (ii) The temperature distribution of the rod on radial direction is negligible. (iii) The heat transfer coefficient between the rod and gas is constant and far smaller than the one between the rod and water. (iv) The temperature of the gas is constant along the rod.

From these assumptions, the diffential equation of stationary heat conduction is obtained as follows:

$$\frac{d^2 t_k}{dx^2} - \frac{2 r_k h_k}{k_k A_k}(t_k - t_v) = 0$$

$$\text{B.C.} \quad x = 0 \; ; \quad t_k = t_l \qquad x = \infty \; ; \quad t_k = t_v \tag{a}$$

Solving Eq. (a),

$$t_k = t_v - (t_v - t_l) e^{-\sqrt{\alpha} x} \tag{b}$$

$$\alpha = 2 h_k / k_k r_k \tag{c}$$

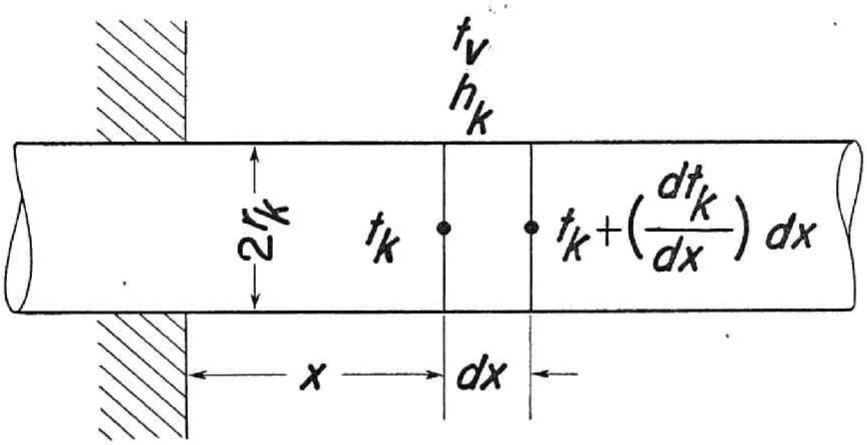

Fig. (6-1-A) Schematic diagram of fine glass rod

Differentiating Eq. (b) with x gives Eq. (d).

$$\left.\frac{dt_k}{dx}\right|_{x=0} = (t_v - t_l) \qquad (d)$$

Eq. (6-1-8) is derived from Eq. (d).

Nomenclature

A	= surface area of drop	[cm^2]
C_p	= specific heat of gas at constant pressure	[cal/g·°C]
D_p	= diameter of drop	[cm]
D_v	= diffusivity of water vapor in air	[cm^2/sec]
F_A	= angle factor for radiation	[-]
F_E	= emissivity factor for radiation	[-]
G	= mass flow rate of gas	[g/cm^2· sec]
h_c	= heat transfer coefficient	[cal/cm^2· sec·°C]
h_c'	= apparent value of heat transfer coefficient	[cal/cm^2· sec·°C]
h_k	= heat transfer coefficient between the glass rod and the main gas stream	[cal/cm^2· sec·°C]
j_h	= j-factor for heat transfer	[-]
k	= thermal conductivity of gas	[cal/cm·sec·°C]
k_G	= mass transfer coefficient	[mol/cm^2· sec·mmHg]
k_k	= thermal conductivity of the glass rod	[cal/cm·sec·°C]
M	= molecular weight	[g/mol]
N	= correction factor of Ackermann's effect	[-]

Nu = $h_c D_p/k$, Nusselt number [-]

p = partial pressure [mmHg]

P = $C_p \mu/k$, Prandtl number [-]

q = rate of heat transfer to drop [cal/cm^2. sec]

q_c = rate of heat transfer to drop by conduction and convection of gas [cal/cm^2. sec]

r = radius [cm]

Re_p = $D_p G/\mu$, Reynolds number [-]

Sc = $\mu/\rho D_v$, Schmidt number [-]

Sh = $k_G M_m D_p p_{Bm}/\rho_m D_v$, sherwood number [-]

t = temperature [°C]

V = volume of drop [cm^3]

x = distance [cm]

Greek letters

Δ = difference in value of variable across the transfer path [g/cm·sec]

μ = viscosity of gas [g/cm·sec]

θ = time [sec]

λ = latent heat of vaporization [cal/g]

ρ = density [g/cm^3]

Subscripts

A = for diffusing component

B = for diffusing component

k = for glass rod

l = for liquid

m = average value in the transfer path for gas mixture

r = for radiation

s = for wall of test section

T = total value

v = for gas mixture

π = total value

0 = at the interface

∞ = in the main stream

Literature Cited

1) N. Frössling; Gerlands Beiter. Geophys., 52, 170 (1938)

2) W. E. Ranz and W. R. Marshall; Chem. Eng. Progr., 48 141, 173 (1952)

3) J. C. Chu, A. M. Lane and D. Conklin; Ind. Eng. Chem., 45, 1583 (1953)

4) L. Wenzel and R. R. White; Ind. Eng. Chem., 43, 1829 (1951)

5) J. C. Chu, S. Finelt, W. Hoerrner and M. Lin; Ind. Eng. Chem., 51, 275 (1959)

6) E. Pohlhausen; Z. angew. Math. u. Mech., 1, 115 (1921)

7) R. C. Cairns and G. H. Roper; Chem. Eng. Sci., 3, 97

(1954)

8) L. E. Westkaemper and R. R. White; A. I. Ch. E. Journal, 3, 69 (1957)

9) H. L. Shulman and L. J. Delany; A. I. Ch. E. Journal, 5, 290 (1959)

10) E. Hori; J. Japan Soc. Aero. Space Sci., 11, 229 (1963)

11) J. D'Ans and E. Lax; Taschenbuch Fur Chemiker u. Physiker, 1108 (1949)

12) W. Licht and D. G. Stechert, Jr.; J. Phys. Chem., 48, 23 (1944)

13) K. Sato; "Bussei-Josu-Suisanho", p. 51, 123 (1961)

14) F. G. Keyes; Tech. Rept., 37, Project Squid. (Apr. 1, 1952)

15) "Kagaku-Kogaku-Binran" p. 41, 54 (1961)

16) H. H. Landolt and R. Börnstein; Zahlenwerte u. Funktionen aus Physik. Chemie, 4 Band, 1 teil, p. 543, 615 (1955)

17) R. Toei, S. Hayashi, T. Kai and J. Hasegawa; Chem. Eng., Japan, 25, 814 (1961)

18) U. Sano and S. Nishikawa; Chem. Eng., Japan, 28, 275 (1964)

19) J. O. Hirschfelder, R. B. Bird and E. L. Sportz; J. Chem. Phys., 16, 968 (1948)

20) R. B. Bird, W. E. Stewart and E. N. Lightfoot; Transport Phenomena, 667 (1960)

21) W. V. Hanks and W. H. Mcadams; Ind. Eng. Chem., 21, 1034 (1929)

22) J. W. Hinchley and G. W. Himus; Trans. Inst. Chem. Engr. (London,) 2, 57 (1924)

23) S. H. Wade; Trans. Inst. Chem. Engr. (London,) 20, 1 (1942)

24) L. M. K. Boelter, H. S. Gordon and J. R. Griffin; Ind. Eng. Chem., 38, 596 (1946)

25) E. R. Gilliland and T. K. Sherwood; Ind. Eng. Chem., 26, 516 (1934)

26) H. Kramers; Physica, 12, 61 (1946)

Section 6-2 Heat Transfer Coefficients on the Super-heated Steam Drying of Porous Solids

There have been several discussions whether there is a difference between the heat transfer coefficient in super-heated steam drying and in the usual hot air drying. It was confirmed in the previous section 6-1[3] that there was no difference in the case of evaporation from a single droplet in the stream of steam-air mixtures. The present investigation was undertaken to examine the effect of the composition of gas on the heat transfer coefficient between the gas stream and the surface of the porous solid.

In the stream of super-heated steam and various steam-air mixtures, the drying of a single sphere of biscuit ware and through-flow drying of a fixed bed of spheres were performed. From the constant drying rate, the heat transfer coefficients between the spheres and the stream were obtained. The physical properties of the spheres used are shown in Table (6-2-1). The spheres of the fixed bed were made by baking a mixture of clay and sawdust.

The correlation of Nu vs. $Re_p^{1/2}Pr^{1/3}$ obtained from the constant drying rate of the single sphere is shown in Fig. (6-2-1.a). The results show no significant difference from the gas composition and agree with the following experimen-

Table (6-2-1) Spherical biscuit ware used

Experiment	Single sphere	Fixed bed
Material	clay	caly and sawdust
Size D_p [cm ϕ]	1.00 ∿ 1.85	0.282 ∿ 0.909
Bulk density [g/cm^3]	1.63	1.47
Porosity [-]	0.36	0.50
Void fraction ε [-]	-	0.412 ∿ 0.462

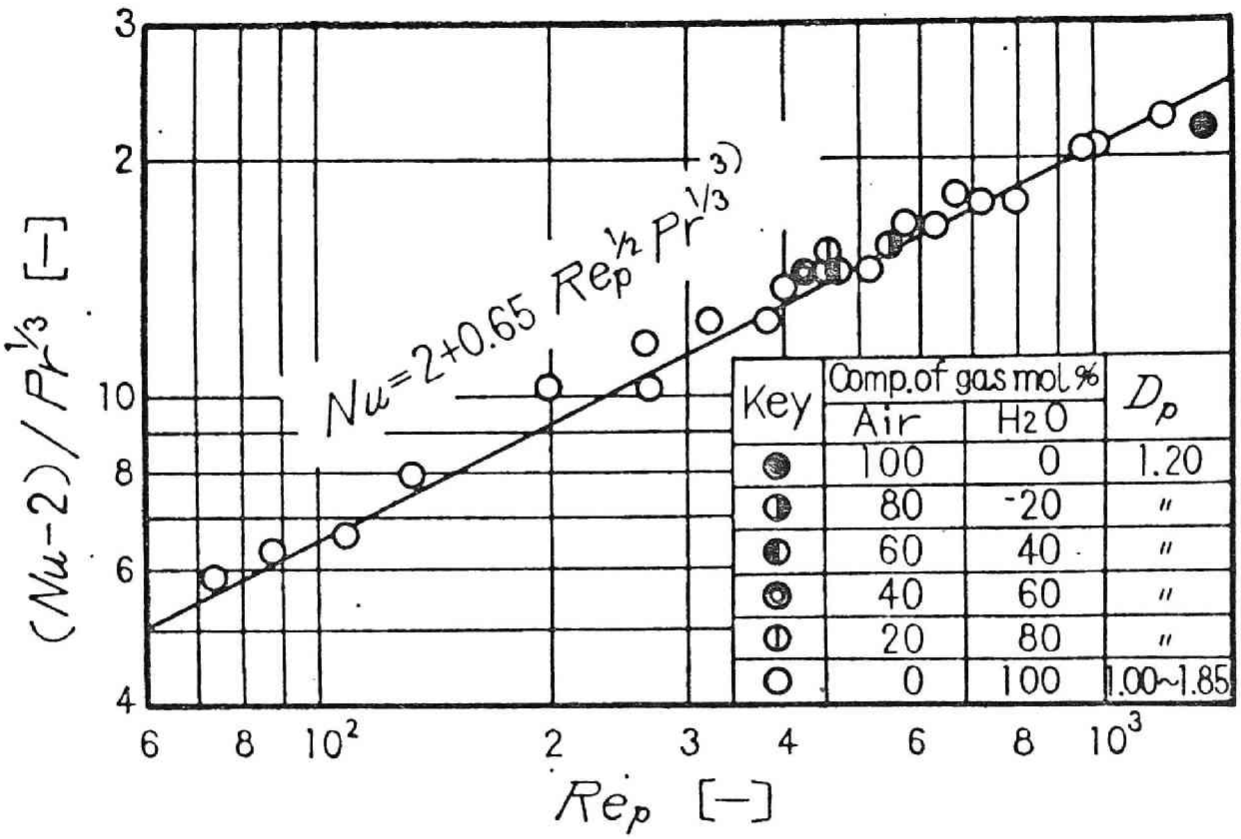

for single sphere

Fig. (6-2-1.a) Experimental results of heat transfer coefficient

tal formula obtained from the single water droplet evaporation in the stream of steam air mixtures (Re_p = 9 ∿ 120) by the authors[3].

$$Nu = 2 + 0.65Re_p^{1/2}Pr^{1/3} \quad (Re_p = 73 \sim 1400) \qquad (6\text{-}2\text{-}1)$$

The correlation of j_h vs. Re_p obtained from the through through-flow drying of a fixed bed using super-heated steam only is shown in Fig. (6-2-1.b), and practically agrees with the following experimental formulas obtained by Wilke et al.[5] and Gamson et al.[2].

$$j_h = 1.95Re_p^{-0.51} \qquad Re_p < 350 \qquad (6\text{-}2\text{-}2)\ [5]$$

$$j_h = 1.06Re_p^{-0.41} \qquad Re_p > 350 \qquad (6\text{-}2\text{-}3)\ [2]$$

As a result, it was confirmed that the heat transfer coefficients on the super-heated steam drying of spherical porous solids are not different from those on air drying, under moderate drying conditions.

Literature Cited

2) Gamson, B. W., Thodos, G. and Hougen, O. A.: Trans. Am. Inst. Chem. Eng., 39, 1 (1943)

3) Toei, R., Okazaki, M., Kubota, K., Ohashi, K., Kataoka, K. and Mizuta, K.: Chem. Eng. (Japan), 30, 43 (1966)

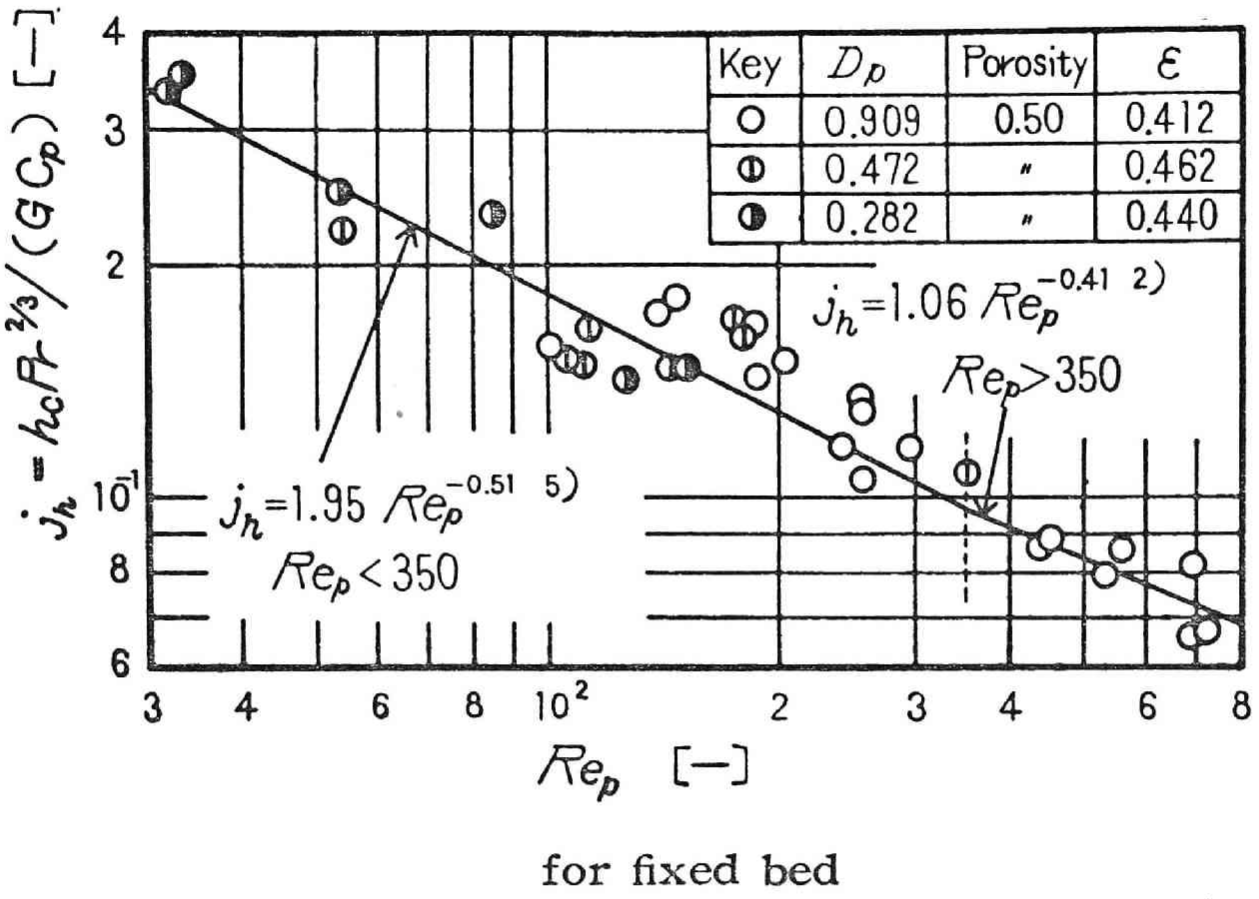

Fig. (6-2-1.b) Experimental results of heat transfer coefficient

5) Wilke, C. R. and Hougen, O. A.: Trans. Am. Inst. Chem. Eng., 41, 445 (1945)

Section 6-3 Drying Characteristics of a Porous Solid in Super-heated Steam Drying

The super-heated steam drying of solid is coming to play a very important part in drying technique. It is interesting to investigate the drying process during super-heated steam drying, but there has been little work published in this field. Therefore the present work was undertaken in order to evaluate the drying mechanism, especially the drying characteristics of a porous sphere in the stream of super-heated steam[1,2].

The properties of the sample used are shown in Table (6-3-1). This sample had considerably fine pores about 100Å in radius.

The characteristic curve of the drying rate obtained at various constant drying rates are shown in Fig. (6-3-1). As the constant drying rate is the smaller, the constant drying rate period continues on to the lower moisture content. The effects of the gas phase composition on the drying rate characteristics under the same constant drying rate are shown in Fig. (6-3-2). There were differences between air drying and super-heated steam drying in the drying rate characteristic curves. The constant drying rate period of super-heated steam drying continued on longer than

Table (6-3-1) Spherical biscuit ware used

Material	Clay
Diameter [cm]	1.20
Density (true) [g/cm^3]	2.57
Density (bulk) [g/cm^3]	1.63
Porosity [-]	0.366
Thermal conductivity [kcal/m·hr·°C]	ψ = 0 : 0.383
	ψ = 1 : 1.10
Thermal capacity [cal/g.°C]	0.217

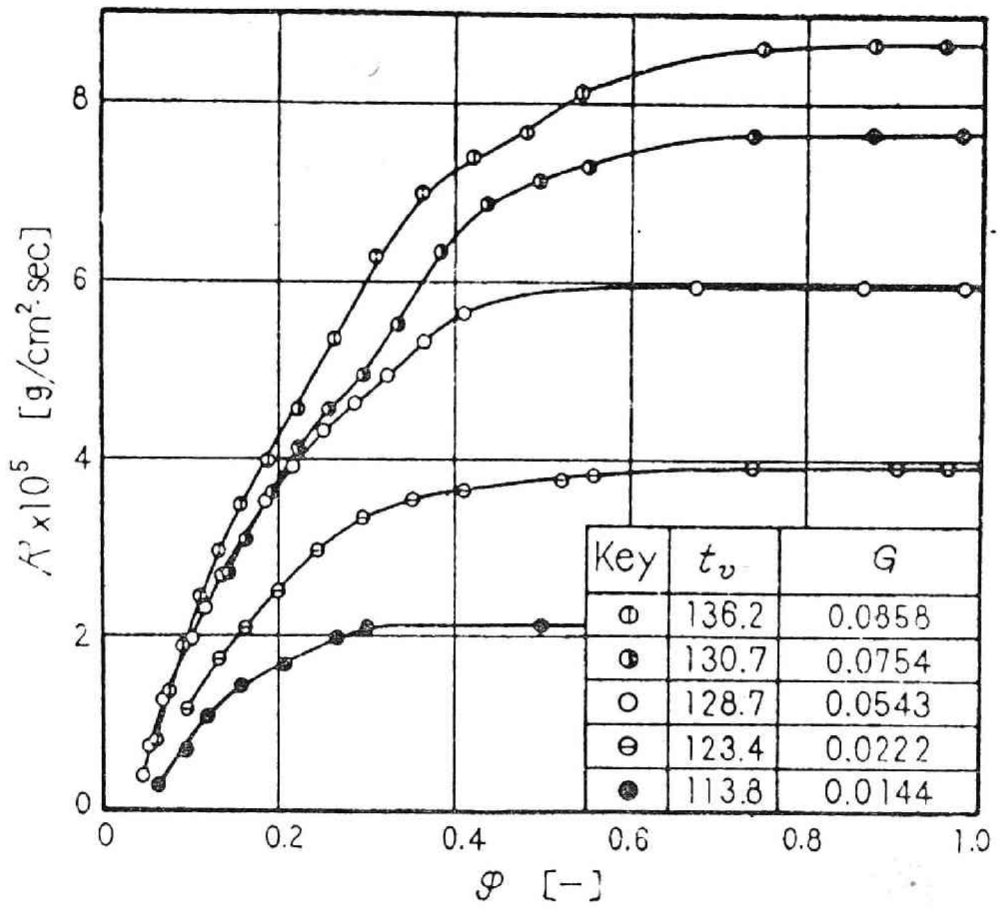

Fig. (6-3-1) Drying characteristic curves of single sphere by super-heated steam

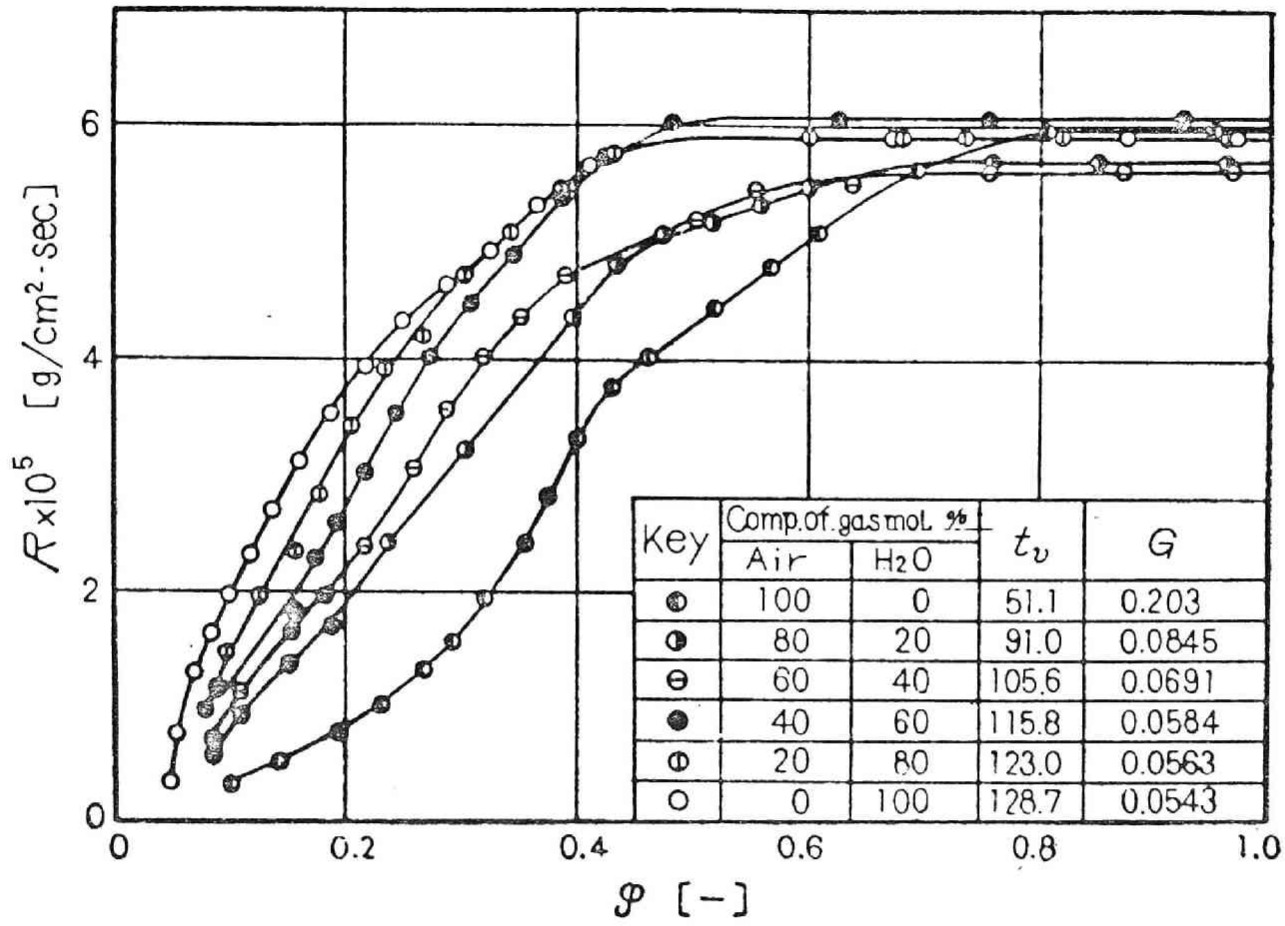

Fig. (6-3-2) Effect of gas phase composition on drying characteristic curve (single sphere)

the one of air drying. The falling drying rate was affected by the gas phase composition also.

The falling drying rate at the same water content becomes higher as the fraction of steam increases and the maximum value was taken in the super-heated steam vapor. So it may be concluded that the super-heated steam drying can save largely the drying time. About the precise drying mechanism, the study of moisture transfer in the bodies should be continued.

Nomenclature

D_p = diameter of sphere [cm ϕ]

G = mass flow rate of gas [g/cm^2. sec]

R = drying rate [g/cm^2. sec]

t = temperature [C°]

ψ = volumetric water fraction based on total pore volume [-]

Subscripts

v = vapor

Literature Cited

1) Toei, R., Okazaki, M., Kimura, M. and Ueda, H.: Chem. Eng. (Japan), 30, 947 (1966)

2) Toei, R., Okazaki, M., Kubota, K., Ohashi, K., Kataoka, K. and Mizuta, K.: Chem. Eng. (Japan), 30, 43 (1966)

CHAPTER 7

A SIMPLE CALCULATIONS OF PLANE POISEUILLE FLOW RATE OF RAREFIED GAS

Introduction

Previous works on the flow of rarefied gases between two infinite parallel plates (plane Poiseuille flow) have not undertaken so many compared to those on the tube flow. Gaede[4], Dong[2] and recently Iuchi et al.[6] reported the experimental results of flow rates, which agree with each other in the range of relatively low Knudsen number, however are scattered in the range of high Knudsen number. Some theoretical analysis by means of the non-equilibrium gas kinetic theory has been done by several workers. Takao[12] has obtained an approximate solution of the B-G-K equation, and after him the same equation was solved numerically by Cercignani & Daneri[1], and analytically by Huang & Stoy[5] based on the discrete ordinate method.

Further analytical solutions of Maxwell moment equation using the two-sided Maxwellian model were obtained by Liu[9] and Kanki & Iuchi[7]. However, on the other hand, the analysis using the elementary kinetic theory, which might be more convenient for technical purposes than the non-

equilibrium kinetic theory, has not been performed by any one other than Iuchi et al[7] whose solution includes an arbitrary parameter to be determined experimentally. The purposes of the present work are to consider the flow mechanism and to derive a simple analytical solution in which there is no experimental parameter.

1. Theoretical Treatment

1.1 Course of analysis

As in the previous analysis of rarefied gas flow through long tube by the elementary theory, the flow rate between two parallel plates may be divided into the three flow terms, those are the term of viscous flow, ship flow and free molecule flow. The former two terms can be easily determined by applying a correction factor introduced by Fryer[3] on tube flow. On the calculation of the last term, however the Smoluckowsky's method[8] which is useful to tube flow cannot be applied because of the divergency of it in this case. Hence it is calculated as the sum of the skin and bulk self-diffusion term.

In the course of the calculation, the following assumptions were introduced.

1. The collision of gas molecule on the wall is diffusely.

2. The pressure gradient in the direction of flow is sufficiently small to give the expression of

$$p' = p + x\frac{dp}{dx} \quad \text{or} \quad n' = n + x\frac{dn}{dx}$$

3. The two parallel plates are infinitely large.
4. Assuming that the degree of non-equilibrium is very small, the velocity distribution function of gas molecules approximately follows the Maxwell distribution function.

1.2 Viscous and slip flow term

Fig. (7-1) shows the macro-scopic flow pattern in the regime of slip flow. As in the figure, there is a slip of velocity just on the wall, and further it might be thought that the velocity profile of Poiseuille flow caused by the viscosity of gas is built up on its slip velocity.

The pV flow rate $Q'[cm^3 \cdot atm/sec \cdot cm^2]$ is given as followings, in the usual manner. From balancing of forces acting on the surface of the shell denoted by hatching in Fig. (7-2), the following equations are given.

$$\mu\frac{d^2u}{dz^2} = \frac{dp}{dz} \tag{7-1}$$

Boundary conditions

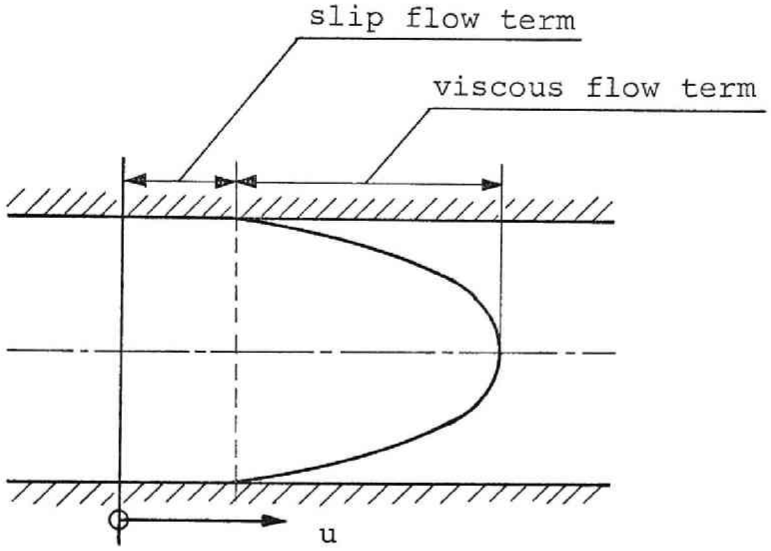

Fig. (7-1) Profile of macroscopic velocity

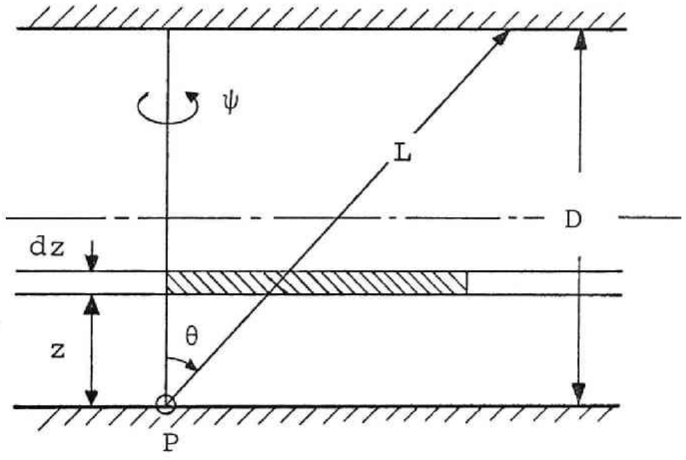

Fig. (7-2) Plane poiseuille flow

$$\text{at} \quad z = \frac{D}{2} \quad ; \quad \frac{du}{dz} = 0 \tag{7-2}$$

$$\text{at} \quad z = 0 \quad ; \quad v = \zeta \frac{du}{dz} \tag{7-3}$$

The solution of Eq. (7-1) with Eq's (7-2) and (7-3) is

$$u = - \frac{1}{2\mu} \frac{dp}{dx}(zD - z^2 + \zeta D) \tag{7-4}$$

Then the flow rate Q' is

$$Q' = \frac{2p}{D}\int_0^{D/2} udz = - \frac{D^2 p}{12\mu} \frac{dp}{dx}(1 + \frac{6\zeta}{D}) \tag{7-5}$$

By substituting the Chapman-Enskog's solution of viscosity, Eq. (7-6), the Knudsen's expression of slip velocity Eq. (7-7) and Eq. (7-8) into Eq. (7-5), Eq. (7-9) is obtained.

$$\mu = 0.499\rho\bar{v}\lambda \simeq \frac{1}{2}\rho\bar{v}\lambda \tag{7-6}$$

$$\zeta = \frac{4}{3}\lambda \tag{7-7}$$

$$\rho = pM/RT \ , \quad \bar{v} = 2\sqrt{\frac{2RT}{M\pi}} \ , \quad \delta = D/\lambda \tag{7-8}$$

$$Q' = Q'_p + Q'_s = - \frac{D\delta}{24} \sqrt{\frac{2\pi RT}{M}}(1 + \frac{8}{\delta}) \frac{dp}{dx} \tag{7-9}$$

where the first term of right hand side is the viscous flow term and the second is the slip flow term. However it should be noted that Eq. (7-9) might be valid only for the bulk of flow, that is the gas molecules having a macroscopic velocity "u", and consequently we must make some

corrections on it. For this purpose, the following correction has been proposed by Fryer[3] who performed a theoretical analysis on the tube flow. Concerning with the slip flow term, he thought that molecules whose last collision was at the wall can have no slip velocity (it being assumed that such molecules are diffusely reflected with no average flow velocity). When N_i and N_w denote the number of intermolecular and wall collision respectively, the fraction of such molecules may be evaluated as the ratio of N_w to $(N_w + N_i)$. The remaining molecules, whose fraction F is $N_i/(N_w + N_i)$, are the only molecules to possess the calculated slip velocity, and hence the corrected slip flow term is given as FQ'_s. To correct the viscous flow term, Fryer applied the factor proposed by Scott & Dullien[11] who had thought that the molecules which, on the average, did not collide with other molecules between two wall collisions should be excluded to obtain the net term of viscous flow.

For the present analysis, the former correction factor, F, introduced by Fryer[3] to correct both the terms, was applied taking into account of the following considerations. In the elementary theory it is always assumed that the velocity distribution obeys the Maxwell's law shown by Eq. (7-10).

$$f = n\left(\frac{m}{2\pi kT}\right)^{2/3} \exp\left[-\frac{m}{2kT}\{(v_x - v_{x0})^2 + v_y^2 + v_z^2\}\right] \quad (7\text{-}10)$$

where as the motion of gas is in one dimensional, the macroscopic velocities v_{y0} and v_{z0} disappear. v_{x0} in Eq. (

7-10) represents the macroscopic velocity which is concerned with the flow pattern caused by the viocosity of the gas and the slip velocity at the wall. The motion of gas under a pressure gradient may be expressed by the elementary theory as the summation of the macro seopic flow contributed by V_{x0} and the diffusional flux caused by the gradient of number density of molecules. The generation of macro scopic velocity results from the viscosity of gas, that is the changes of momentum by intermolecular collisions. According to the mentioned above, it might be reasonably regarded that molecules whose last collision was at the wall had no macroscopic velocity. The molecules having V_{x0} should be the ones whose last collision is an intermolecular collision. The problem that how many intermolecular collisions are required to get perfectly V_{x0} is difficult to solve only by elementary theory. However it is well said that a group of molecules having an appreciabll deviation from the Maxwell's distribution approaches close to it after only one random intermolecular collision for each molecule. Therefore in the present calculation it was assumed that one collision was enough to get V_{x0}. According to above consideration it is reasonably concluded to apply the Fryer's factor to evaluate both the two flow terms.

The total number of wall collisions per unit length and width of the channel in unit time is $n\bar{v}b/2$, and the total number of intermolecular collisions is $Dbn\bar{v}/\lambda$. Hence the proportion of molecules at any instant whose last collision was at the wall is given as follows.

$$\frac{n\bar{v}b/2}{(n\bar{v}b/2) + (Dn\bar{v}b/\lambda)} = \frac{1}{1 + 2\delta} \tag{7-11}$$

Then the correction factor F for plane Poiseuille flow is

$$F = 1 - 1/(1 + 2\delta) = 2\delta/(1 + 2\delta) \tag{7-12}$$

Therefore the corrected terms of viscous and slip flow are given by the following equations, respectively.*

$$Q_{PC}/Q_A = FQ'_P/Q_A = \frac{\pi}{32}\delta\left(\frac{2\delta}{1 + 2\delta}\right) \tag{7-13}$$

$$Q_{SC}/Q_A = FQ'_S/Q_A = \frac{\pi}{4}\left(\frac{2\delta}{1 + 2\delta}\right) \tag{7-14}$$

where Q_A is the rate of plane Poiseuille flow derived by formalized application of free molecule flow through long tube.

---

*) Since the molecules whose last collision are at the wall distribute more densely near the wall than near the center, strictly speaking, it is incorrect to mutiply directly Eq. (7-9) by the correction factor. But the factor does not become effective untill δ reaches to the extent $\delta \leqq 3$ where the distribution of macroscopic velocity considerably approaches to uniform. Hence the effect of the distribution of the molecules might be negligible.

$$Q_A = -\frac{8}{3\pi}\frac{S}{s}\sqrt{\frac{2\pi RT}{M}}\frac{dp}{dx} = -\frac{4D}{3\pi}\sqrt{\frac{2\pi RT}{M}}\frac{dp}{dx} \tag{7-15}$$

If the factor proposed by Scott & Dullien[11], instead of the above factor, is applied, the flow terms can be expressed as follows. The fraction of molecules engaged on wall-to-wall paths to total number of molecules which collide at a point P of the wall as shown in Fig. (7-2), and are reflected diffusely is given as Eq. (7-16).

$$F_p = \int_0^{\frac{\pi}{2}}\int_0^{\frac{\pi}{2}} \sin\theta\cos\theta e^{-(\delta/\cos\theta)}\, d\theta d\psi \Big/ \int_0^{\frac{\pi}{2}}\int_0^{\frac{\pi}{2}} \sin\theta\cos\theta d\theta d\psi$$

$$= (1-\delta)e^{-\delta} - \delta^2 Ei(-\delta) \tag{7-16}$$

where

$$Ei(-\delta) = -\int_{\delta}^{\infty}\frac{e^{-t}}{t}dt = \log\delta + \gamma + \sum_{r=1}^{\infty}\frac{(-1)^r\delta^r}{r\, r!} \tag{7-17}$$

Then the viscous and slip flow terms are

$$Q_{PP}/Q_A = \frac{\pi}{32}\delta(1 - F_p) \tag{7-18}$$

$$Q_{SP}/Q_A = \frac{\pi}{4}\delta(1 - F_p) \tag{7-19}$$

1.3 Self-diffusion terms

In the former section, the flow rates concerned to the macroscopic velocity $\underline{v_0}$ of the Maxwell distribution were

calculated. Then let us consider the flow caused by the gradient of number density, n. The molecules passing across an element of cross section of the channel are divided into the molecules which come flying directly from the wall where they have collided and the ones whose last collision are an intermolecular collision. Then, let us name the flux of the first molecules as the skin self-diffusion term and the second as the bulk self-diffusion term.

1.3.1 Skin self-diffusion term

Consider the flow of molecules across an arbitrary cross section of the channel and consider first the flow across an element of area dS of this cross section, as shown in Fig. (7-3). These molecules that cross dS come from various points on the wall, where they underwent reflection; let us select those that come from an element dS' on the wall distant x from the cross section, and also distant r' from dS in a direction making angles θ with the normal to dS and α with the nomal to dS', respctively. As molecules strike dS' they will leave it after diffuse reflection in the same manner as if they came from a gas in equilibrium with density n' and mean speed $\bar{v}$ of the gas in the neighborhood of dS', and

$$dN = \frac{\bar{v}F}{4\pi} n' \bar{v} \cos\alpha d\Omega dS'$$

$$= \frac{\bar{v}F}{4\pi}\left(n + x\frac{dn}{dx}\right)\cos\alpha d\Omega dS' \qquad (7\text{-}20)$$

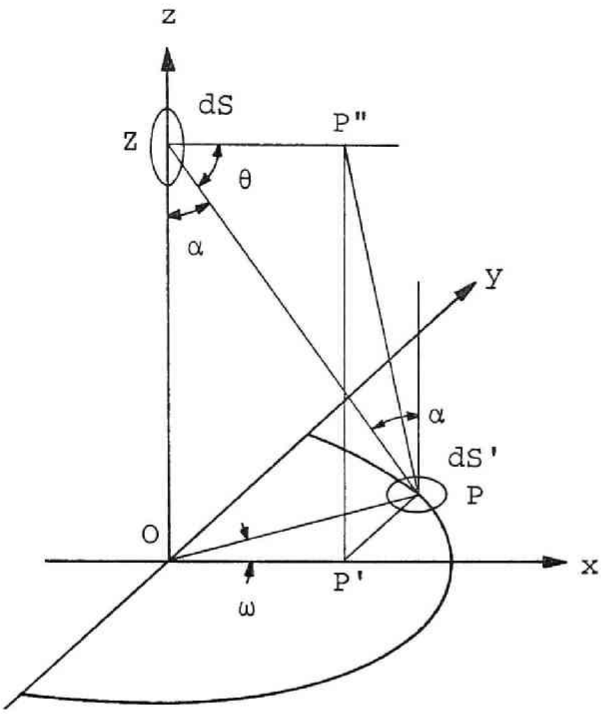

$\overline{OZ}$ = z
$\overline{OP'}$ = x
$\overline{OP}$ = r
$\overline{ZP}$ = r'
ZP"// OP'
P'P"// OZ

Fig. (7-3) Skin self-diffusion

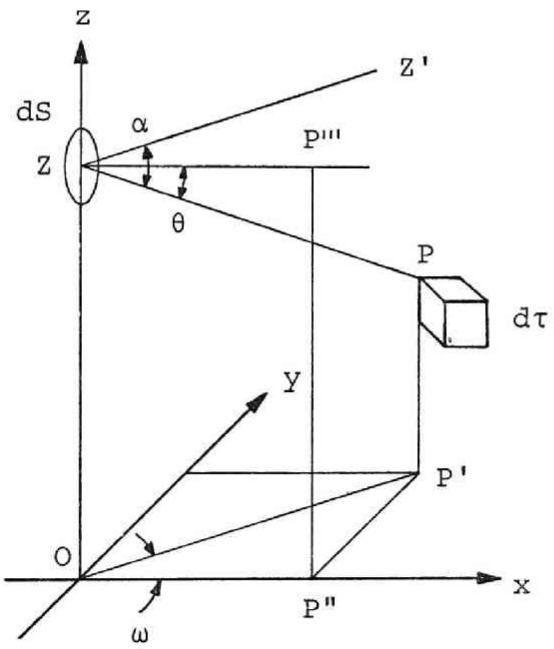

$\overline{OZ}$ = z
$\overline{OP''}$ = x
$\overline{ZP}$ = r
$\overline{OP'}$ = r'
ZZ'// ZP'''
P"P'''// P'P // OZ

Fig. (7-4) Bulk self-diffusion - 1

of them will pass downward through dS per second, here $d\Omega$ is the solid angle subtended by dS at dS', and F is the probability to arrive at dS from dS' without any intermolecular collision.

$$\begin{aligned} \overline{PP'} &= r\sin\omega \\ d\Omega &= \cos\theta dS/r' \\ \overline{ZP} &= r' = \sqrt{z^2 + r^2} \\ x &= r\cos\omega \\ \cos\alpha &= z/\sqrt{z^2 + r^2} \\ \cos\theta &= (r/r')\cos\omega \end{aligned} \tag{7-21}$$

Therefore the following equation is given.

$$dN = \frac{\bar{v}}{4\pi}\left(n + x\frac{dn}{dx}\right)\frac{zr\cos\omega}{(z^2 + r^2)^2} F\, dSdS' \tag{7-22}$$

where $dS = dydz$

and $dS' = rd\omega dr$

Method - 1A As the manner of Pollard & Present [10] for tube flow, let F be $\exp.(-r'/\lambda)$. Hence by integration of Eq. (7-22) over the whole surface, dN can be given as follows.

$$dN = \frac{\bar{v}}{4\pi}\frac{dn}{dx}dS\,\frac{zr^3\cos^2\omega}{(z^2 + r^2)^2}\exp\left(-\sqrt{z^2 + r^2}/\lambda\right)d\omega dr \tag{7-23}$$

In Eq. (7-23), n is omitted because in the last integration the term in n vanishes. The flow rate Q is,

$$Q = -\left(\frac{mRT}{M}\right)\frac{\bar{v}}{D\pi}\frac{dn}{dx}\int_0^D I(z)\,dz \tag{7-24}$$

where $I(z)$ in this case is

$$I(z) = \int_0^{\infty}\int_0^{\pi}\frac{zr^3\cos^2\omega}{(z^2 + r^2)^2}\exp\left(-\sqrt{z^2 + r^2}/\lambda\right)d\omega dr \tag{7-25}$$

After some calculations and dividing by Q_A, the flow rate Q_{DP} is given as follows

$$\frac{Q_{DP}}{Q_A} = \frac{3}{32}\left\{\left(\delta - 1 - \frac{2}{\delta} - \frac{2}{\delta^2}\right)e^{-\delta} + \frac{2}{\delta^2} + (\delta^2 - 4)\,Ei(-\delta)\right\} \tag{7-26}$$

Method - 2A For simplicity, instead of introducing the probability F, let us assume that all molecules have the same free path λ and further the molecules reflected on dS' whose distance from dS, r', is less than λ can pass through dS without any inter-moleculas collision, and the other molecules can never do so. Hence, the integral $I(z)$ becomes

$$I(z) = \int_0^{\sqrt{\lambda^2 - z^2}}\int_0^{\pi}\frac{zr^3\cos^2\omega}{(z^2 + r^2)^2}d\omega dr \tag{7-27}$$

Therefore the flow rate Q_{DMS} is

$$\frac{Q_{DMS}}{Q_A} = \frac{3}{8}\left(\frac{\delta^2}{4} - \ln\delta\right) \quad , \quad \delta \leq 1$$

$$= \frac{3}{32\delta^2} \quad , \quad \delta > 1 \tag{7-28}$$

Method - 3A Ignoring some errors in the range of large δ, by changing the upper bound of r in Eq. (7-27) from $\sqrt{z^2 - \lambda^2}$ to λ, the following equation is obtained.

$$\frac{Q_{DMC}}{Q_A} = \frac{3}{16}\ln\left(1 + \frac{1}{\delta^2}\right) \quad , \quad 0 \leqq \delta \leqq \infty \tag{7-29}$$

1.3.2 Bulk self-diffusion term

In the above section, we have evaluated the contribution of the molecules directly coming from the wall. Next let us consider the contribution of the molecules whose last collision is an intermolecular collision.

Method - 1B Corresponding to Method - 1A, in order to get the number of molecules coming just after intermolecular collisions in the volume element $d\tau$, as shown in Fig. (7-4), and passing downward through dS per second by the method of Pollard & Present[10].

We note that the collision frequency in $d\tau$ is $n\bar{v}d\tau/\lambda$, so that

$$dN = \left(\frac{n'\bar{v}}{\lambda}\right)\left(\frac{d\Omega}{4\pi}\right)e^{-r/\lambda}d\tau \tag{7-30}$$

where,

$$\begin{aligned} x &= r\cos\alpha\cos\omega \quad , \quad \cos\theta = \cos\alpha\cos\omega \\ d\tau &= r^2\cos\alpha d\alpha dr d\omega \quad , \quad d\Omega = \cos\theta dS/r^2 \end{aligned} \tag{7-31}$$

Hence

$$dN = \frac{\bar{v}dS}{4\pi\lambda}\left(n + x\frac{dn}{dx}\right)\cos^2\alpha\cos\omega\ e^{-r/\lambda}dr d\alpha d\omega$$

$$I(z) = \frac{1}{2\lambda}\int_0^{2\pi}\int_0^{\frac{\pi}{2}}\int_0^{z/\sin\alpha} r\cos^3\alpha\cos^2\omega\ e^{-r/\lambda}\,dr\,d\alpha\,d\omega \tag{7-32}$$

By substituting Eq. (7-32) into Eq. (7-24) and dividing by Q_A,

$$\frac{Q_{BP}}{Q_A} = \frac{3}{4\delta^2}\{\frac{2}{3}\delta - 1 + (1 + \frac{\delta}{3} + \frac{\delta^2}{3})e^{-\delta}\}$$

$$- \frac{\delta^2}{4}[\frac{\ln\delta}{4} - \frac{1}{16} + \frac{\gamma}{4} + \sum_{r=1}^{\infty}\{\frac{(-1)^r\delta^r}{r(r+4)\cdot r!}\}] \tag{7-33}$$

Method - 2B In Method - 2A, assuming that there is no distribution of free path and all molecules have the same free path λ, the contribution of the molecules coming from the part of the wall intercepted by the two parallel plates was evaluated. By extending this assumption on the evaluation of the flow contribution of the molecules whose last collision is an intermolecular collision, it can be calculated as the contribution of the molecules coming from the intercepted partial spherical plane with one path. In Fig. (7-5) the number of these molecules across downward through dS coming from dS' which is an element of the partial spherical plane is

$$dN = \frac{\bar{v}}{4\pi}(n + x\frac{dn}{dx})\,d\Omega dS'$$

$$= \frac{\bar{v}}{4\pi\lambda^2}(n + x\frac{dn}{dx})\cos\alpha\cos\omega dS dS' \tag{7-34}$$

where

$$x = \lambda\cos\alpha\cos\omega \quad , \quad \cos\theta = \cos\alpha\cos\omega \tag{7-35}$$

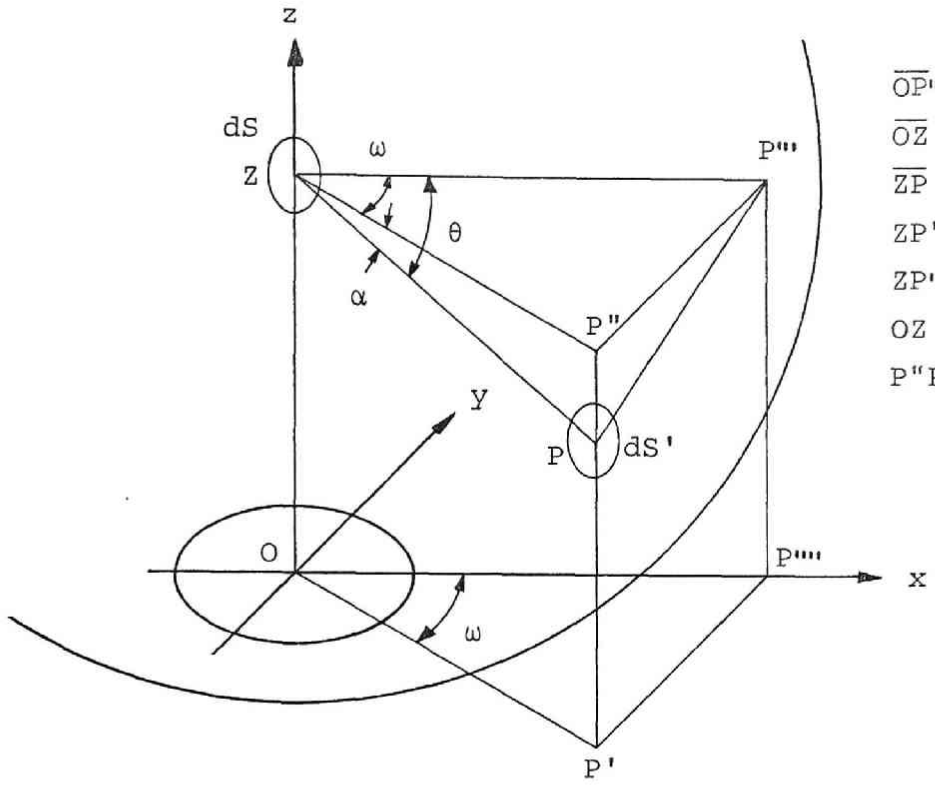

$\overline{OP''''} = x$
$\overline{OZ} = z$
$\overline{ZP} = \lambda$
ZP"// OP'
ZP'''// OP''''
OZ // P'P"// P'''P''''
P"P'''// P'P''''

Fig. (7-5) Bulk self-diffusion - 2

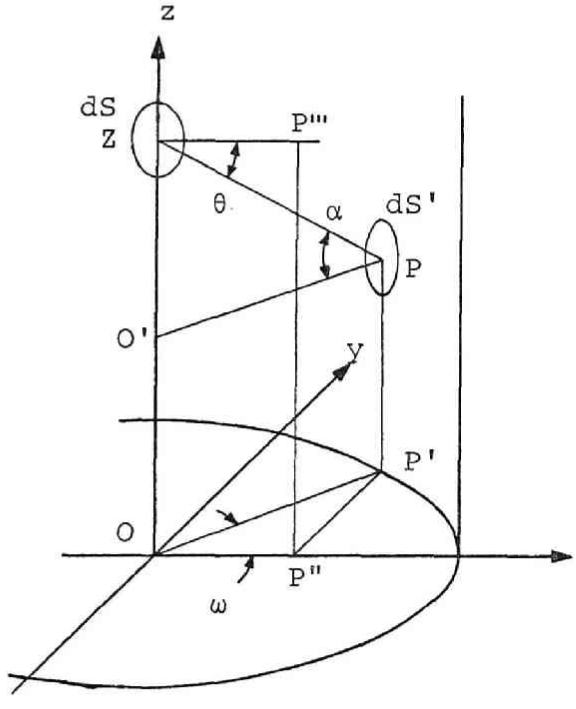

$\overline{OO'} = h$
$\overline{OZ} = z$
$\overline{OP"} = x$
$OP' = O'P = \lambda$
OP"// ZP'''
PP'// OO'
O'P // OP'

Fig. (7-6) Bulk self-diffusion - 3

$$I(z) = \lambda \int_0^{2\pi} \int_0^{\mathrm{Sin}^{-1}(z/\lambda)} \cos^3\alpha \cos^2\omega \, d\alpha d\omega \qquad (7\text{-}36)$$

Therefore

$$\frac{Q_{BMS}}{Q_A} = \frac{1}{16}(6 - \delta^2) \quad , \quad \delta \leq 1$$
$$= \frac{1}{16\delta^2}(8\delta - 3) \quad , \quad \delta > 1 \qquad (7\text{-}37)$$

Method - 3B In Method - 3A, the contribution of the intercepted part of wall by the cylindrical plane whose radius is mean free path λ was evaluated. Corresponding to Method - 3A, the bulk self-diffusion term of this case must be calculated as the contribution of the molecules coming from the intercepted cylindrical plane by the two plates.

In Fig. (7-6) the number of these molecules across downward through dS, coming from dS' which is an element of the cylindrical plane , is

$$dN = \frac{\bar{v}}{4\pi}(n + x\frac{dn}{dx}) \cos\alpha d\Omega dS' \qquad (7\text{-}38)$$

where

$$x = \lambda\cos\omega \quad , \quad \cos\alpha = \lambda / \sqrt{\lambda^2 + (z - h)^2} \qquad (7\text{-}39)$$

$$I(z) = \int_0^{2\pi} \int_0^{D} \frac{\lambda^4 \cos^2\omega}{\{\lambda^2 + (z - h)^2\}^2} dh d\omega \qquad (7\text{-}40)$$

Hence finally the follwing equation is given as the flow

rate Q_{BMC}.

$$\frac{Q_{BMC}}{Q_A} = \frac{3}{8\delta}\mathrm{Tan}^{-1}\delta \quad , \quad 0 \leqq \delta \leqq \infty \tag{7-41}$$

2. Discussion

All calculated terms are plotted in Fig. (7-7), respectivelly.

As seen in Fig. (7-7), both the viscous flow terms, Q_{PC} and Q_{PP}, decrease steeply as δ decreases, and approximately vanish at $\delta \cong$ o.2. However Q_{PP} is larger than Q_{PC}, the difference is not appreciable in the range of δ where this term becomes significant.

The slip flow terms both moderately increase as δ increase, and asymptote to the constant value $\frac{\pi}{4}$ at $\delta > 10$. The difference between them reaches a maximum 13% at $\delta \cong 2$, but those coincides with each other at $\delta \to 0$ and $\delta \to \infty$.

The terms of skin self-diffusion gradually increase as δ decreases, and show a linear increasing on the semi-log chart at $\delta < 0.1$. However in the neighbourhood of $\delta = 1$, where the contribution of this term to the total flow rate is not controlling, Q_{DMC} is slightly larger than Q_{DMS}, the difference of them might be neglisible in practice. Meanwhile Q_{DP} calculated by the method of Pollard & Present[10] is somewhat appreciably smaller than the others.

Similar to the skin self-diffusion terms, Q_{BMC}

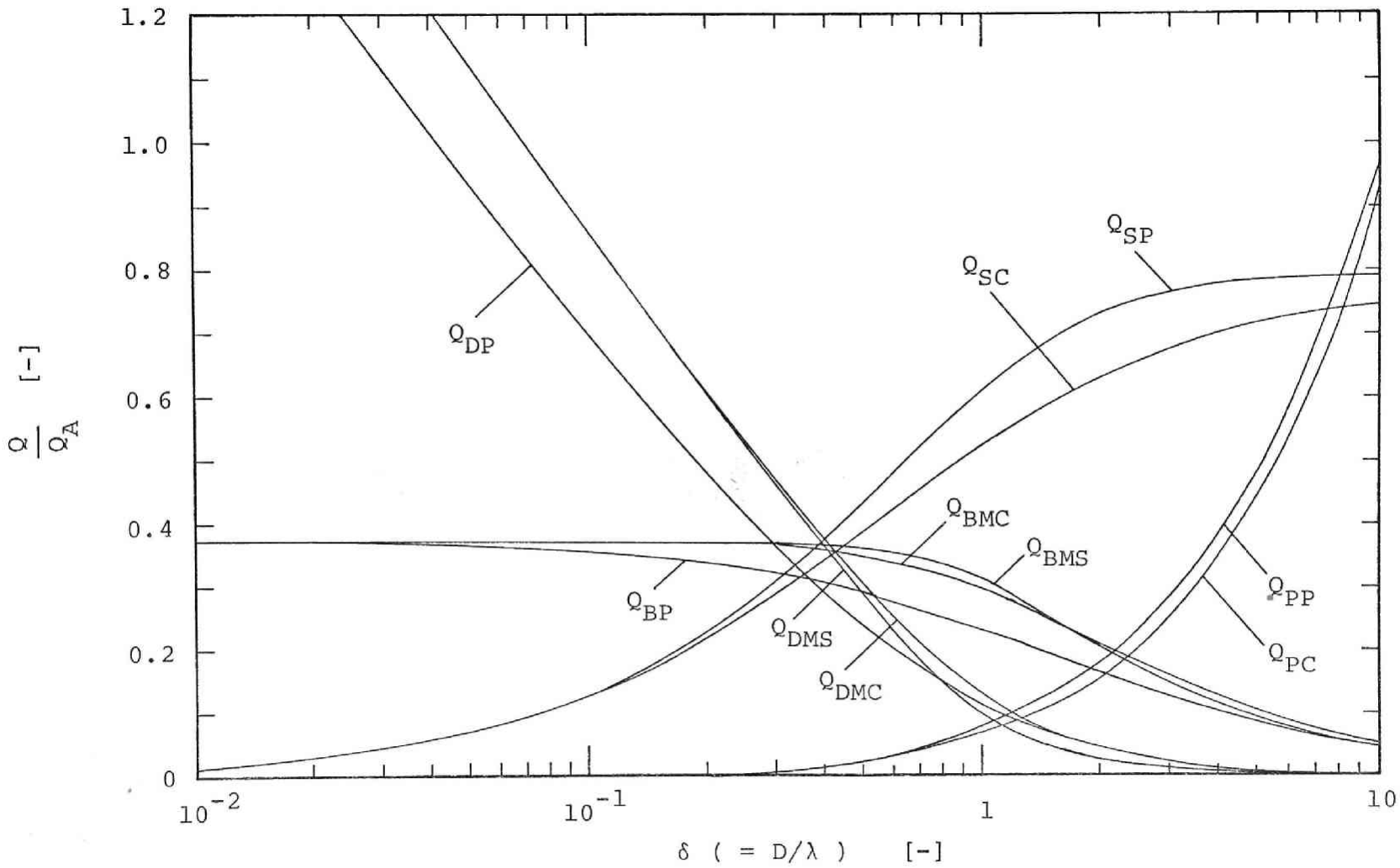

Fig. (7-7) Comparisons of individual flow terms

practically agrees with Q_{BMS} in the whole range of δ, and those asymptote to 3/8 at $\delta \to 0$. Q_{DP} agrees with them at $\delta \to 0$ and $\delta \to \infty$, but appreciably smaller than those in the intermediate range of δ.

There might be various combinations of the terms to give the total flow rate. However in the view of the physical picture of the flow mechanism, as the correction factor of the viscous and slip flow terms, Eq. (7-12) seems to be more reasonable than Eq. (7-16). Hence the typical combination are given as follows.

$$Q_{T1}/Q_A = (Q_{PC} + Q_{SC} + Q_{DP} + Q_{BP})/Q_A \tag{7-42}$$

$$Q_{T2}/Q_A = (Q_{PC} + Q_{SC} + Q_{DMS} + Q_{BMS})/Q_A \tag{7-43}$$

$$Q_{T3}/Q_A = (Q_{PC} + Q_{SC} + Q_{DMC} + Q_{BMC})/Q_A \tag{7-44}$$

Fig. (7-8) shows these three total flow rates comparing with the previous theoretical solutions and experimental data, and the characteristics of the solutions are listed in Table (7-1).

Both Q_{T2} and Q_{T3}, which practically agree with each other in the whole range of δ, show a farily good agreement with the numerical solution of the B-G-K equation calculated by Cercignani & Daneri[1] expect in the range of small δ, but even where the relative difference of them is very small. Therefore Q_{T3} is more combinient to use than Q_{T2} because of the simplicity of formula. On the other hand, Q_{T1} is somewhat smaller than the others at $\delta < 2$, however the principal characteristic of Q_{T1} seems to be approximately

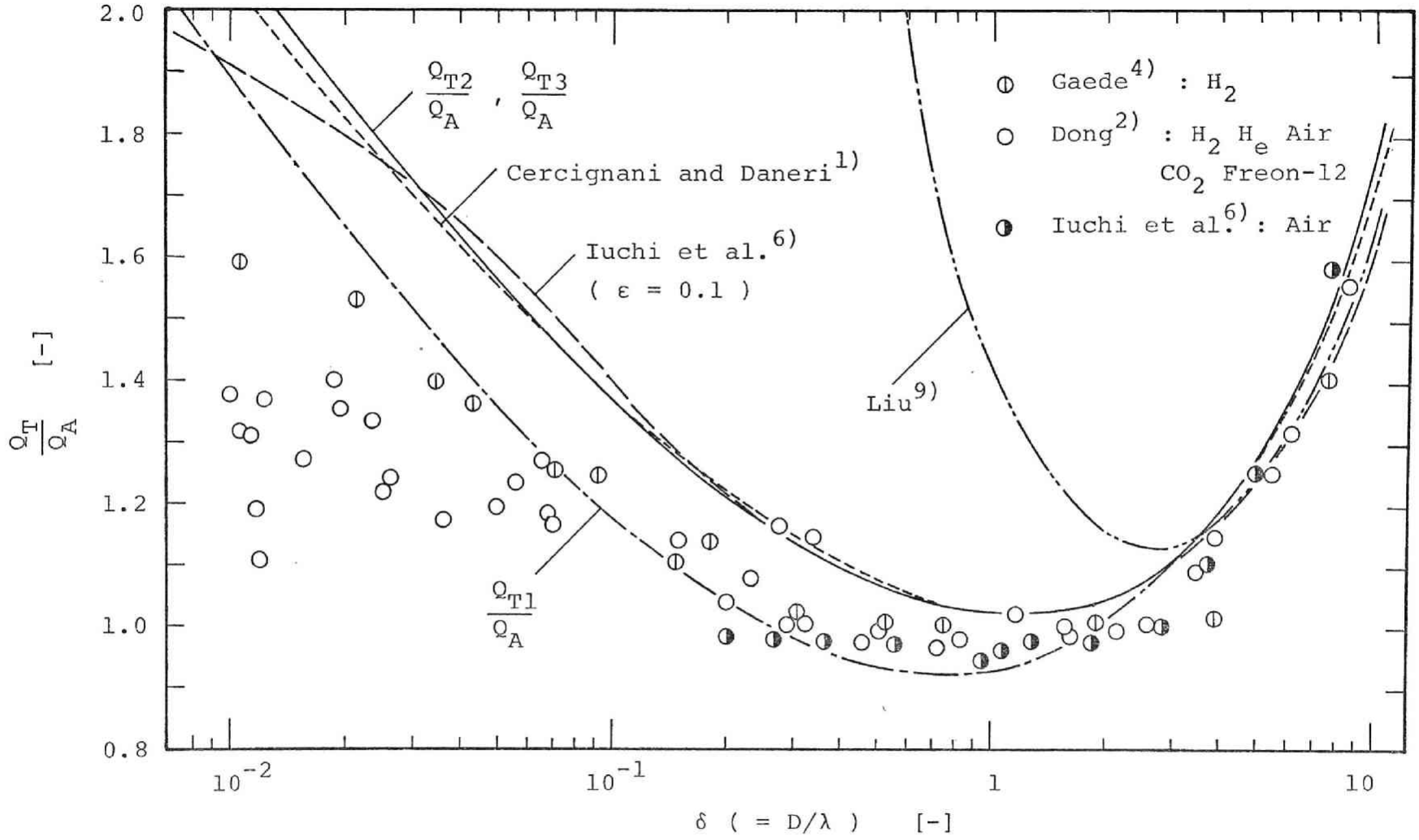

Fig. (7-8) Comparisons of observed data and various theoretical equations

Table (7-1) Camparison of theoretical solutions

	Cercignani & Daneri[1]	Liu[9]	Iuchi et. al.[6]	Present work
Method of Calculation	Numerical Soln. of B.G.K.eq.	Momemt Method (Two-sided Maxwellian)	Elementary Theory	Elementary Theory
$Q_T/Q_A\|_{\delta\to 0}$	$\frac{3}{8}(0.12 - \ln\delta)$	$\frac{3}{4\delta}$	func. of exp. parameter	$\frac{3}{8}(1 - \ln\delta)$
$(Q_T/Q_A)_{min}$	1.02	1.15	func. of exp. parameter	1.02
δ_{min}	1.2	2.8	1.0	1.2
$Q_T/Q_A\|_{\delta\to\infty}$	$\frac{\pi\delta}{32} + 0.68$	$\frac{\pi\delta}{32} + 0.59$	$\frac{\pi\delta}{32}$	$\frac{\pi\delta}{32} + 0.79$

equal to the one of the others. However the solution of Iuchi et al.[6], calculated as the arbitrary parameter $\varepsilon = 0.1$, roughly coincides with the present solutions, it gives somewhat the smaller minimum flow rate. Liu's[9] solution of the two-sided Maxwellian functions shows appreciable diviation from the others.

Compared with the experimental results of Gaede[4], Dong[2] and Iuchi et al.[6], the present solutions give larger value in the left hand side of the minimum flow points, neverthless in the right hand side they are in a good agreement. The reason why there seems to be upperbounds for the experimental data at $\delta \to 0$ in spite of the divergency of the theoretical results except only the one of Iuchi et al.[6], may be very difficult to be considered quantitatively at the present stage. The influence of the side wall of the channel used in the experiments might be considered to be the one of the most significant cause of that. However it is impossible to obtain a final conclusion till the quantitative analyis for the side wall effect is accomplished.

Conclusion

The Poiseuille flow between two parallel plates was analysed by the elementary kinetic theory to investigate the flow mechanism and finally to derive the flow rate

equation in a simple analytical form. As the result of the present analysis, it was verified that the total flow rate was composed of the four flow terms, those are the terms of viscous flow, slip flow and skin and bulk self-diffusion, and that the simple calculation procedures proposed here give the fairly good agreement with the experimental data in the range of the right hand side of the minimum flow point and with the numerical solutions of the B-G-K equation that has been regarded as the most reliable result. Hence it might be said that these calculation procedures are useful to evaluate of the flow rates of gases through various channels. The difference between the experimental results and theoretical ones must be examined quantitatively in future.

Nomenclature

b = width [cm]

D = interstice between two parallel plates [cm]

$Ei(x) = \int_{\infty}^{-x} e^{-u} u^{-1} du$ [-]

F = correction factor [-]

f = Maxwell's velocity distribution function of gas molecules [-]

k = Boltzmann's constant (= Rm/M) [$cm^3 \cdot atm/molecule \cdot °K$]

M = molecular weight [g/mol]

m = weight of molecule [g/molecule]

N	= number flow rate of molecule	[molecule/sec]
N_i, N_w	= frequency of collision	[1/sec]
n	= number density of molecule	[molecule/cm^3]
p	= pressure	[atm]
Q	= pV flow rate	[$cm^3 \cdot$ atm/sec$\cdot cm^2$]
Q'	= pV flow rate uncorrected	[$cm^3 \cdot$ atm/sec$\cdot cm^2$]
Q_A	= pV Knudsen flow rate formally equivalent to circular tube	[$cm^3 \cdot$ atm/sec$\cdot cm^2$]
R	= gas constant	[$cm^3 \cdot$ atm/mol$\cdot$°K]
r	= distance	[cm]
S	= area	[cm^2]
s	= wetted perimeter of channel	[cm]
T	= absolute temperature	[°K]
u	= macroscopic velocity of gas	[cm/sec]
$\underline{v}$	= velocity of molecule	[cm/sec]
$\bar{v}$	= averaged peculiar speed of molecule	[cm/sec]
x	= longitudinal coordinate	[cm]
y	= transversal coordinate parallel to plates	[cm]
z	= transversal coordinate perpendicular to plates	[cm]

α	= angle	[radian]
γ	= 0.577215...: Euler's constant	[-]
δ	= inverse Knudsen number	[-]
ζ	= slip coefficient	[cm]
θ	= angle	[radian]
λ	= mean free path	[cm]
μ	= viscosity	[g/cm$\cdot$sec]

ρ = density [g/cm^3]

Ω = solid angle [-]

ψ = angle [radian]

ω = angle [radian]

Subscripts

o = average

Literature Cited

1) Cercignani, C. and A. Daneri: J. Appl. Phys., 34, 3509 (1963)

2) Dong, W.: Univ. Calif. Report UCRL-3353 (1956)

3) Fryer, G. M.: Proc. Roy. Soc. (London) A293, 329 (1966)

4) Gaede, W.: Ann. Phys., 41, 289 (1913)

5) Huang, A. and R. L. Stoy: Phys. Fluids, 9, 2327 (1966)

6) Iuchi, S., T. Kanki and S. Miki: Kagaku Kogaku (Chem. Eng., Japan), 36, 996 (1972)

7) Kanki, T. and S. Iuchi: Kagaku Kogaku (Chem. Eng., Japan), 37, 1110 (1973)

8) Kennard, E. H.: Kinetic Theory of Gases, 302 (New York, McGraw Hill, 1938)

9) Liu, C. Y.: Phys. Fluids, 11, 481 (1968)

10) Pollard, W. G. and R. D. Present: Phys. Rev., 73, 762 (1948)

11) Scott, D. S. and F. A. L. Dullien: A. I. Ch. E. Journal, 8, 293 (1962)

12) Takao, K: Rarefied Gas Dynamics, 465 (Pergamon Press, 1961)

CHAPTER 8

MASS TRANSFER THROUGH RAREFIED GAS BETWEEN CONCENTRIC SPHERES

Introduction

Mass transfer operations under reduced pressures, such as freeze-drying, molecular distillation, metallizing under vacuum and so on, are accompanied with phase change in all cases and play a very important roll in chemical engineering. Condidering the mass transfer phenomena with phase change, for example, sublimation, condensation and evaporation, two kinds of resistance for mass transfer should be evaluated. One is the resistance through the surrounding space, so called the resistance of gaseous diffusion and the other is the one for phase change at the interface, which is concerned in accomodation, condensation or evaporation coefficients.

For mass transfer through the surrounding space three regimes classified by the Knudsen number, K_n, have been considered. Those are the free molecular regime under highly rarefied condition, $K_n > 10$, the continuum regime under ordinary, $K_n < 0.01$, and the transition regime between them, $0.01 < K_n < 10$. The mass transfer under this transition regime has given a great interest to investigators of physics

and technology. Especially its applications are very important for chemical engineering but few theoretical and experimental works[3,4,8,11] have been performed because of its complexity.

It has been generally accepted apriori by the previous investigators[8] that Stefan's equation with the pressure-jump boundary condition which is analogous to Maxwell-Smoluchowski's temperature-jump boundary condition for heat transfer would be correct. But there has been no theoretical basis on applying Stefan's equation to the mass transfer with large degree of rarefaction, high mass flux and large pressure gradient between evaporating (or sublimating) and condensating surface.

The present work was undertaken to derive a theoretical equation of mass transfer under reduced pressures, especially transition regime, through the gas kinetic theory and compare with the experimental results.

The Maxwell moment method utilizing the two-sided Maxwellian distribution function[2,6,7] was applied to the mass transfer between concentric spheres. The analytical solution obtained was compared with the experimental results obtained by the sublimation of naphthalene under reduced pressures ($10^{-1} \sim 10^{-3}$ mmHg in total pressure).

1. Theoretical Works

1.1 Distribution function and mean quantities

Let us consider a sphere of radius R_I placed at the center of hollow sphere of radius R_{II}, with $R_I < R_{II}$ (Fig. 8-1).

Sublimation (or evaporation) of molecule A occurs at the outer surface of the inner sphere and condensation at the inner surface of the outer sphere. The annular region ($R_I < R < R_{II}$) is filled with diffusion gas A and innert gas B.

By applying Lee's model[2], the "two-sided Maxwellian" velocity distribution functions are defined at an arbitrary point in the annular space as follows (Fig. 8-1); all outwardly directed molecules with velocity vector ξ,

$$\xi = (\xi_R^2 + \xi_\theta^2 + \xi_\phi^2)^{1/2} \tag{8-1}$$

$$\psi = \tan^{-1}\{(\xi_\theta^2 + \xi_\phi^2)^{1/2}\xi_R^{-1}\} \tag{8-2}$$

lying inside "the wedge of influence"[2] (region 1 in Fig. 8-1) are characterized by one Maxwellian f_1,

$$f = f_1 = n_1\left(\frac{m}{2\pi kT}\right)^{3/2}\exp\left(-\frac{m\xi^2}{2kT}\right) \tag{8-3}$$

for

$$-\frac{\pi}{2} + \alpha < \psi < \frac{\pi}{2} - \alpha$$

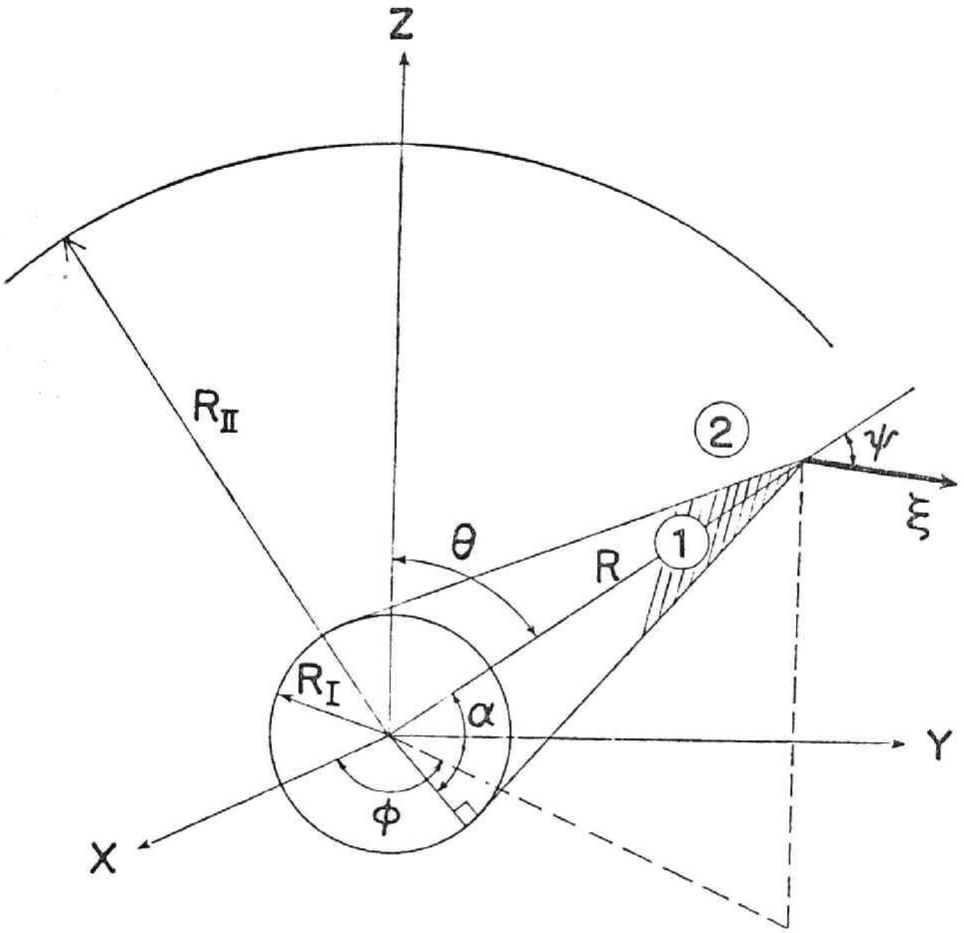

Fig. (8-1) Spherical polar coordinate

in which

$$\alpha = \mathrm{Cos}^{-1}\left(\frac{R_I}{R}\right) \tag{8-4}$$

Then, all molecules with velocity vector $\underline{\xi}$ lying outside of region 1 are characterized by f_2,

i. e.,

$$f = f_2 = n_2\left(\frac{m}{2\pi kT}\right)^{3/2}\exp\left(-\frac{m\xi^2}{2kT}\right) \tag{8-5}$$

for

$$\frac{\pi}{2} - \alpha < \psi < \frac{3}{2}\pi + \alpha$$

where $n_1(R)$ and $n_2(R)$ are unknown functions of radial distance.

In the above difinitions, we consider the case that the temperature difference between two spheres is small so the each temperature of two spheres can be approximately denoted as the same absolute temperature T[°K]. The Maxwellian velocity distribution for stationary gas is assumed applicable when the net flow of molecule A between concentric spheres is relatively small.

Knowing the distribution function f, one can evaluate all mean quantities < Q > by averaging over whole velocity space,

$$< Q > = \int Qfd\underline{\xi} = \int_I Qf_1 d\underline{\xi} + \int_{II} Qf_2 d\underline{\xi} \tag{8-6}$$

$$\int fd\underline{\xi} = n = \frac{1}{2}\{n_1(1 - \sin\alpha) + n_2(1 + \sin\alpha)\} \tag{8-7}$$

$$\int f\xi_R d\underline{\xi} = u_R = \frac{1}{4}\left(\frac{2kT}{m\pi}\right)^{1/2}(1 + \cos 2\alpha)(n_1 - n_2) \tag{8-8}$$

$$- \int m\xi_R^2 f d\underline{\xi} = P_{RR}$$

$$= - \frac{kT}{2}\{n_1(1 - \sin^3\alpha) + n_2(1 + \sin^3\alpha)\} \quad (8\text{-}9)$$

$$p = - \frac{1}{3}\{P_{RR} + P_{\theta\theta} + P_{\phi\phi}\}$$

$$= \frac{kT}{2}\{n_1(1 - \sin\alpha) + n_2(1 + \sin\alpha)\} \quad (8\text{-}10)$$

1.2 The Maxwell integral equation of transfer

In spherical co-ordinates the Maxwell integral equation of transfer for the spherical symmetric case is as follows:

$$\frac{1}{R^2}\frac{\partial}{\partial R}(R^2\int f\xi_R Q d\underline{\xi}) + \frac{1}{R\tan\theta}\int f\xi_\theta Q d\underline{\xi} - \int f(\frac{\xi_\theta^2}{R} + \frac{\xi_\phi^2}{R})\frac{\partial Q}{\partial \xi_R} d\underline{\xi}$$

$$+ \int f(\frac{\xi_R\xi_\theta}{R} - \frac{\xi_\phi^2}{R\tan\theta})\frac{\partial Q}{\partial \xi_\theta} d\underline{\xi} + \int f(\frac{\xi_R\xi_\phi}{R} + \frac{\xi_\theta\xi_\phi}{R\tan\theta})\frac{\partial Q}{\partial \xi_\phi} d\underline{\xi} = \Delta Q \quad (8\text{-}11)$$

where ΔQ is the collision integral.

There are two kinds of molecule, diffusing molecule A and non-diffusing molecule B and one should take the distribution functions for each molecule into account. Therefore there are four unknown parameters, n_{A1}, n_{A2}, n_{B1} and n_{B2}, and they could be evaluated by utilizing four Maxwell integral equations as follows.

(a) Mass Conservation for Molecule A Setting $Q = m_A$, we find $\Delta Q = 0$ because the mass is invariant during collisions, and obtain the ordinary continuity equation as

follows;

$$\frac{1}{R^2}\frac{\partial}{\partial R}(R^2\int f_A m_A \xi_{AR} d\underline{\xi}_A) = 0 \tag{8-12}$$

From Eqs. (8-8) and (8-12), we obtain the following relation;

$$\frac{1}{4R^2}\left(\frac{2m_A k}{\pi}\right)^{1/2}\frac{\partial}{\partial R}\{R^2(1 + \cos 2\alpha)(n_{A1} - n_{A2})T^{1/2}\} = 0 \tag{8-13}$$

On the other hand;

$$R^2(1 + \cos 2\alpha) = 2R_I^2 = \text{const.}$$

then the following equation is obtained.

$$n_{A1} - n_{A2} = \gamma = \text{const.} \tag{8-14}$$

(b) Mass Conservation for Molecule B Setting $Q = m_B$,

$$\frac{1}{4R^2}\left(\frac{2m_B k}{\pi}\right)^{1/2}\frac{\partial}{\partial R}\{R^2(1 + \cos 2\alpha)(n_{B1} - n_{B2})T^{1/2}\} = 0 \tag{8-15}$$

Here molecule B is the non-diffusing component, then

$$n_{B1} - n_{B2} = 0 \tag{8-16}$$

(c) R-momentum Conservation Summing up the momentum transfer equations for molecule A and B, the collision integral becomes zero as the R-momentum is conservative as a whole. Substituting $Q = m_A\xi_{AR}$ or $Q = m_B\xi_{BR}$ into Eq. (8-11),

$$\frac{\partial}{\partial R}\left(\int f_A m_A \xi_{AR}^2 d\underline{\xi}\right) + \frac{3}{R}\int\{-\frac{1}{3}(f_A m_A \xi_{AR}^2 + f_A m_A \xi_{A\theta}^2 + f_A m_A \xi_{A\phi}^2) + f_A m_A \xi_{AR}^2\}d\underline{\xi} = \Delta Q_{AB} \tag{8-17}$$

Then we obtain the next equation,

$$\frac{d}{dR}\{(n_{A1} + n_{A2})T\} - \sin^3\alpha\frac{d}{dR}\{(n_{A1} - n_{A2})T\} = \frac{2}{k}\Delta Q_{AB} \tag{8-18}$$

likewise

$$\frac{d}{dR}\{(n_{B1} + n_{B2})T\} - \sin^3\alpha\frac{d}{dR}\{(n_{B1} - n_{B2})T\} = \frac{2}{k}\Delta Q_{BA} \tag{8-19}$$

Summing up Eqs. (8-18) and (8-19),

$$\frac{d}{dR}(n_{A1} + n_{A2} + n_{B1} + n_{B2}) = 0 \tag{8-20}$$

$$n_{A1} + n_{A2} + n_{B1} + n_{B2} = \delta' = \text{const.} \tag{8-21}$$

where δ' is an integral constant.

(d) Mass Flux for Molecule A[5] Since we are primarily interested in radial mass transfer, the mass flux equation is given by taking $Q = m_A\xi_{AR}$. In the mass flux equation, the collision integral ΔQ_{AB} is evaluated with Maxwell's inverse-fifth-power force law $F = \tilde{K}_{AB}/r^5$ [5], for simplicity. Then it should be noted that mass flux is influenced only by the collision integral ΔQ_{AB} involving the collisions between molecule A and B.

Assuming that a molecule A collides with a molecule B from a direction P (see Fig. 8-2), the collision integral ΔQ_{AB} is expressed as follows:

$$\Delta Q_{AB} = \iiiint (Q' - Q) f_A f_B V d\underline{\xi}_A d\underline{\xi}_B b db d\varepsilon \tag{8-22}$$

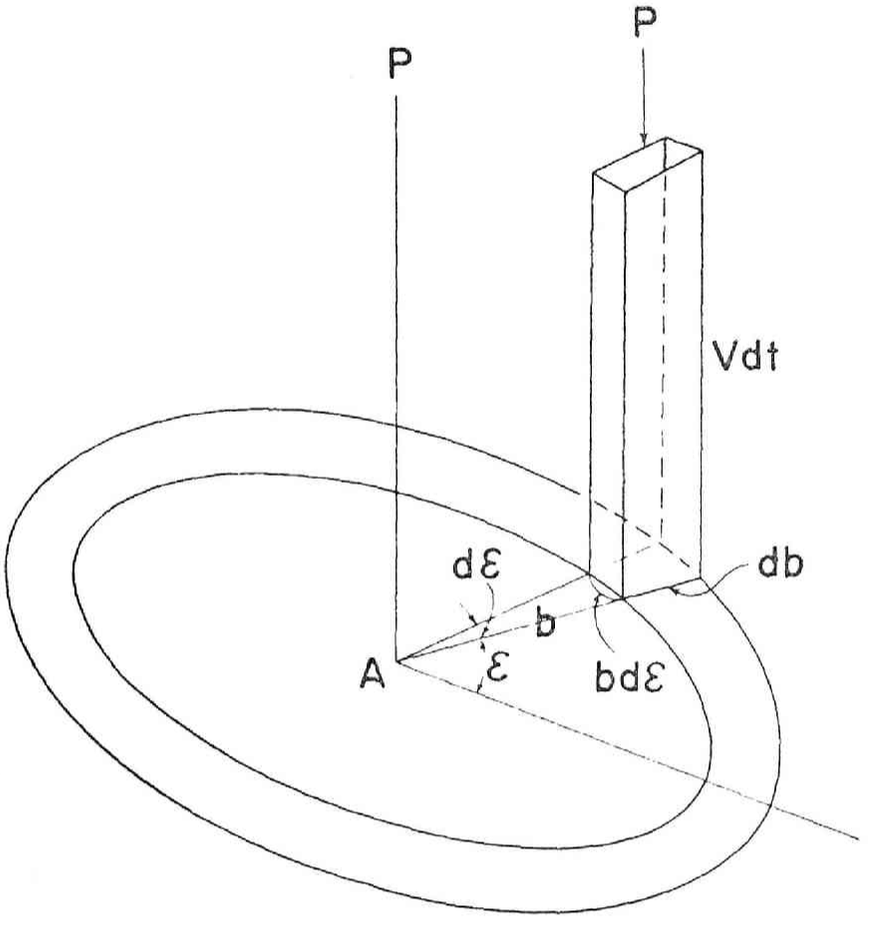

Fig. (8-2) Binary encounter of molecules

and by Maxwell[5],

$$\int_0^{2\pi} (Q' - Q)d\varepsilon = \int_0^{2\pi} m_A(\xi_{AR}' - \xi_{AR})d\varepsilon$$

$$= \frac{m_A m_B}{m_A + m_B}(\xi_{BR} - \xi_{AR})4\pi\sin^2\theta' \tag{8-23}$$

$$bdb = \{\frac{\tilde{K}_{AB}(m_A + m_B)}{V^2 m_A m_B}\}^{1/2} \beta d\beta \tag{8-24}$$

$$A_1 = \int_0^{\infty} 4\pi\beta d\beta \sin^2\theta' = 2.6595 \tag{8-25}$$

Therefore

$$\Delta Q_{AB} = A_1 (\frac{m_A m_B}{m_A + m_B}\tilde{K}_{AB})^{1/2} \iint f_A f_B (\xi_{BR} - \xi_{AR}) d\underline{\xi}_A d\underline{\xi}_B$$

$$= A_1 (\frac{m_A m_B}{m_A + m_B}\tilde{K}_{AB})^{1/2} (n_A u_{BR} - n_B u_{AR}) \tag{8-26}$$

Taking molecule B being at rest into account:

$$\Delta Q_{AB} = -A_1 (\frac{m_A m_B}{m_A + m_B}\tilde{K}_{AB})^{1/2} u_{AR} n_B$$

$$= -A_1 \{\frac{m_B kT \tilde{K}_{AB}}{2\pi(m_A + m_B)}\}^{1/2} \gamma' n_{B1} (\frac{R_I}{R})^2 \tag{8-27}$$

The diffusion coefficient for the Maxwell molecule is evaluated by the following equation[1],

$$[D_{AB}] = \frac{3\pi}{4nA_1\Gamma(2\frac{1}{2})}\{\frac{kT(m_A + m_B)}{2\pi m_A m_B}\}^{1/2} (\frac{2kT}{\tilde{K}_{AB}})^{1/2} \tag{8-28}$$

Eliminating $\tilde{K}_{AB}$ of Eq. (8-27) using Eq. (8-28), we obtain

$$\Delta Q_{AB} = - \frac{kTn_{B1}\gamma'}{2n[D_{AB}]}\left(\frac{2kT}{m_A\pi}\right)^{1/2}\left(\frac{R_I}{R}\right)^2 \tag{8-29}$$

$$\frac{d}{d\bar{R}}(n_{A1} + n_{A2}) = - \frac{R_I}{n[D_{AB}]}\left(\frac{2kT}{m_A\pi}\right)^{1/2} n_{B1}\gamma'\left(\frac{1}{\bar{R}}\right)^2 \tag{8-30}$$

where

$$\bar{R} = \frac{R}{R_I}$$

Converting n to p by utilizing the relation p = nkT, we obtain the following set of equations;

$$p_{A1} - p_{A2} = \gamma = \text{const.} \tag{8-31}$$

$$p_{B1} - p_{B2} = 0 \tag{8-32}$$

$$p_{A1} + p_{A2} + p_{B1} + p_{B2} = \delta = \text{const.} \tag{8-33}$$

$$\frac{d}{d\bar{R}}\left(\frac{p_{A1} + p_{A2}}{2}\right) = - \zeta\gamma p_{B1}\left(\frac{1}{\bar{R}}\right)^2 \tag{8-34}$$

where

$$\zeta = \frac{R_I}{2p_t[D_{AB}]}\left(\frac{2kT}{m_A\pi}\right)^{1/2} = \text{const.} \tag{8-35}$$

Then the following equations are obtained from Eqs. (8-31) ∿ (8-34),

$$p_{A1} = \frac{1}{2}\{\gamma + \delta + M\exp(-\frac{\zeta\gamma}{\bar{R}})\} \tag{8-36}$$

$$p_{A2} = \frac{1}{2}\{-\gamma + \delta + M\exp(-\frac{\zeta\gamma}{\bar{R}}) \tag{8-37}$$

and

$$p_{B1} = p_{B2} = - \frac{M}{2}\exp(-\frac{\zeta\gamma}{\bar{R}}) \tag{8-38}$$

where M is an integral constant.

The set of Eqs. (8-36) ∿ (38) can be solved by using the boundary conditions in 1-3.

1.3 Boundary conditions and solutions

On defining the accomodation coefficient for mass transfer, it was assumed that when a number of molecules are impinging on a surface, the fraction a of them are stuck and condensated, and the fraction (1-a) are reflected diffusely.

Then

$$\text{at } \bar{R} = \frac{R_I}{R_I} = 1 \; ; \quad p_{A1} = p_{A1I} = (1 - a)p_{A2I} + ap_{AI} \tag{8-39}$$

$$\text{at } \bar{R} = \frac{R_{II}}{R_I} = \bar{R}^* \; ;$$

$$p_{A2} = p_{A2II} = \frac{1 - a}{2}\{(1 + \cos 2\alpha_{II})p_{A1II} + (1 - \cos 2\alpha_{II})p_{A2II}\} + ap_{AII} \tag{8-40}$$

$$p_{B1} = p_{B2} = p_{B1II} = p_{B2II} \tag{8-41}$$

where a denotes the accomodation for mass transfer, and p_{AI} and p_{AII} are the saturated vapor pressures of substance A at the surfaces of the inner and outer spheres, respectively. Using Eqs. (8-39) ∿ (8-41) and Eqs. (8-36) ∿ (8-38) yield

$$p_{AI} - p_{AII} = \{\frac{1}{a} + \frac{1 - a}{a}(\frac{1}{\bar{R}^*})^2\}\gamma$$

$$+ p_{BlII}[1 - \exp\{-\zeta\gamma(1 - \frac{1}{\bar{R}^*})\}] \qquad (8\text{-}42)$$

On the other hand, the mass flux based on the outer surface of the inner sphere is given as follows;

$$N_{AI} = \int m_A \xi_{AR} f_A d\xi_A = m_A u_{ARI}$$

$$= (\frac{m_A kT}{2\pi})^{1/2}(n_{A1} - n_{A2}) = (\frac{m_A}{2\pi kT})^{1/2}\gamma \qquad (8\text{-}43)$$

$$k_g = \frac{N_{AI}}{p_{AI} - p_{AII}} = (\frac{m_A}{2\pi kT})^{1/2}\frac{\gamma}{p_{AI} - p_{AII}} \qquad (8\text{-}44)$$

$$M = -2p_{BlII}\exp(\frac{\zeta\gamma}{\bar{R}^*}) \qquad (8\text{-}45)$$

$$\delta = 2p_{AI} - (\frac{2}{a} - 1)\gamma - M\exp(-\zeta\gamma)$$

When p_{AI}, p_{AII} and p_{BlII} are known, one can obtain the value of γ from Eq. (8-42) and then the mass transfer rate from Eq. (8-43) also.

It could be easily verified that Eq. (8-43) approaches to Hertz-Kundsen's equation under highly rarefied pressures and to Stefan's equation under ordinary pressures.

If p_{BlII} approaches to zero, Eq. (8-42) reduces to the following equation.

$$\gamma \cong \frac{1}{F(a)}(p_{AI} - p_{AII}) \qquad (8\text{-}46)$$

where

$$F(a) = \frac{1}{a} + \frac{1 - a}{a}\left(\frac{1}{\bar{R}^*}\right)^2 \tag{8-47}$$

Therefore

$$N_{AI} \cong \frac{1}{F(a)}\left(\frac{m_A}{2\pi kT}\right)^{1/2}(p_{AI} - p_{AII}) \tag{8-48}$$

This is Hertz-Knudsen's equation.

If p_{BlII} takes so large value that the first term in the right hand side of Eq. (8-42) is negligibly smaller than the second, then one obtains

$$\exp\{-\zeta\gamma(1 - \frac{1}{\bar{R}^*})\} \cong \frac{1}{p_{BlII}}(p_{AII} + p_{BlII} - p_{AI}) \tag{8-49}$$

and

$$p_{AII} + p_{BlII} - p_{AI} \cong p_t - p_{AI} \cong p_{BlI} \tag{8-50}$$

$$\gamma \cong -\{\zeta(1 - \frac{1}{\bar{R}^*})\}^{-1}\ln\left(\frac{p_{BlI}}{p_{BlII}}\right) \tag{8-51}$$

because the value of p_t is approximately constant.

Therefore

$$N_{AI} \cong -\left(\frac{m_A}{2\pi kT}\right)^{1/2}\left(\frac{m_A\pi}{2kT}\right)^{1/2}\frac{2p_t[D_{AB}]}{R_I(1 - 1/\bar{R}^*)}\ln\left(\frac{p_{BlI}}{p_{BlII}}\right)$$

$$\cong \frac{m_A p_t[D_{AB}]}{kTR_I(1 - 1/\bar{R}^*)}\frac{p_{AI} - p_{AII}}{(p_B)_{lm}} \tag{8-52}$$

The above equation is Stefan's equation.

The distributions of the total pressure and the partial pressure of component A are expressed by

$$p_t = \frac{1}{2}\{(1 - \sin\alpha)(p_{A1} + p_{B2}) + (1 + \sin\alpha)(p_{A2} + p_{B2})\}$$

$$= \frac{1}{2}(\delta - \gamma\sin\alpha) \qquad (8\text{-}53)$$

and

$$p_A = \frac{1}{2}\{\delta + M\exp(-\frac{\zeta\gamma}{\bar{R}}) - \gamma\sin\alpha\} \qquad (8\text{-}54)$$

2. Experimental Apparatus and Procedures

The experimental apparatus used is schematically shown in Fig. (8-3).

The measurements of the sublimation rate of naphthalene coated on the inner sphere were performed under reduced pressure. The inner sphere was placed at the center of the outer sphere working as a condensating surface.

The outer sphere, the sublimation chamber ($150^{mm\phi}$I. D. x $160^{mm\phi}$O. D.), was made of bronze and jacketed by the copper cooling pipe through which methanol cooled by a refrigerator, 0 ∿ 40°C, was circulated.

The inner sphere (about 22 ∿ $30^{mm\phi}$) was the copper spherical shell having 1.5mm thickness in which the electric heater was provided, and was coated with naphtalene about to 2mm thickness and located concentrically in the outer sphere (see Fig. 8-3 and Fig. 8-4). The coating of naphthalene was carried out by dipping the inner sphere into a bath of molten naphthalene purified by recrystallization. The inner sphere

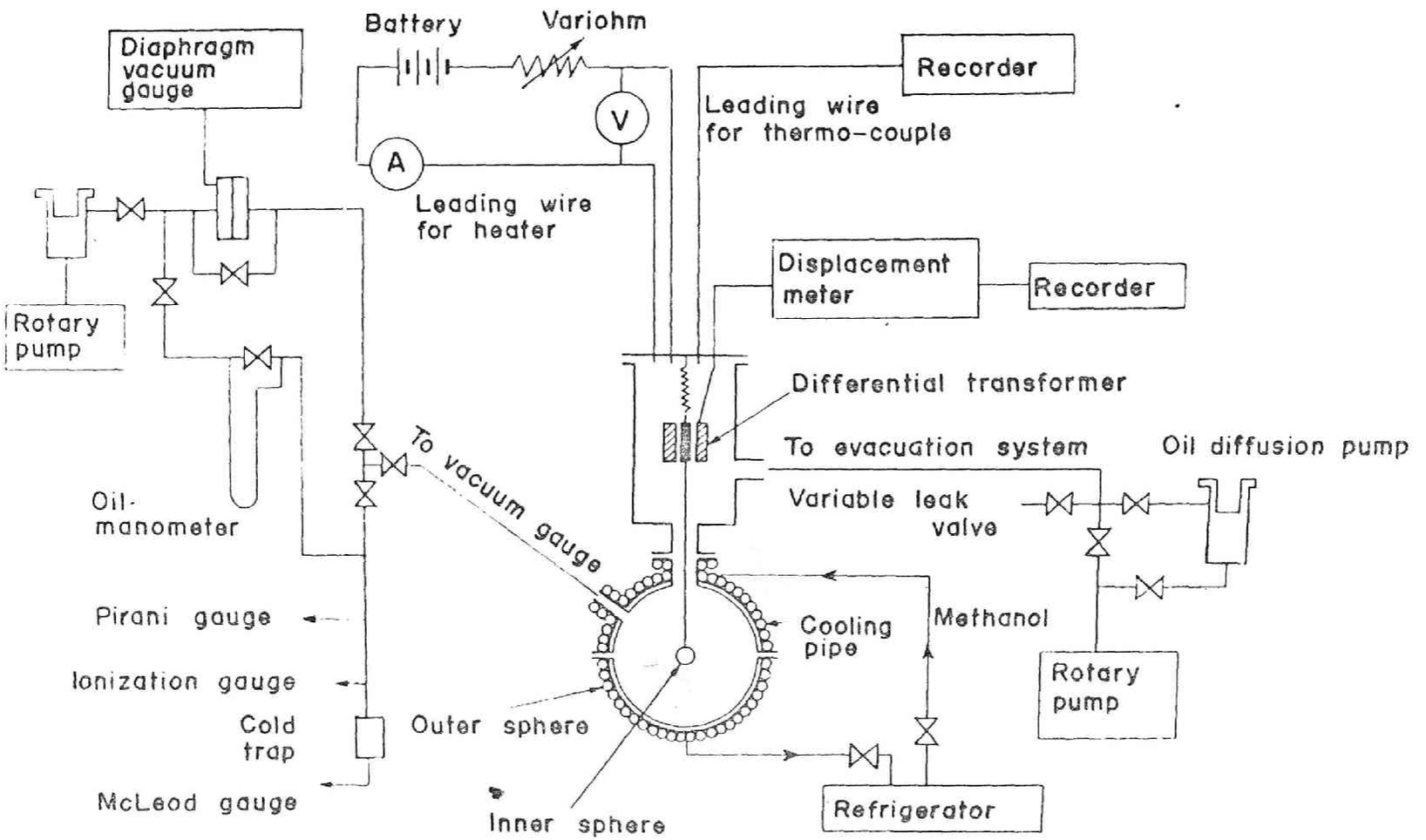

Fig. (8-3) Schematic diagram of apparatus

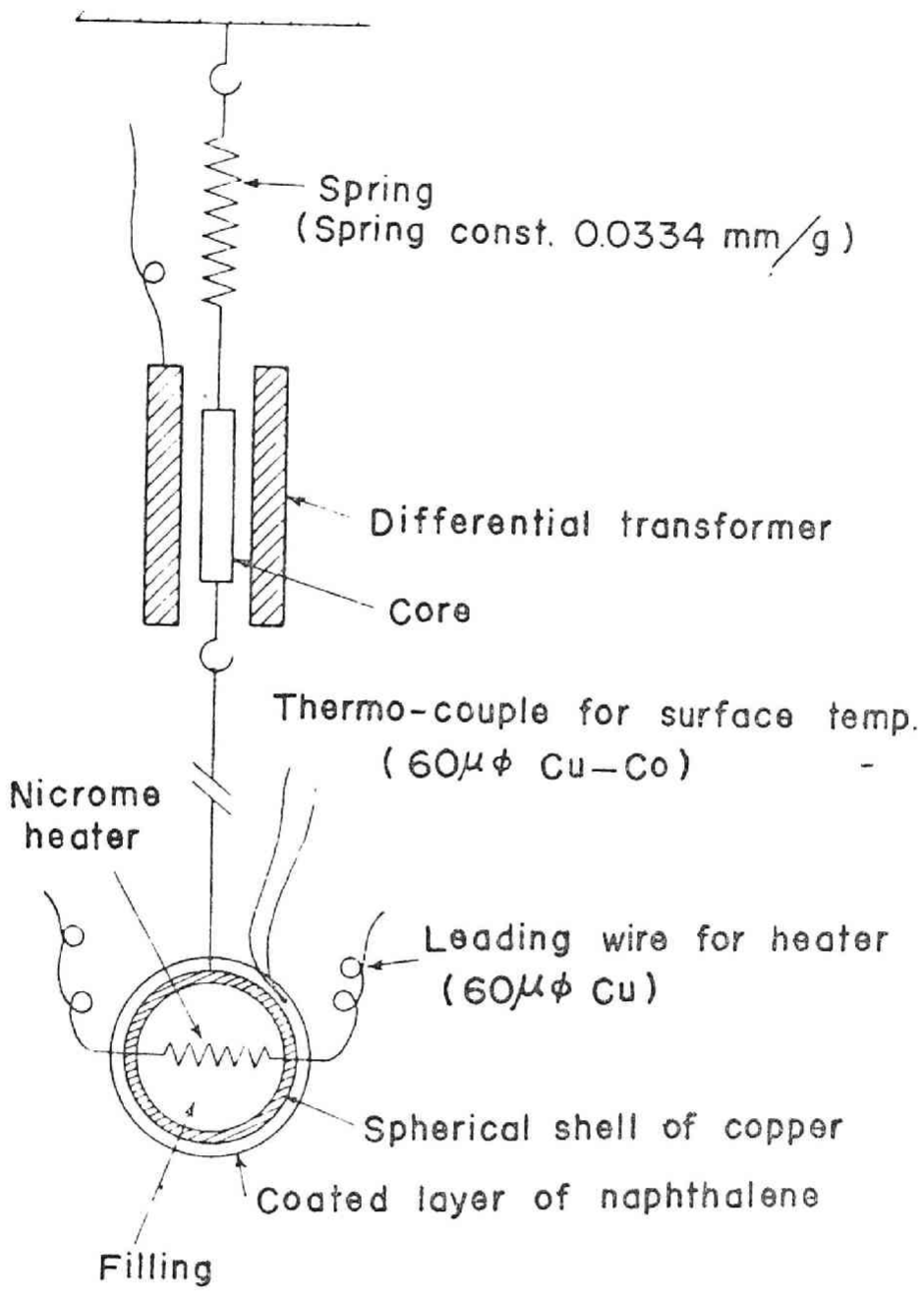

Fig. (8-4) Inner sphere and weighing mechanism

was electrically heated by supplying D. C. current and the surface temperature of naphthalene was regulated to be constant by a variohm and determined from the temparature of the surface of inner sphere taking account of the difference through the layer.

To determine the rate of sublimation, the weight loss of naphthalene on the inner sphere was measured by the displacement meter using the differential transformer (see Fig. 8-3 and Fig. 8-4) and recorded continuously.

For pressure measurement, Atlas-MMM diaphragm vacuum gauge for relatively low pressures and oil manometer for relatively high pressures were used. The measured value of the pressure at the outer sphere by using vacuum gauge, p_D, is

$$p_D = \frac{1}{2}\{(1 + \cos 2\alpha_{II})p_{A1II} + (1 - \cos 2\alpha_{II})p_{A2II}\} + p_{B1II}$$

$$= \left(\frac{1}{\bar{R}^*}\right)^2 p_{A1II} + \{1 - \left(\frac{1}{\bar{R}^*}\right)^2\} p_{A2II} + p_{B1II} \qquad (8\text{-}55)$$

From Eq. (8-55), the value of p_{B1II} can be calculated.

In the experiments, the total pressures of the apparatus were kept constant in the range $10^{-1} \sim 10^{-4}$ mmHg by a variable leak valve.

The procedures of the experiments were as follows; after hanging the coated inner sphere from a hook below the core of differential transformer, the sublimation chamber was evacuated for several minutes to the prescribed pressure and the outer sphere was cooled to the prescribed temperature.

Then the inner sphere was electrically heated for the surface temperature to be constant. The weight loss of the inner sphere and the temperatures of the surfaces were recorded continuously.

The measurements and regulations of the temperatures of the inner and outer sphere were carried out within $\pm 0.1°C$ and $\pm 0.4°C$ in errors, respectively.

The relative error on the determination of sublimation rate was estimated to be in $\pm 2\%$.

3. Experimental Results and Discussions

The mass transfer rate based on the surface of the inner sphere, N_{AI}, was calculated from the rate of weight loss of naphthalene by using the following equation,

$$N_{AI} = - \frac{1}{4\pi R_I^2} \frac{dW}{dt} \tag{8-56}$$

The value of p_{BlII} was calculated from the value of p_D measured by the vacuum gauge by using Eqs. (8-55), (8-31) and (8-36).

$$p_D = (\frac{1}{\bar{R}^*})^2 \gamma + p_{BlII} + \frac{1}{2}\{-\gamma + \delta + M\exp(-\frac{\zeta\gamma}{\bar{R}^*})\} \tag{8-57}$$

From Eqs. (8-45) and (8-57), we obtain the following equation;

$$p_{BlII} = p_D - p_{AII} - \frac{1}{a}(\frac{1}{\bar{R}^*})^2 \gamma \tag{8-58}$$

The experimental results are shown in Table (8-1). Further the values of p_{BIII} in Table (8-1) were calculated from Eq. (8-58) assuming that the value of a was equal to unity, because the error produced by this approximation was negligibly small in the final value.

In Fig. (8-5), the observed values of the sublimation rate are compared with the calculated values from Eq. (8-43). The observed values fairly agree with the calculated ones from the continuum to the transition region. It can be observed that in the free molecular region the observed values are a little smaller than the calculated ones as shown in Fig. (8-5).

The observed values of k_g are also compared with the calculated values from Eq. (8-44) in Fig. (8-6). From Fig. (8-6) it may be said that the accomodation coefficient a for maphthalene is equal about to 0.9. It has been reported by Sherwood et al.[9] that this coefficient was equal to 0.88 about at -60°C.

The distributions of the total pressure and the partial pressures of component A and B are calculated by using Eqs. (8-53) and (8-54). An example is shown in Fig. (8-7). The pressure-jump is observed distinctly on the surface on inner sphere and the total pressure changes steeply near the inner sphere.

Table(8-1) Experimental data

Run No.	t_I' [°C]	Δt_I [°C]	t_I [°C]	t_{II} [°C]	$p_{AI} \times 10^3$ [mmHg]	$p_{AII} \times 10^3$ [mmHg]	$p_D \times 10^3$ [mmHg]	$p_{BIII} \times 10^3$ [mmHg]	$N_{AI} \times 10^5$ [g/cm^2 sec]	$k_g \times 10^3$ [g/cm^2 sec mmHg]
1	10.4	0.7	9.7	-0.2	18.0	5.90	84.1	78.1	3.62	3.00
2	10.4	0.5	9.9	-0.3	18.2	5.82	143.0	137.1	2.32	1.80
3	0.2	1.2	-1.0	-10.9	5.40	1.65	10.7	9.00	5.14	13.7
4	-0.3	0.6	-0.9	-9.3	5.48	2.01	28.7	26.7	2.96	8.54
5	-9.7	0.8	-10.5	-30.9	1.75	0.118	2.25	2.10	3.78	23.2
6	-10.4	0.9	-11.3	-30.0	1.58	0.133	3.78	3.62	3.50	24.1
7	-9.7	0.7	-10.4	-30.0	1.75	0.133	7.56	7.40	2.98	18.4
8	-10.2	0.5	-10.7	-28.3	1.70	0.169	22.0	21.8	1.51	9.84
9	-10.0	0.4	-10.4	-29.3	1.75	0.146	61.6	61.4	0.621	3.88
10	-19.3	0.2	-19.5	-26.9	0.55	0.205	2.09	1.88	0.703	20.1
11	-20.2	0.4	-20.6	-29.0	0.485	0.152	2.90	2.74	1.10	33.0
12	-19.7	0.2	-19.9	-29.3	0.530	0.146	7.25	7.10	0.700	18.3
13	-20.0	0.2	-20.2	-29.0	0.510	0.153	23.3	23.2	0.281	7.87
14	-19.3	0.2	-19.5	-28.1	0.560	0.174	24.0	23.8	0.355	9.20
15	-20.2	0.2	-20.4	-29.7	0.495	0.139	72.5	72.4	0.127	3.58
16	0.0	0.6	-0.6	-9.8	5.60	1.90	35.2	33.3	2.50	6.74
17	-10.0	0.8	-10.8	-30.5	1.67	0.124	5.14	4.97	3.69	23.8
18	-10.0	0.8	-10.8	-29.3	1.67	0.146	6.32	6.14	3.67	24.1
19	-9.9	0.6	-10.5	-29.5	1.74	0.143	13.2	13.0	2.43	15.1
20	-9.9	0.6	-10.5	-30.0	1.74	0.133	16.5	16.3	2.00	12.4
21	-10.0	0.9	-10.9	-31.0	1.65	0.115	3.26	3.10	4.32	28.1
22	-9.9	0.9	-10.8	-30.5	1.67	0.125	4.31	4.15	3.94	25.4
23	-9.9	0.5	-10.4	-30.8	1.76	0.119	24.9	24.8	1.25	7.62
24	-10.0	0.7	-10.7	-30.8	1.70	0.119	8.68	8.53	3.13	19.8
25	-9.7	0.4	-10.1	-29.8	1.83	0.136	40.5	40.4	0.965	5.71
26	-10.0	0.7	-10.7	-30.6	1.70	0.122	9.33	9.18	3.21	20.3

t_I : temperature of the surface of copper shell

Δt_I : temperature difference through the coated layer of naphthalene

The data of vapor pressure, thermal conductivity and diffusivity of naphthalene were cited from I. C. T..

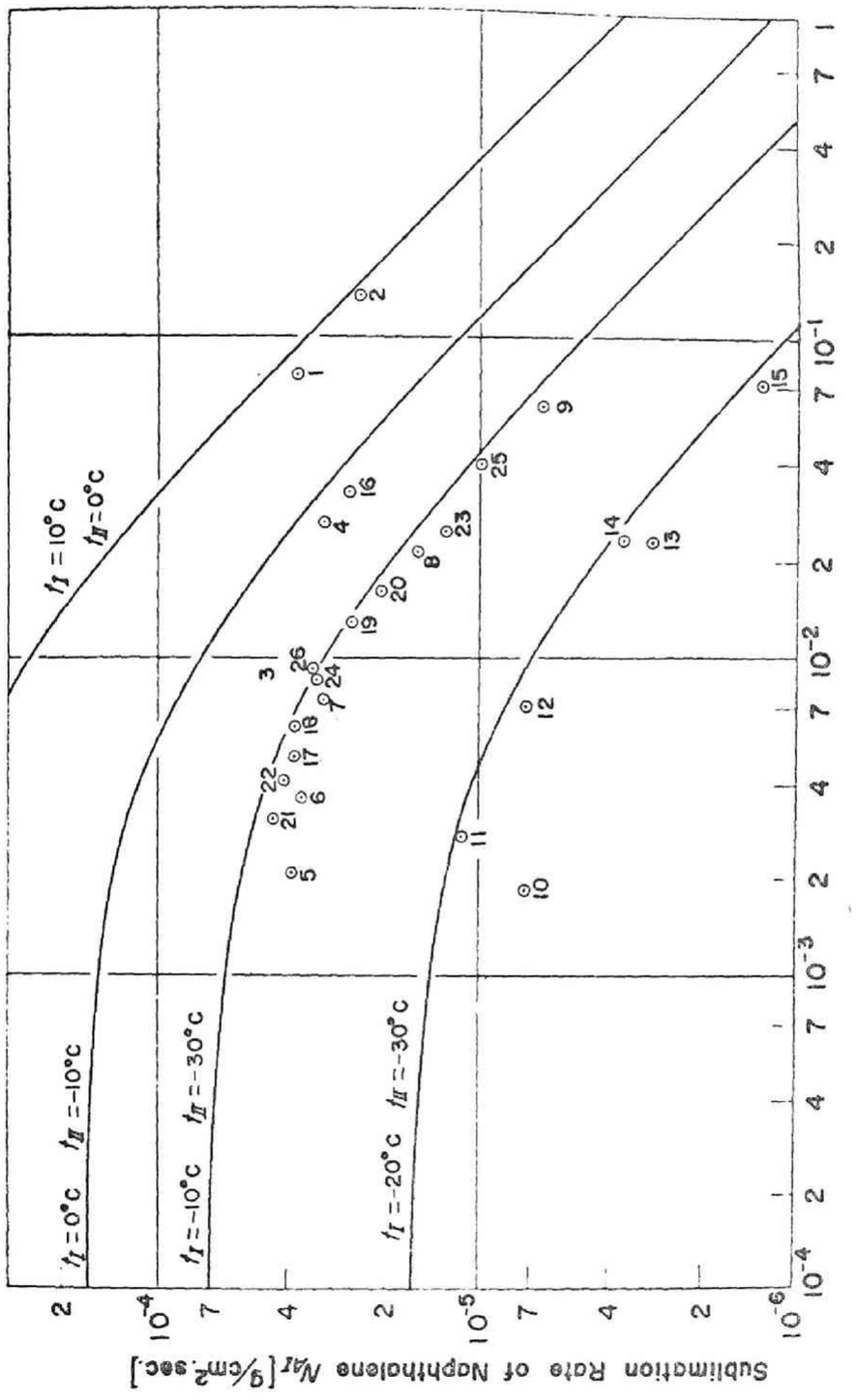

Fig. (8-5) Comparison between experimental and theoretical results

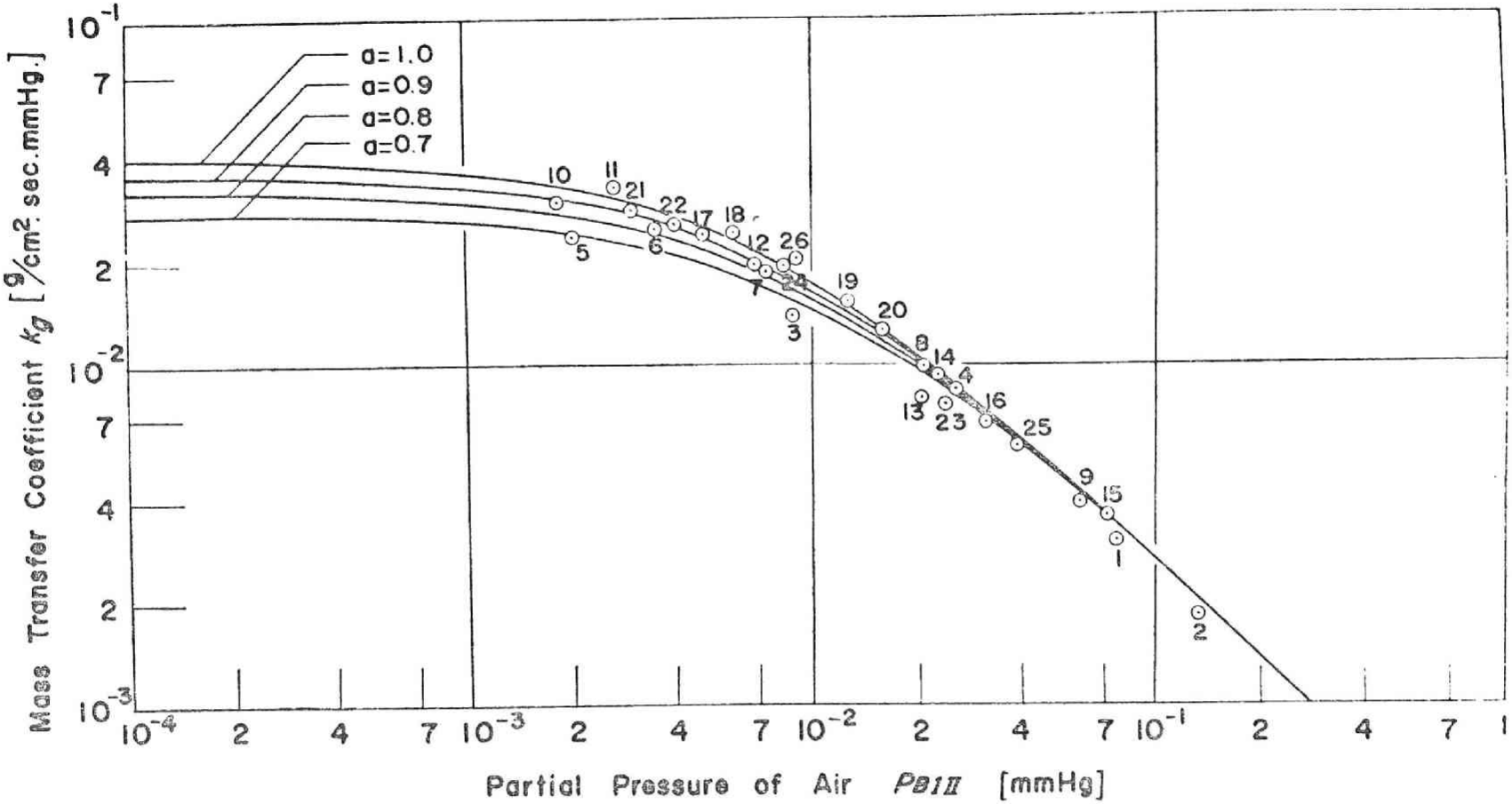

Fig. (8-6) Correlation of mass transfer coefficient vs. partial pressure of air

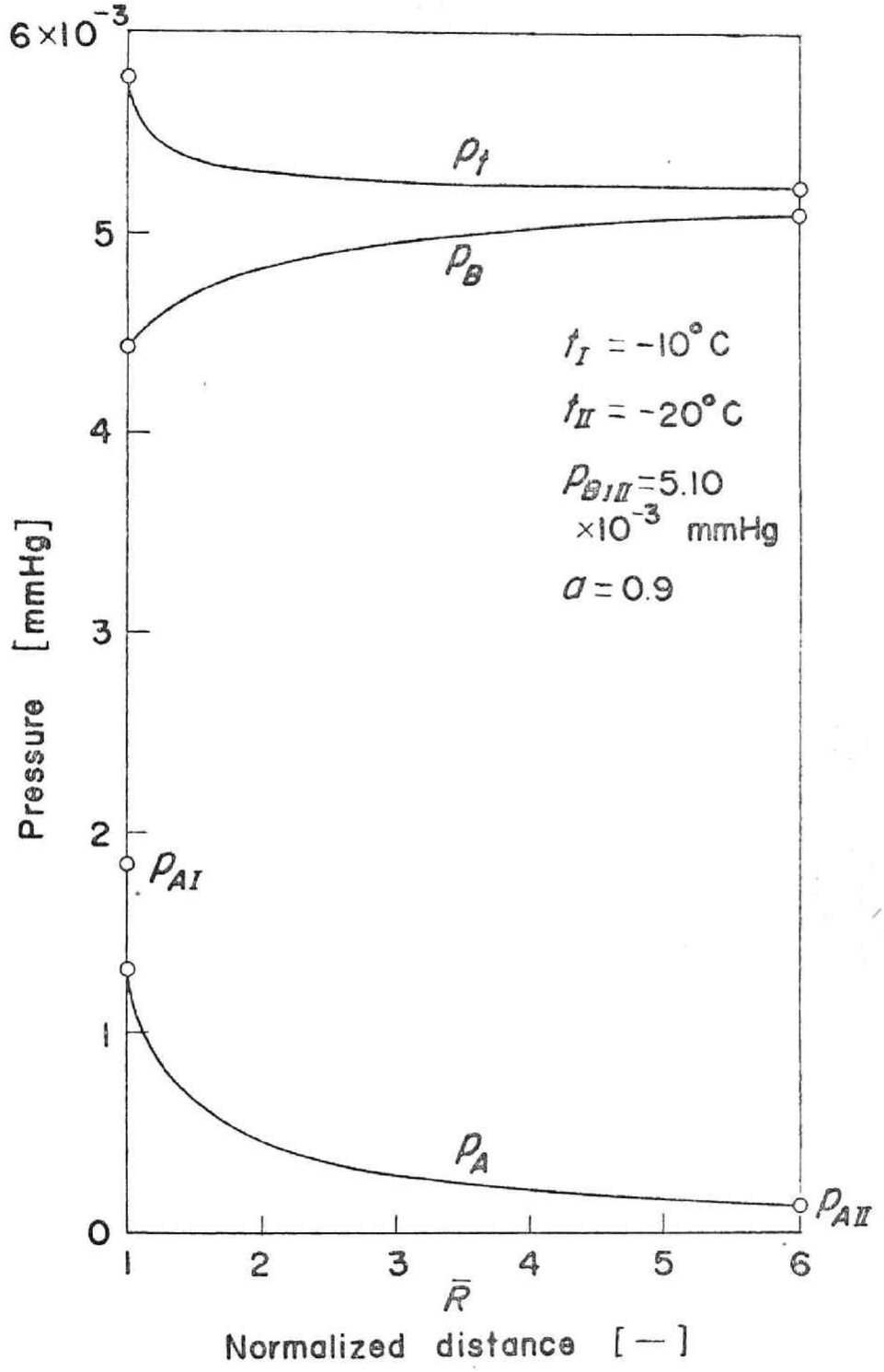

Fig. (8-7) Theoretical distributions of partial pressures between concentric spheres

Conclusion

The equation of mass transfer between concentric sphere under reduced pressures, especially under the transition regime, was derived through the gas kinetic theory using the two-sided Maxwellian distribution function. The observed values of the sublimation rate of naphthalene were compared with the values calculated from the equation derived in the present work and both were in good agreement.

Nomenclature

A_1 = constant defined by Eq. (8-25) [-]

a = accomodation coefficient for mass transfer [-]

b = impact parameter, or perpendicular distance from molecule A to initial trajectory of molecule B (see Fig. 8-2) [cm]

$[D_{AB}]$ = diffusion coefficient of molecule A through molecule B [cm^2/sec]

F = intermolecular force for the Maxwell molecule

F(a) = the function of accomodation coefficient:

$$\frac{1}{a} + \frac{1 - a}{a}\left(\frac{1}{\bar{R}^*}\right)^2 \quad [-]$$

f = velocity distribution function of molecule [-]

$\tilde{K}_{AB}$ = constant in expression for central force field, $F = \frac{\tilde{K}_{AB}}{r^5}$

k = Boltzmann constant [mmHg·cm^3/°K]

k_g = mass transfer coefficient [g/cm^2· sec·mmHg]

M = integral constant defined in Eqs. (8-36) ∿ (8-38) [mmHg]

m = mass of a molecule [g]

N_{AI} = mass transfer rate based on the inner sphere [g/cm^2 sec]

n = number density of molecule [1/cm^3]

P = component of pressure tensor [mmHg]

p = pressure defined by $p = nkT$ [mmHg]

Q = physical quantity

ΔQ = change in Q produced by collision; collision integral

R = radial distance from the center of the inner sphere [cm]

$\bar{R}$ = normalized distance from the center of the inner sphere sphere; $\bar{R} = R/R_I$ [-]

$\bar{R}^*$ = R_{II}/R_I [-]

r = distance between two molecules colliding each other [cm]

T = absolute temperature [°K]

t = time [sec]

V = relative velocity between two interacting molecules [cm/sec]

W = weight of the inner sphere [g]

Greek Letters

α = angle defined by Eq. (8-4) [-]

β = variable concerned in variable b (cf. literature 5)

γ = integral constant defined by Eq. (8-31) [mmHg]

γ' = integral constant defined by Eq. (8-14) [1/cm^3]

δ = integral constant defined by Eq. (8-21) [$1/cm^3$]

ε = angle between plane of the orbit and plane containing the original relative velocity and the X-axis in a binary collision (see Fig. 8-2) [-]

θ' = scattering angle, or angle between relative velocity before and after collision [-]

ξ = velocity of molecule [cm/sec]

$\underline{\xi}$ = velocity vector of molecule [cm/sec]

ψ = angle defined in Fig. (8-1) [-]

ζ = constant defined by Eq. (8-35) [1/mmHg]

Suffix

A = diffusing component

B = stagnant component

R = radial direction on polar co-ordinate

D = pressure directed outwardly at the inner surface of the outer sphere

t = total pressure

θ = θ-direction on polar co-ordinate

ϕ = ϕ-direction on polar co-ordinate

1 = inside of the wedge of "influence" (see Fig. 8-1)

2 = outside of the wedge of "influence" (see Fig. 8-1)

I = the inner sphere

II = the outer sphere

$< >$ = averaged value

' = after collision

Literature Cited

1) Chapman, S. and T. G. Cowling: "The Mathematical Theory of Non-Uniform Gases" (Cambridge, 1964)

2) Lees, L. and C. Liu: Phys. Fluid. 5, 1137 (1962)

3) Madden, A. J.: A. I. Ch. E. J., 5, 135 (1959)

4) Madden, A. J. and F. J. Halfen: A. I. Ch. E. J., 7, 160 (1961)

5) Maxwell, J. C.: Phil. Trans. Roy. Soc. 157, 49 (1867)

6) Mikami, H., Y. Endo and Y. Takashima: Int. J. Heat Mass Transfer, 9, 1435 (1966)

7) Mott-Smith, H. M.: Phys. Review, 82, 885 (1951)

8) Sherwood, T. K. and N. E. Cooke: A. I. Ch. E. J., 3, 37 (1957)

9) Sherwood, T. K. and C. Johannes: A. I. Ch. E. J., 8, 590 (1962)

10) Smoluchowski, M.: Ann. Phys., 35, 984 (1911)

11) Uyeha, H., T. Kajiura and O. Yoshikawa: Chem. Eng. (Japan), 24, 274 (1960)

POSTFACE

This thesis is a collection of several works on drying of solids which have performed by author for twelve years since he came back to the laboratory of professor R. Toei of Kyoto University in 1962.

This work covers only a small part of the study on drying mechanism, and there have been left many important problems unsolved.

Especially as mentioned in CHAPTER 1, the one of the most important problems to know how to proceed drying of moist material is the evaluations of the transport properties controlling the drying process.

Among the properties, the liquid water transfer coefficient of moist porous materials is the most difficult to evaluate, in spite of the extensive studies of Krischer and many other workers. It would seem then more profitable on the future to study the mechanisms of liquid water movement in porous materials from a more fundamental standpoint.

ACKNOWLEDGMENTS

The author would like to express his sincere appreciation to Professor Ryozo Toei of Department of Chemical Engineering, Kyoto University for his valuable suggestions and encouragement in all stage of this work.

The author wishes to acknowldge to Professor Shinya Hayashi of Kobe University, Professor Ryuichi Matsuno and Messrs. Masashi Asaeda and Takeshi Furuta of Kyoto University for their encouragements and helpful advices.

Thanks are also due to Messrs. Katsuyuki Kubota, Kunio Kataoka, Koji Ohashi, Mutsumi Kimura, Hiromasa Ueda, Toshihiro Okuma, Teruhiko Sugimori, Hiroshi Iwasaki, Akira Uragami, Yuji Takaki, Takuo Harado, Toshiaki Maruyama, Katashi Shioda, Keizo Masuda, Narihiko Akamatsu, Ikuo Ito, Yukimichi Okamoto and Shoji Yamamoto, and Miss Kuniko Yamanaka for their helps to this study.

Thanks are also due to Misses Eiko Miura and Kuniko Yamanaka for their helps in the preparation of this thesis.

M. OKAZAKI

Kyoto, February 1975